Photoelectron Spectroscopic Investigations of Porphyrins and Phthalocyanines on Ag(111) and Au(111): Adsorption and Reactivity

Photoelektronenspektroskopische Untersuchungen zur Adsorption und Reaktivität von Porphyrinen und Phthalocyaninen auf Ag(111) und Au(111) Oberflächen

Der Naturwissenschaftlichen Fakultät der

Friedrich-Alexander-Universität Erlangen-Nürnberg

zur

Erlangung des Doktorgrades Dr. rer. nat.

vorgelegt von

Yun Bai

aus Jingzhou, China

Als Dissertation genehmigt

durch die Naturwissenschaftliche Fakultät

der Friedrich-Alexander-Universität Erlangen-Nürnberg

Tag der mündlichen Prüfung: _____

Vorsitzende/r der Promotionskommission: Prof. Dr. Bänsch

Erstberichterstatter/in: Prof. Dr. H.P. Steinrück

Zweitberichterstatter/in: Prof. Dr. R. Fink

Table of Contents

Acronyms

Techniques

DFT density functional theory
LEED low-energy electron diffraction
NEXAFS near edge X-ray absorption fine structure
(NI)XSW (normal-incidence) X-ray standing wave technique
STM scanning tunnelling microscopy
TPD temperature programmed desorption
UPS UV photoelectron spectroscopy
XPS X-ray photoelectron spectroscopy

Chemical compounds

2HOEP octaethylporphyrin
2HPc phthalocyanine
2HTPP 5,10,15,20-tetraphenylporphyrin
2HTTBPP 5,10,15,20-tetrakis(3,5-di-tert-butylphenyl)porphyrin
MOEP cobalt octaethylporphyrin (M = Co, Ni, etc.)
MPc metallo-phthalocyanine (M = Fe, Co, etc.)
MTPP metallo-tetraphenylporphyrin (M = Fe, Co, Zn, etc.)
MTTBPP metallo-tetrakis(3,5-di-tert-butylphenyl)porphyrin (M = Fe, Co, etc.)

Further acronyms

DFG Deutsche Forschungsgemeinschaft
SFB Sonderforschungsbereich der DFG

1. Introduction

Functionalization of surfaces on the nanoscale is the key to designing novel catalysts, sensors, and other devices that are based on the interaction of an active surface with the surrounding medium. Metalloporphyrins and similar planar metal complexes are especially suitable for this task, because they combine a structure forming element (e.g., the porphyrin framework) with an active site, usually the coordinated metal center. In the free complex, this metal center is often coordinated by only the tetradentate planar ligand (porphyrin, phthalocyanine, or corrole, in the following referred to as tetrapyrroles), thus is coordinatively unsaturated. This unsaturated character, resulting in two vacant axial coordination sites, is a central reason for the outstanding importance of this class of molecules in biological systems and in technology. In biological system they represent the active centers of many enzymes, such as the ubiquitous heme-thiolate proteins for oxygen reduction. Other examples of porphyrins in nature include magnesium porphyrins in chlorophyll, cobalt corrin in cobalamin (vitamin B12), and iron porphyrin in hemoglobin for the oxygen transport in the blood of mammals. In modern technologies, metalloporphyrin monolayers or thin films have been employed in catalysis,[Hu07] as sensors,[Sc05] and in dye solar cells,[Ra00] etc. In many of these applications the metal center plays an important role.

To develop a fundamental understanding of the functional principles of the tetrapyrrole complexes in nature, and to increase the probability of their application in industry, the formation, the electronic structure, and the reactivity of various tetrapyrrole complexes have been studied on well-defined metal single crystal surfaces using photoelectron spectroscopy and complementary techniques. This research work is supported by the Deutsche Forschungsgemeinschaft (DFG) through Sonderfprschungsbereich (SFB) 583.

1.1. The subproject A9 in SFB 583 - Adsorption and reactivity of the redox active metalloporphyrins

The SFB 583 is focused on three fields:
A. molecular architectures for molecular activation,
B. Molecular architectures for charge transfer, and
C. Physical and Theoretical quantification of the functionality

Our project A9, "Adsorption and Reactivity of Redox-Active Metalloporphyrins", is a part of the project area A. In project A9, we investigate well defined layers, especially monolayers of metalloporphyrins on metal and oxide surfaces of single crystal and polycrystalline substrates. The focus is on new surface reactions such as the direct

metalation of adsorbed porphyrins (especially for the preparation of reactive metalloporphyrins) and the activation of inert molecules (CO_2, N_2, N_2O) on the porphyrin-coordinated metal centers. The reactivity of these metal centers (Fe, Ti, V, Cr, Mo) will be controlled by the interaction with the substrate, where both the type of the substrate (Ag, TiO_2, graphite, (2x2)-S/Ni (111) etc.) as well as the distance between the redox center and the substrate are varied. For the variation of the distance, different peripheral substituents on the porphyrin framework are used. Of particular interest are the intra-molecular conformations of the adsorbed porphyrins and their long-range order, even in the presence of coadsorbates. To gain insight into the catalytic effects of metal complexes supported on an oxide, the system $CoTPP/TiO_2$, which catalyzes the NO reduction with H_2 or CO, should be investigated both on TiO_2 (110) and on polycrystalline TiO_2. For the aforementioned investigations mainly scanning tunneling microscopy (STM) and photoelectron spectroscopy (XPS / UPS) are used. Additionally X-ray standing waves (XSW) as well as X-ray absorption measurements (EXAFS) should be carried out for precise determination of the distance between the metal center and the substrate. Collaborations with other projects also exist within the SFB 583.

1.2. Objectives of the thesis

From the ongoing sub-project A9 a number of remarkable results and findings have been obtained, including elucidation of the geometrical structure of adsorbed porphyrin layers, investigation of the electronic structure of adsorbed porphyrin layers, and chemical reactions of adsorbed porphyrins and metalloporphyrins.[Go06] [Bu07A] [Bu07B] [Co07] [Fl07A] [Fl07B] [Kr07] [Lu07] [Sh07] The objective of this thesis is to study the extended tetrapyrrole system on well–defined metal surfaces:

A. To determine the Co-Ag distance in CoTPP and CoTTBPP monolayers on Ag(111) surface;

B. To study the behaviour of adsorbed planar porphyrins on a Ag(111) surface in comparison to porphyrins which are distorted in the adsorbed state;

C. To explore influence of the molecular structure of the tetrapyrrole complex and the nature of the substrate on the interaction between the metal center and the substrate.

2. Materials: substrates and adsorbates

The physical and chemical properties of the materials used in this work are described briefly in this chapter.

2.1. Silver

Silver has the atomic number 47 with the atomic symbol Ag and belongs to the first side group of the periodic system. Its atomic radius is 144.5 pm and its most common isotope has an atomic weight of 107.868. Its melting point is 1,234 K and boiling point is 2,435 K. The ground state electron configuration of silver is [Kr] $5s^14d^{10}$.[La05]

Pure silver has a brilliant white metallic luster and is very ductile. It has the highest electrical and thermal conductivity of all metals, and possesses the lowest contact resistance. Ag is stable in pure air and water, but tarnishes when exposed to ozone, hydrogen sulfide, or air containing sulfur. The most common oxidation state of silver is +1, although +2 and +3 also exist in silver complexes.[La05]

A silver single crystal with a (111) oriented surface was used as one of the substrates in this work. Figure 2-1 shows a model of the unit cell of the silver crystal and the (111) plane.
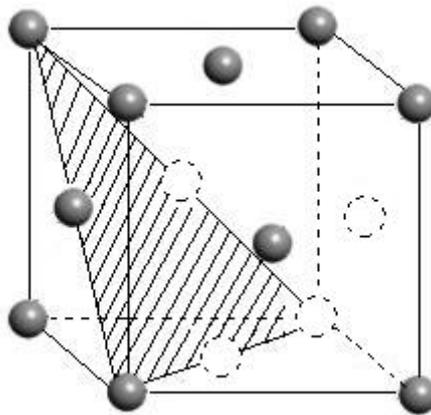
Figure 2-1. Model of a silver face centered cubic (fcc) unit cell and the (111) plane (the shaded plane).

2.2. Gold

Gold with the atomic symbol Au has the atomic number 79 and also belongs to the first side group of the periodic system. Its atomic radius is 144.2 pm and its atomic weight is 196.966. Its melting point is 1,337 K and boiling point is 3,080 K. The electron configuration of gold at ground state is [Xe] $4f^{14}$ $5d^{10}$ $6s^1$.[La05]

Gold is the most malleable one of all metals. It is a good conductor of heat and electricity and reflects infra red radiation strongly. Chemically, Au is unaffected by air, moisture and most corrosive reagents. Common oxidation states of gold include +1 (gold(I) or aurous compounds) and +3 (gold(III) or auric compounds).[La05]

A gold single crystal with a (111) oriented surface was used as one of the substrates in this work. Although gold single crystal has a close packed fcc structure, its (111) surface undergoes the so called "herringbone" reconstruction, which is shown in Figure 2-2.[Mo07]
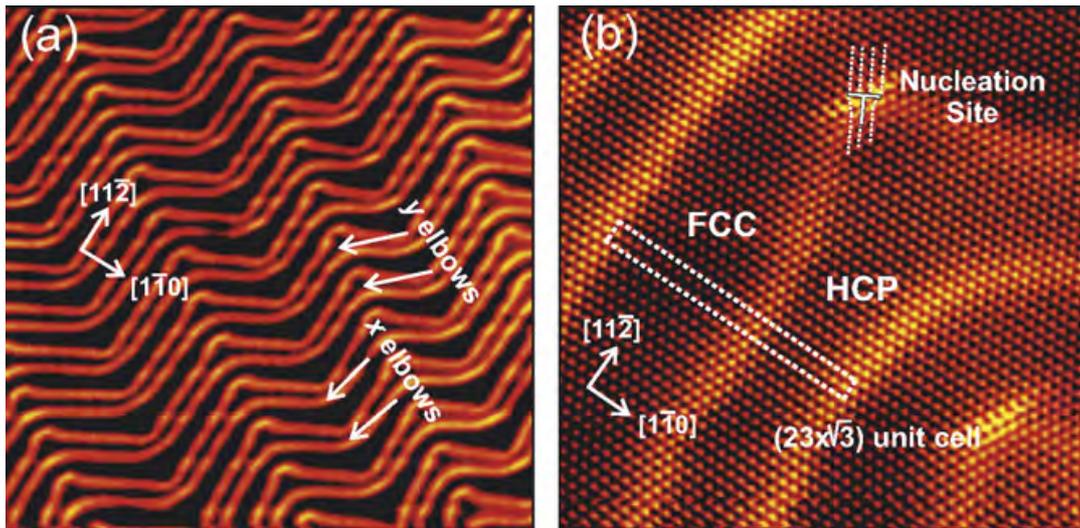
Figure 2-2. STM pictures of a Au(111) surface. (a) Overview on a large area (80.2 × 79.5 nm^2) (b) With atomic resolution (14.1 × 13.5 nm^2).[Mo07]

The Au(111) reconstruction consists of partial dislocation ridges resulting from the uniaxial 4.2% contraction along the [1$\bar{1}$0] directions, where there are 23 atoms for every 22 sites leading to a 23x$\sqrt{3}$ unit cell.[Ha85] [Wö89] [Ba90] These ridges result from atoms in bridge sites (at elevated positions) and separate regions where atoms are in the hollows sites of fcc and hcp stacking. The larger spacing between individual ridges corresponds to regions of fcc stacking (more energetically favored) while the narrower regions correspond to hcp stacking. On sufficiently large terraces the reconstruction forms a superstructure where the ridges alternate by 120° along [11$\bar{2}$]

directions. The double ridges change orientation about every 280 nm. This leads to the herringbone structure.

2.3 Iron

Iron with the atomic symbol Fe has the atomic number 26 and belongs to the side group VIII of the periodic system. Its atomic radius is 124.1 pm and atomic weight is 55.845. Its melting point is 1808 K and boiling point is 3023 K. The electron configuration of iron is [Ar] $3d^6 4s^2$ at ground state.[La05]

Fresh iron surfaces are lustrous and silvery-grey in color, but oxidise in air to form a red or brown coating of ferrous oxide or rust. Iron as Fe^{2+} (ferrous ion) is a necessary trace element used by almost all living organisms. Iron-containing enzymes, usually containing heme prosthetic groups, participate in catalysis of oxidation reactions in biology, and in transport of a number of soluble gases.[La05]

Iron has a diverse redox chemistry, which is primarily due to the easily accessible and convertible oxidation states +2 and +3 ($\varepsilon_0(Fe^{2+} / Fe^{3+}) = + 0.771$ V). There also exist other oxidation states from -2 to +6, but they are rather insignificant compared with the oxidation stages +2 and +3.[La05]

In this thesis iron was used as metalation agent for metal-free porphyrin and phthalocyanine molecules.

2.4 Porphyrins and metalloporphyrins

Adsorbed thin layers of porphyrins and metalloporphyrins on a well-defined metal surface are the main objects studied in this thesis.

Porphyrins are a group of chemical compounds of which many occur in nature, such as in green leaves and red blood cells, and in bio-inspired synthetic catalysts and devices. They are heterocyclic macrocycles characterised by the presence of four modified pyrrole subunits interconnected at their α carbon atoms with methine bridges (=CH-). Porphyrins are aromatic; therefore, the macrocycle is a highly-conjugated system. It has 26 π electrons. The parent porphyrin is porphine, whose structure is shown in Figure 2-3. Substituted porphines are called porphyrins.
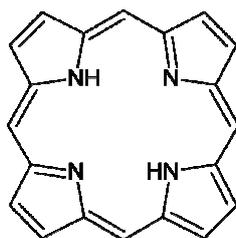
Figure 2-3. Structure of porphine (the simplest porphyrin).

Porphyrins bind metals to form complexes. Most metals can be inserted into the metal-free porphyrins to form metalloporphyrins. If the metalation reaction happens in solution, metalloporphyrins are formed with the loss of two protons. A schematic equation for the synthese in solution is shown as:

$$H_2\text{porphyrin} + [ML_n]^{2+} \rightarrow M(\text{porphyrinate})L_{n-4} + 4\,L + 2\,H^+$$

If the metalation reaction happens in vacuum, as will be described in Chapter 5, metalloporphyrins are produced with the loss of dihydrogen.

A porphyrin in which no metal is inserted in its cavity is sometimes called a *free base*. Some iron-containing porphyrins are called hemes. Heme-containing proteins, or hemoproteins, are found extensively in nature, e.g., hemoglobin and myoglobin are two O_2-binding proteins that contain iron porphyrins.

2.5 Phthalocyanines and metallophthalocyanines

Other objects for the research in this thesis are adsorbed thin layers of phthalocyanines and metallophthalocyanines on a well-defined metal surface.

A phthalocyanine is a macrocyclic compound having an alternating nitrogen atom-carbon atom ring structure. The structure of a phthalocyanine molecule is closely related to that of the naturally occurring porphyrin systems. The relation of the phthalocyanine with the porphyrin macrocycle is shown in Figure 2-4. Similar to porphyrins, phthalocyanine molecules are able to coordinate metal cations in their centers by coordinate bonds with the four central nitrogen atoms, forming metallophthalocyanines. The central metal ion of a metallophthalocyanine molecule can carry additional ligands. Most of the elements are able to coordinate to the phthalocyanine macrocycle. Therefore, a variety of phthalocyanine complexes exists.
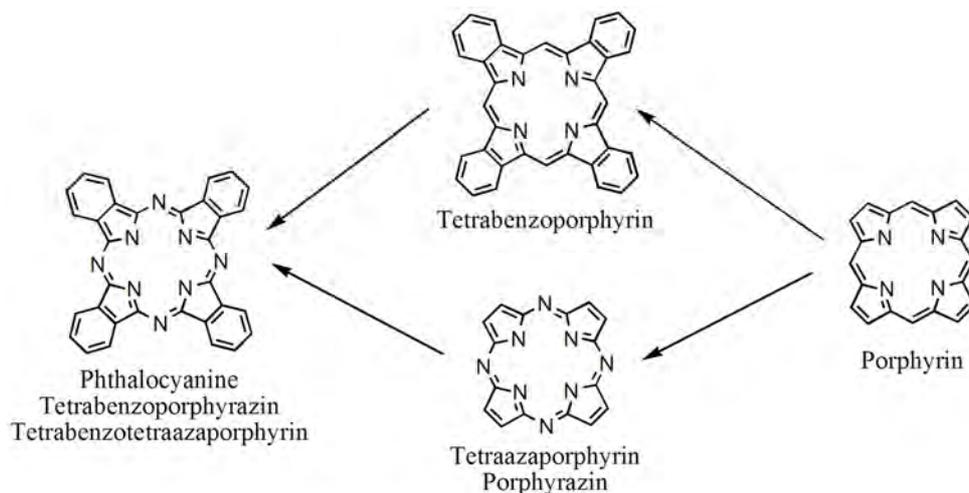
Figure 2-4. Relationship between phthalocyanine and porphyrin macrocycles

2.6. Oxygen

Due to the low-coordinated nature of the metal center in a metalloporphyrin or metallophthalocyanine molecule adsorbed on a surface, it is possible to attach a small molecule to the metal center, which enables the application of such systems in catalysis and as gas sensors, or simply for gas transportation. A natural example is the transportation of dioxygen in the blood of mammals with haemoglobin. In this thesis oxygen was attached to the FeTPP molecules on Ag(111) surface to mimic the attachment of dioxygen to hemoglobin molecules.

Oxygen has the atomic number 8 with the atomic symbol O, and belongs to the chalcogen group on the periodic table. Oxygen gas is colorless, tasteless and odorless. It reacts readily with almost all other elements. Oxygen is the most abundant element by mass in the earth's crust. Diatomic oxygen gas constitutes 20.9% of the volume of air. It is essential for most of the life-form on earth, and also plays an important role in industry. [La05]

2.7 Carbon monoxide

The molecule carbon monoxide contains one carbon atom and one oxygen atom. It is a highly toxic gas to human beings and animals, although it is colorless and odorless. In the human body it combines with hemoglobin to produce carboxyhemoglobin, which is ineffective for delivering oxygen to bodily tissues, thus causes poisoning even with a concentrations as low as 100 ppm[Prockop, 2007]. Despite its high toxicity, carbon monoxide is widely used in industry in chemical manufacturing, such as the production of aldehydes and acetic acid, etc.

3. Research methods and facilities

3.1. Photoelectron spectroscopy (PES)

When a photon impinges on a substance, its energy can be transferred to an electron in that substance, causing the electron to be emitted. This effect is called the photoeffect (or photoelectric effect), and the electron emitted in this manner is called photoelectron. Photoelectrons can be produced by irradiation with X-rays, ultra-violet (UV) light, laser, etc. Photoelectron spectroscopy (sometimes also called photoemission spectroscopy) refers to the energy measurement of the emitted electrons generated via photoeffect. In this thesis two types of photoelectron spectroscopy have been used, which are X-ray photoelectron spectroscopy (XPS) and UV photoelectron spectroscopy (UPS).

3.1.1. The general principles of photoelectron spectroscopy

Figure 3-1 shows a schematic diagram of the photoeffect. Photoemission takes place when photons with energy $h\nu$ impinge on a sample, causing the electrons in the sample to be emitted with kinetic energy E_k^S given by Equation 3.1:

$$E_k^S = h\nu - E_b^F - \phi_S, \tag{3.1}$$

where $h\nu$ is the energy of the incident photon, E_b^F is the binding energy (relative to the Fermi level) of the atomic orbital from which the electron originates, and ϕ_S is the work function of the sample. A photoelectron spectrum is obtained as a plot with the number of detected electrons per energy interval (intensity) versus their kinetic energy.
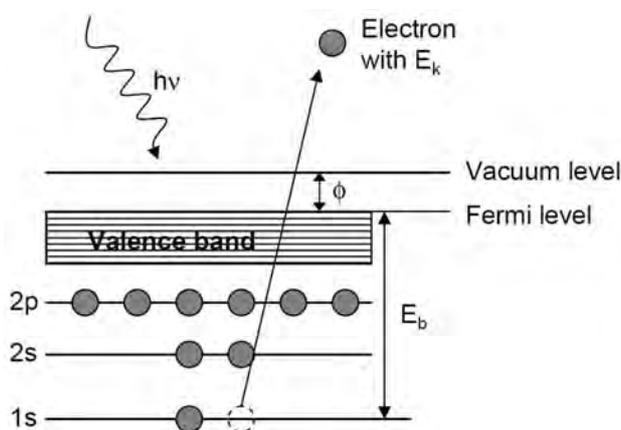
Figure 3-1. The principle of PES

3.1.2 X-ray Photoelectron spectroscopy (XPS)

X-ray photoelectron spectroscopy (XPS), sometimes also called ESCA (Electron Spectroscopy for Chemical Analysis), is a type of photoelectron spectroscopy in which the photons are X-rays. It is the essential method used for the research project in this thesis. It was developed in the mid-1960s by Kai Siegbahn and his research group at the Uppsala University, Sweden.

In XPS usually monoenergetic X-rays are used as probe, which can be Mg K_α (1253.6 eV), Al K_α (1486.6 eV) X-ray, or synchrotron radiation. Although the X-ray photons have penetrating depth in a solid on the order of 1-10 micrometers, the detected electrons only originate from a depth in the range of 0-10 nm, because the inelastic mean free path (IMFP) of electrons in solids is very small. Figure 3-2 shows the universal IMFP curve for electrons with different kinetic energies, based on the experimental data for various materials[Se79] As can be seen on the curve, the mean free paths are very high at low energies, fall to 0.1-0.8 nm for energies in the range 30-100 eV and then rise again as the energy increases further.[Se79] This makes XPS a unique surface-sensitive technique for chemical analysis.
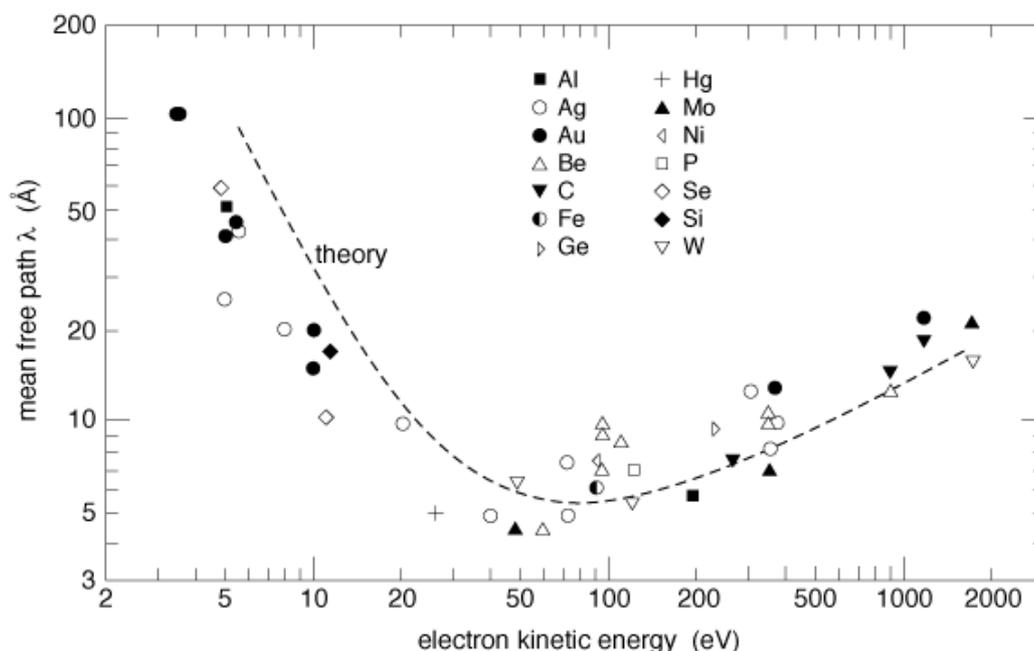
Figure 3-2. Universal curve of the inelastic mean free path (IMFP) for electrons, based on experimental data for various materials.[Se79]

In an XPS measurement one can improve the surface sensitivity by increasing the detection angle ϑ. The relation between the information depth d' of the measurement and the inelastic mean freen path d of the electrons in the material is given by d´= d ×

cos ϑ. As ϑ increased, d' decreases, thus the surface sensitivity is improved. This effect is illustrated in Figure 3-3.
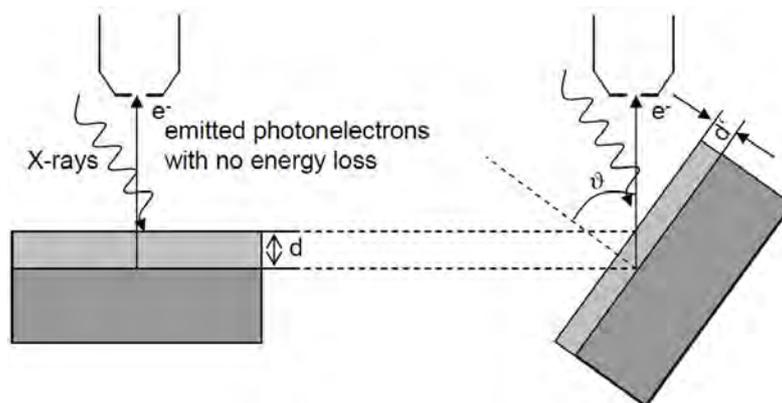
Figure 3-3. Dependence of the information depth d´ on the detection angle ϑ in XPS. The information depth d´ of the measurement decreases as the detection angle increases, thus the measurement becomes more surface sensitive.

While the kinetic energy of the emitted electrons varies with the energy of the incoming X-rays, the binding energy stays unchanged for electrons from a certain element in a certain chemical state. Therefore an XPS spectrum is conventionally plotted with the intensities of the emitted electrons versus their binding energies, which can be obtained from the alternative form of Equation 3.1:

$$E_b{}^F = h\nu - E_k{}^S - \phi_s \qquad (3.2)$$

Because each element has a unique set of binding energies, XPS can be used to identify and determine the concentration of the elements in the surface region. In the practical application, it is inconvenient to use the work function of the sample since for each sample the work function has a specific value. Therefore, the sample is usually conductively connected to the analyser, whose work function ϕ_A is fixed, and the kinetic energy of the electrons ($E_k{}^A$) is measured according to the vacuum level of the analyser, i.e.,

$$E_b{}^F = h\nu - E_k{}^A - \phi_A \qquad (3.3)$$

An XP spectrum is formed by electrons which leave the surface without energy loss, while the electrons that undergo inelastic loss processes before emerging from the surface form the background.

Variations in the binding energies for a certain core level arise from different effects, which can be divided into two groups, namely initial and final state effects. The initial state effects describe the phenomena independent on the photoemission event. For instance, the total charge that an electron experiences depends on the neighbouring atoms, both intermolecular and intramolecular. An example of the intermolecular case is the influence of the substrate on the adsorbed molecule. For example, in this thesis, the Ag substrate can cause a binding energy shift around 2.0 eV of the central Co ion

10

in a Co(II) porphyrin monolayer compared with a multilayer (for more details see Chapter 5), this is partially due to the change transfer from the Ag substrate to the Co ion. An example for the intramolecular influence is the different binding energies for iminic and pyrrolic nitrogen atoms in a metal-free porphyrin (for more details see Chapters 5 and 6).

If changes of the binding energy happen during the emission of the photoelectron, it is called final state effect. The loss of a core electron leads to relatively increased nuclear charge to the valence electrons. Under this influence the valence electrons undergo relaxation processes. The relaxation energy leads to an increase of the kinetic energy of the photoelectrons. Relaxation processes includes intra-atomic effects (effects on electrons from the ionized atom itself) and extra-atomic effects (effects on electrons from surrounding atoms or from the valence band). The extra-atomic relaxation processes can be further divided into intra-molecular effects (effects on electrons from the molecule from which the photoelectron is emitted) and extra-molecular effects (effects on electrons from other molecules). Another effect is the excitation of one valence electron to a higher unfilled energy level, which is referred to "shake-up".[Br90] The energy required for this process leads to reduced kinetic energy of the primary photoelectrons and leads to the discrete structure on the high binding energy side of the photoelectron peak, the shake-up satellite(s) structures. If the valence electrons are completely ionized, i.e. excited to an unbound continuum state, this process is called "shake-off", which leaves an ion with vacancies in both the core level and a valence level.[Br90] Another final state effect is that initially unoccupied valence orbitals of a metal can be lowered beneath the Fermi level by Coulomb attraction of the core hole in the photoion and consequently be occupied by electrons from the Fermi sea. This concept was first suggested by Gunnarson and Schönhammer,[Gu78] and is applied to explain satellite structures in metal atom XP spectra in this thesis, for more details see Chapters 5 and 6. According to the Gunnarson-Schöhammer model, the peak at lowest binding energy position in a XP spectrum usually corresponds to most efficiently screened core holes, while the satellites at higher binding energies result from less efficiently screened core holes.

The electrons leaving the sample are analyzed by an electron spectrometer according to the distribution of their kinetic energy. The analyzer is usually operated as an energy window (varying with the pass energy), which accepts only those electrons having energy within the range of this window. To maintain a constant energy resolution, the pass energy is fixed. Incoming electrons are adjusted to the pass energy before entering the energy analyzer. Scanning for different energies is accomplished by applying a variable electrostatic field (electronic lenses) before the energy analyzer. Electrons are detected as discrete events, and the number of electrons for a given detection time and a given energy is stored by the software and after a sweep of the electrons with all different energies in a desired energy range, the

stored data are displayed as an XP spectrum. For better statistics, this sweep procedure is usually repeated until a good quality of the spectrum is obtained. The final spectrum is then the sum of all the sweeps.

For quantitative analysis of the XP spectra, it is necessary to describe the photoemission lines by model functions, since the intensities of overlapping contributions can only be determined by fitting the XP spectra with such functions. In simple cases, the width of a line contains the experimental broadening of the spectrum together with the natural line width. The former includes the line width of the photos and the resolution of the electron energy analyser, and is usually described by a Gaussian function. The natural line width results from the lifetime of the excited state and leads to a line shape which can be described by a Lorentz function. More details about the fittings are described in Section 4.7.

3.1.3. Quantitative analysis for XPS

The photoelectron intensity of core levels can be employed as a way to determine the concentration of an element in a sample. However, the absolute intensity from the experiment cannot be directly compared for different elements or for different core levels of the same element, because the probability P for the excitation of an electron from a particular state to vacuum, the cross section, is different for the different transition, which directly influences the intensity. To calculate the cross section, the time-dependent perturbation theory is used, which leads to Fermi's golden rule.

Fermi's golden rule

In quantum physics, Fermi's golden rule is a way to calculate the transition rate (probability of a transition per unit time) from a certain energy eigenstate of a quantum system into a continuum of energy eigenstates, due to a perturbation. In general conceptual terms, a transition rate depends on the strength of the coupling between the initial and final state of a system and upon the number of ways the transition can happen (i.e., the density of the final states). Assume the system is described by a Hamiltonian H, the time dependent Schrödinger Equation can be written as:

$$(H_0 + H')\psi = i\hbar \frac{\partial \psi}{\partial t}\psi \tag{3.4}$$

where H_0 is the unperturbed Hamiltonian, for which the eigenfunctions ψ_n are known, and H' is the time-dependent perturbation. The eigenfunctions satisfy $H_0\psi_n = E_n\psi_n = \hbar\omega_n\psi_n$, with $\langle\psi_a|\psi_b\rangle = \delta_{ab}$. With the assumption that the perturbation

H' is small, the wave function for the perturbed case can be expanded in a series of the orthonormal wave functions of the unperturbed case:

$$\psi(t) = \sum_n c_n(t)\psi_n e^{-i\omega_n t} \tag{3.5}$$

With the solution of the unperturbed case:

$$H_0\psi_n = \hbar\omega_n\psi_n, \text{ with } \langle\psi_a|\psi_b\rangle = \delta_{ab}, \tag{3.6}$$

one obtains:

$$i\hbar\frac{dc_k(t)}{dt} = \sum_n H'_{kn}c_n(t)e^{i\omega_{kn}t}, \tag{3.7}$$

where $H'_{kn} \equiv \langle\psi_k|H'(t)|\psi_n\rangle$ and $\omega_{kn} \equiv \omega_k - \omega_n$. \hfill (3.8)

H'_{kn} is often called the matrix-element or transition amplitude, which connects the states $k \rightarrow m$. Equation 3.7 is equivalent to the Schrödinger equation, but is expressed in terms of the coefficients $c_n(t)$.

In problems involving a continuum of states, equation (3.7) is generally solved approximately by a "perturbation expansion." The order-(p + 1) approximation is found from the order-(p) solution by

$$i\hbar\frac{d}{dt}c_k^{(p+1)}(t) \approx \sum_n H'_{kn}c_n^{(p)}(t)e^{i\omega_{kn}t}, \tag{3.9}$$

with the "0-th"-order approximation $dc_k^{(0)}(t)/dt = 0$, which implies that $c_k^{(0)}$ is constant and no transitions occur.

As a first approximation, the system is assumed to be initially in the state m, in which case, $c_n^{(0)}(t) = \delta_{nm}$, and Equation 3.9 can be integrated to give

$$i\hbar c_k^{(1)}(t) = \int_{-\infty}^{t} dt' H'_{km}(t')e^{i\omega_{km}t'}. \tag{3.10}$$

Next, it is assumed the perturbation H' is turned on at $t = 0$ and is constant over the interval $0 \leq t' \leq t$, Equation 3.9 can be integrated to give

$$i\hbar c_k^{(1)}(t) \approx 2H'_{km}e^{i\omega_{km}t/2}\left(\frac{\sin\omega_{km}t/2}{\omega_{km}}\right). \tag{3.11}$$

For our purpose, the perturbation expansion is stopped after the first order term. The transition probability from state m to state k is

$$P_k(t) = |c_n(t)|^2 = \frac{4|H'_{km}|^2}{\hbar^2}\frac{\sin^2(\frac{\omega_{km}t}{2})}{\omega_{km}^2}. \tag{3.12}$$

The transition probability per unit time, the transition rate, is then

$$w_k = \frac{P_k(t)}{t} = \frac{4|H'_{km}|^2}{\hbar^2}\frac{\sin^2(\frac{\omega_{km}t}{2})}{\omega_{km}^2 t}. \tag{3.13}$$

For times t $\rightarrow \infty$, which are long enough such that the scattering process has been completed, the function $\dfrac{\sin^2(\dfrac{\omega t}{2})}{\omega^2 t}$ has the property of a δ-function, meaning

$$f(\omega,t) = \frac{\pi}{2}\delta(\omega)\text{, which gives } \int_{-\infty}^{\infty} d\omega \frac{\sin^2(\dfrac{\omega_{km}t}{2})}{\omega_{km}^2 t} = \frac{\pi}{2}. \tag{3.14}$$

Because the strongest intensity for $f(\omega,t)$ appears at $\omega = 0$, Equation 3.12 requires that states to which transitions can occur must have $\omega_{km} \approx 0$, forcing energy conservation. In general, there will be some number of states d_n within an interval $d\omega_{km}$. The number of possible transition states can be written as:

$dn = \rho(k)\ dE_k$ with $dE_k = \hbar d\omega_{km}$, where $\rho(k)$ is the density of states per unit energy interval near E_k. For the total transition rate to states near the state k, one has:

$$w_k = \frac{1}{t}\sum_{k'\,near\,k}P_{k'}(t) = \frac{1}{t}\int P_{k'}(t)\rho(k')dE_{k'} = \int dE_k \rho(k)\frac{4|H'_{km}|^2}{\hbar^2}(\frac{\sin^2 \omega_{km}t/2}{\omega_{km}^2 t})$$

$$= \frac{4}{\hbar}|H'_{km}|^2 \rho(k)\int_{-\infty}^{\infty} d\omega \frac{\sin^2 \omega t/2}{\omega^2 t}\text{, together with Equation 3.14, one obtains the so}$$

called Fermi's Golden Rule:

$$w_k = \frac{2\pi}{\hbar}|H'_{km}|^2 \rho(k) \tag{3.15}$$

Photoelectric cross section

In photoelectric process, the probability per unit area, per unit time that a photon of a given energy can be absorbed by an atom to excite the photoelectrons is defined as the photoelectric cross section. It is an imaginary area representing the fraction of incoming photons that will be absorbed in the photoelectric process. By this definition, the photoelectric cross section is written as

$$\sigma = \frac{n}{j_i}, \tag{3.16}$$

where n is the number of photons adsorbed per unit time and j_i is the incident photoflux($j_i = \dfrac{A_0^2 \omega}{8\pi\hbar c}$). σ has the unit barn (10^{-24} cm^2) or megabarn (10^{-18} cm^2).

According to Fermi's golden rule, the transition probability P_{if} under a time dependent perturbation $H' = H_0 exp(-i\omega t)$ is given by:

$$P_{if} = \frac{2\pi}{-h}|\langle f|H'|i\rangle|^2, \tag{3.17}$$

with $H' = \dfrac{e}{mc}\vec{A}\cdot\vec{p}$, where $\vec{A}$ is the vector potential of the electromagnetic field

($\vec{A} = \dfrac{A_0}{2}(e^{i(\vec{k}\cdot\vec{x}-\omega t)} + e^{-i(\vec{k}\cdot\vec{x}-\omega t)})\hat{e}$, which describes a plane wave with the unit vector $\hat{e}$),

e is the elementary change, c is the speed of light, and $\vec{p}$ is the momentum operator.

Together with the definition of σ and j_i, one obtains the photoelectric cross section σ:

$$\sigma = \frac{4\pi^2 e^2}{m^2 c\omega}\left|\left\langle f\left|e^{i(\vec{k}\cdot\vec{x})}\hat{e}\cdot\vec{p}\right|i\right\rangle\right|^2 \delta(\hbar\omega + E_i - E_f) .\tag{3.18}$$

Damping effect

Another parameter influencing the intensity is the mean free path of electrons in solids. Electrons from deeper layers will be inelastically scattered by the overlying material, which attenuates the resulting signal. Since the amount of the overlying material, i.e. the thickness, varies with the experiment, for instance, by changing the thickness of the adsorbate, this can not be determined by reference measurements, but must be quantified. Thus in an ideal homogeneous solid for total intensity:

$$I_{ges} = \sum_{n=0}^{\infty} I_0 e^{-\frac{nd}{\lambda\cos\theta}} ,\tag{3.19}$$

where I_0 is the intensity without damping, n is the number of layers, d is the distance between two adjacent layers, λ is the mean free path of the electrons and θ is the emission angle. If the system has a total thickness D, one obtains following relation for the intensity:

$$\sum_{n=0}^{D/d} e^{-\frac{nd}{\lambda\cos\theta}} = \frac{1 - e^{-\frac{D}{\lambda\cos\theta}}}{1 - e^{-\frac{d}{\lambda\cos\theta}}} .\tag{3.20}$$

Under the assumption $D \rightarrow \infty$:

$$\sum_{n=0}^{\infty} e^{-\frac{nd}{\lambda\cos\theta}} = \frac{1}{1 - e^{-\frac{d}{\lambda\cos\theta}}} ,\tag{3.21}$$

one acquires the damping factor:

$$\frac{I}{I_0} = 1 - e^{-\frac{d}{\lambda\cos\theta}}\tag{3.22}$$

Other effects

In addition to cross section and damping effect, the intensity and the number of detected electrons also depends on other parameters, which are technical in nature. They depend on the type of equipment, the applied devices and the experimental setup, e.g., sensitivity, angle acceptance, transmission function of the analyzer, detection angle ϑ and intensity of the photon flux. Such influences can be taken into

account with reference measurements, since they do not change and can be considered as constant factor in the intensity. Usually the overall relative intensities are compared rather than absolute ones, which means that only the intensities of spectra measured with the same apparatus can be compared directly.

3.1.4. UV photoelectron spectroscopy (UPS)

UV-photoelectron spectroscopy (UPS) was introduced in the early 1960s. It was also inspired by the photoelectric effect. Due to the relatively low energy of the UV radiation (He I: 21.22 eV and He II 40.81 eV) it is applied to investigate the valence electronic structure of materials. Since the valence orbitals are responsible for the formation of chemical bonds, UV-photoelectron spectroscopy is particularly suitable for the study of electronic structure of adsorbed molecules at surfaces. Thus one can identify the adsorbed compounds by their "fingerprints", as well as obtain information about the type of adsorption (chemi-/physisorption) and about the orbitals involved in the bond. For an unambiguous assignment of UPS signals, it is often necessary to do quantum chemical calculations. Unlike XPS, UPS is not a quantitative method, because at low photon energies the cross sections for different energy levels vary greatly. Furthermore, the low kinetic energies lead to diffraction effects of the electrons. In this thesis, UPS is used to study the valence structure of the adsorbate by comparison of the molecular orbitals of the adsorbed species with those of both the isolated molecule and with calculations. In our system the resolution is limited by resolution of the analyzer and the life time of the photoelectrons.

Determination of work function

Further information, which can be obtained from UP spectra, includes the work function ϕ_S of the sample. For this purpose the energy difference ΔE between the secondary electron cut-off (the minimal kinetic energy of photoelectrons $E^A_{kin, min}$) and the energy of the UV light source (the maximum kinetic energy $E^A_{kin, max}$) are needed, as shown in Figure 3-4:
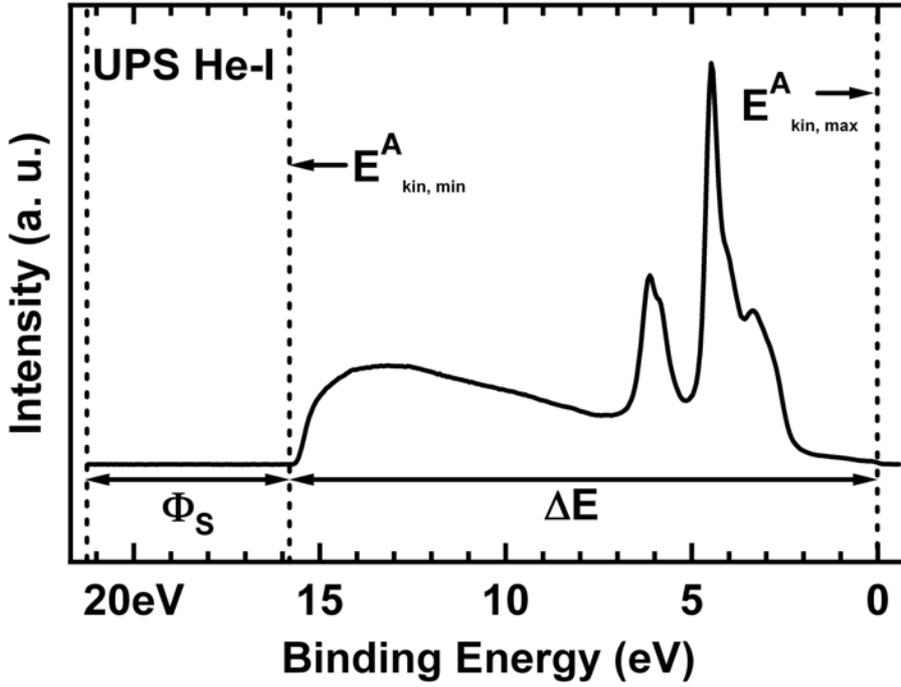
Figure 3-4. UP spectrum of a clean Au(111) surface. The work function is given by the difference between the energy of the incident UV light and ΔE, which is the energy difference between secondary electron cut off and the Fermi edge.

$$\Delta E = E^A_{kin,max} - E^A_{kin,min} \qquad (3.23)$$

Since electrons at the Fermi edge have zero binding energy ($E_b^F = 0$),

$$E^A_{kin,max} = h\nu - \Phi_A, \qquad (3.24)$$

From equations 3.2 and 3.3, one obtains

$$E^A_{kin,min} + \Phi_A = h\nu - E^F_{B,min} = E^S_{kin,min} + \Phi_S . \qquad (3.25)$$

since $E^S_{kin,min} = 0$, $E^A_{kin,min} = \Phi_S - \Phi_A,$ (3.26)

with equation 3.23, one has

$$\Delta E = E^A_{kin,max} - E^A_{kin,min} = h\nu - \Phi_A + \Phi_A - \Phi_S = h\nu - \Phi_S, \qquad (3.27)$$

thus $\Phi_S = h\nu - \Delta E.$ (3.28)

Adsorbate-induced work function changes

Adsorbates usually induce change of the work function, which can be interpreted both electrostatically and quantum mechanically.

Electrostatically, Langmuir's model for adsorbed monolayer on solid substrate can be applied to interpret the adsorbate-induced work function changes. The attractive forces holding adsorbed molecules on surfaces are ordinarily far stronger than those acting among the adsorbed molecules and thus the adsorbed molecules will usually be highly polarized so that they become dipoles having parallel orientations

17

perpendicular to the surface.[La32] The formation of dipole layers upon adsorption results in changes of work function $\Delta\phi$, which is given by the Helmholtz equation:

$$\Delta\phi = \frac{\mu_0\theta}{\varepsilon_0},$$ (3.29)

Here μ_0 is the dipole moment of the adsorbate-substrate complex, and θ is the absolute coverage. If one assumes that μ_0 is independent on θ, the work function change $\Delta\phi$ should be proportional to θ. However, according to the experimental observation, there is a non-linear relationship between coverage and work function change, i.e., the work function changes less and less with increasing coverage. The explanation for this contradiction is that the assumed individual dipoles are mutually depolarized by the Coulomb field of all surrounding dipoles. The work function change is then modified according to the Topping model [To27]:

$$\Delta\phi = \frac{\mu_0\theta}{\varepsilon_0(1+9\alpha\theta^{3/2})},$$ (3.30)

where α is the polarizability of the adsorbate-substrate complex. Hereby one can obtain information of adsorbate-substrate systems: on the one hand, one can distinguish between mono- and multilayer adsorption; on the other hand, one can also compare different adsorbates and can possibly characterize chemical behaviour of the adsorbates qualitatively.

A quantum-mechanical model has also been developed, which was suggested by Gurney [Gu35]. Here it will not be explained in detail.

3.2. Low-energy electron diffraction (LEED)

LEED is a technique for the determination of the surface structure of crystalline materials by bombardment with a collimated beam of low energy electrons (20-200eV) and observation of diffracted electrons as spots on a florescent screen. Figure 3-5 shows the simplified sketch of LEED setup.
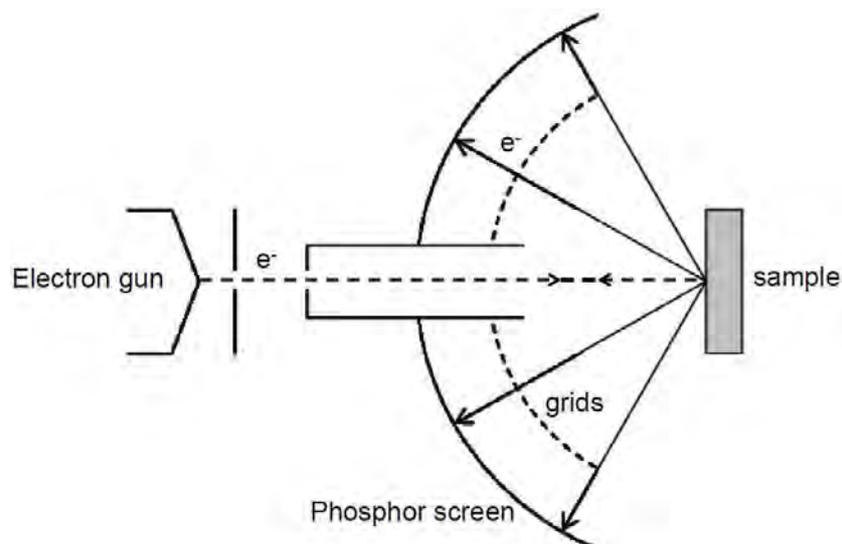
Figure 3-5. Simplified sketch of an LEED setup

Monochromatic electrons are emitted by a cathode filament and then are accelerated and focused into a beam. Some of the electrons incident on the sample surface are backscattered elastically, and diffraction can be detected if the surface is well ordered. LEED is a surface sensitive technique, because the inelastic mean free path of the elastically scattered electrons is only a few angstroms, thus only a few atomic layers are detected by the electron beam, and the contribution of deeper atoms to the diffraction progressively decreases.

3.2.1. Principle of LEED

By the principles of wave-particle duality, the beam of electrons may be equally regarded as electron waves. These waves can be scattered by the surface atoms. The wavelength of the electrons is given by the de Broglie relation $\lambda = h /(mv)$:

$\lambda \approx \sqrt{150 / E_{kin}}$, with E_{kin} in eV and λ in Å.

For instance, electrons with E_{kin} = 100 eV have wavelength 1.22 Å, which is comparable with atomic spacings. This is the necessary condition to observe diffraction effects associated with atomic structures.

The interaction between the scatterers present in the surface and the incident electrons is most conveniently described in reciprocal space. Due to the very short mean free path of electrons, with first principle approximation there are no diffraction conditions in the direction perpendicular to the sample surface. As a consequence the reciprocal lattice of a surface is a 2D lattice with rods extending perpendicular from each lattice point. The rods can be pictured as regions where the reciprocal lattice

points are infinitely dense. Therefore, in the case of diffraction from a surface the reciprocal lattice is two-dimensional, and the primitive reciprocal lattice vectors $\vec{a_1^*}$, $\vec{a_2^*}$ are related to the real space lattice vectors $\vec{a_1}$, $\vec{a_2}$ in the following way:

$$\vec{a_1} \cdot \vec{a_2^*} = \vec{a_1^*} \cdot \vec{a_2} = 0 \text{ and } \vec{a_1} \cdot \vec{a_1^*} = \vec{a_2} \cdot \vec{a_2^*} = 2\pi .$$

For an incident electron with the wave vector $\vec{k_0}$ and scattered wave vector $\vec{k}$ the condition for constructive interference and hence diffraction of scattered electron waves is given by the Laue condition
$$\vec{k} - \vec{k_0} = \vec{G_{hk}} ,$$
where (h, k) is a set of integers and $\vec{G_{hk}} = h\vec{a_1^*} + k\vec{a_2^*}$ is a vector of the reciprocal lattice. The magnitudes of the wave vectors are unchanged, i.e. $|\vec{k_0}| = |\vec{k}|$, since only elastic scattering is considered.

The Laue condition can readily be visualized using the Ewald's sphere construction. Figure 3-6 shows a simple illustration of this principle: The wave vector $\vec{k_0}$ of the incident electron beam is drawn such that it terminates at a reciprocal lattice point O. The Ewald's sphere is then the sphere with radius $|\vec{k_0}|$ and passing through the reciprocal lattice point O (Figure 3-6).
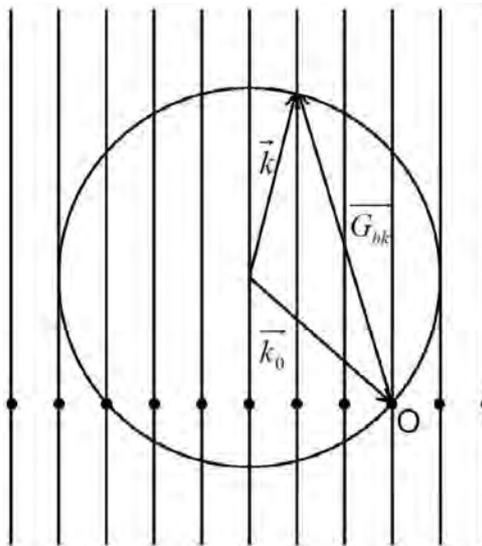
Figure 3-6. Construction of an Ewald's sphere for the case of diffraction from a 2D-lattice. The intersections between Ewald's sphere and reciprocal lattice rods define the allowed diffracted beams.

By constructing every wave vector $\vec{k}$ that terminats at an intersection between a rod and the sphere one can determine the allowed diffracted beams.

3.2.2 Determination of lattice constant of porphyrin monolayer with LEED

LEED patterns can be used to determine the long range order of adsorbed layers. For example, the lattice constant of a two-dimensional ordered porphyrin monolayer can be calculated with its LEED pattern. The principle is that for a given electron energy the ratio of lattice constant a_1^* of the reciprocal lattice of hexagonal Ag (111) surface and the distance d of the Ag reflexes from the 00-reflex in the LEED pattern is equal to the ratio of lattice constants b_1^* of the reciprocal porphyrin and distance d' of the porphyrin reflexes from the 00-reflex in the LEED pattern:

$$\frac{a_1^*}{d} \cdot \frac{[1/m]}{[mm]} = \frac{b_1^*}{d'} \cdot \frac{[1/m]}{[mm]} \tag{3.31}$$

$$b_1^*[1/m] = d'[mm] \cdot \frac{a_1^*}{d} \frac{[1/m]}{[mm]} \tag{3.32}$$

d ' can be directly read from the LEED picture of the porphyrin monolayer. Since the Ag reflexes for the low electron energies, with which the porphyrin layers were investigated, are outside the phosphor screen, the distance d is determined with a straight calibration line. For different acceleration voltages, the distance d between a certain silver reflex and the 00 reflex is measured and plotted versus $1/\sqrt{U}$. The extrapolation gives a straight line, with which the distance d can be determined for any voltage U. After introducing the values d, d', and a_1^* in **Equation 3.32**, one obtains b_1^* or the requested lattice constant b_1[m].

3.3. Synchrotron radiation and the X-ray standing wave technique

3.3.1. Synchrotron radiation

A synchrotron is a particular type of cyclic particle accelerator in which the magnetic field and the electric field are carefully synchronized with the travelling particle beam. The magnetic field is applied to circulate the particles, and the electric field is used to accelerate the particles. When high-energy relativistic charged particles are forced to travel in a curved path by a magnetic field, they lose energy to produce electromagnetic radiations, here synchrotron radiation. The radiation produced may range over the entire electromagnetic spectrum, from radio waves to infrared light, visible light, ultraviolet light, X-rays, and gamma rays. It is distinguished by its

characteristic polarization and spectrum. Synchrotron radiation was seen for the first time at General Electric in the USA in 1947. It was first considered to be a nuisance, because it caused the particles to lose energy. But it was then recognised in the 1960s as electromagnetic radiation with exceptional properties. Synchrotron radiation has a wide range of applications. Many 2nd and 3rd generation synchrotrons have been built especially to utilize it. Among the largest of those 3rd generation synchrotron light sources are the European Synchrotron Radiation Facility (ESRF) in Grenoble, France, the Advanced Photon Source (APS) near Chicago, USA, and SPring-8 in Japan, accelerating electrons up to 6, 7 and 8 GeV, respectively. Figure 3-7 is the simplified sketch of ESRF in Grenoble, France.
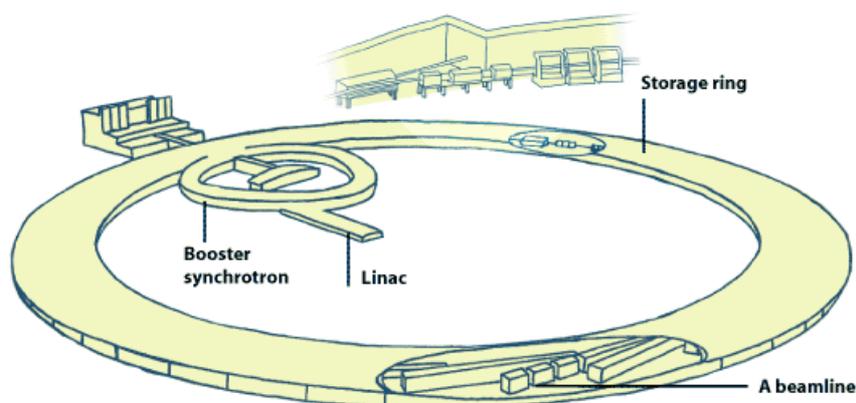
Figure 3-7. Simplified sketch of the European Synchrotron Radiation Facility (ESRF) in Grenoble, France. [ESRF]

At ESRF, electrons emitted by an electron gun are first accelerated in a linear accelerator (linac) and then transmitted to a circular accelerator (booster synchrotron) where they are accelerated to reach an energy of 6.03 GeV. These high-energy electrons are then injected into a large storage ring, 844 metres in circumference, where they circulate in UHV at a constant energy. The main parameters of the electron beam in the storage ring are summarised in Table 3-1. The storage ring includes both straight and curved sections [ESRF]. As they travel round the ring, the electrons pass through different types of magnets, which include bending magnets undulators and focusing magnets. Along the length of the undulators, the static magnetic field is alternating periodically. Electrons traversing the periodic magnet structure are forced to undergo oscillations and radiate synchrotron radiation. The focusing magnets, placed in the straight sections of the storage ring, are used to focus the electron beam on its orbit. The synchrotron beams emitted by the electrons are directed towards the "beamlines" which surround the storage ring in the experimental hall. Each beamline is designed for use with a specific technique or for a specific type of research. Each beamline includes an optics cabin, an experimental cabin and a control cabin. An optics cabin houses the optical systems used to tailor the X-ray

beam to have the desired experimental characteristics; an experimental cabin contains the support mechanism and sample environment for the sample to be studied. One or more detectors record the information produced as a result of the interactions between the X-ray beam and the sample; and a control cabin allows the researchers to control their experiments and to collect the data. XSW measurements in this thesis were performed at beamline ID32. It is suited for 2-25 keV experiments for surface and interface studies, including XRD, XPS, EXAFS and XSW, etc. Table 3-2 shows the source characteristics of beamline ID32[ESRF].

Table 3-1. Summary of the main parameters of the electron beam in the storage ring in ESRF

Energy	6.03 GeV
Maximum Current	200 mA
Horizontal Emittance	4 nm
Vertical Emittance (*minimum achieved)	0.025 (0.010*) nm
Coupling (*minimum achieved)	0.6 (0.25*) %
Revolution frequency	355 kHz
Number of bunches	1 to 992
Time between bunches	2816 to 2.82 ns

Table 3-2. Source characteristics of beamline ID32

Undulators

	1st undulator u35d	2nd undulator u35m	3rd undulator u42u
Magnet period	35 mm	35mm	42mm
K_{max}	2.3957	2.3246	3.2025
Filed B_{max}	2.08 T	2.01 T	1.95 T
Total power	1.8 kW at 0.2 A	1.8 kW at 0.2 A	3.2 kW at 0.2 A
Maximum power density at 30 m	90 Wmm^{-2}	90 Wmm^{-2}	90 Wmm^{-2}
Source size	0.900 x 0.02 mm^2		
Beam divergence	0.030 x 0.020 mrad^2		
Peak flux at 25 m	7.10 ^{14}ph s^{-1} mm^{-2}, 0.1% bw, 0.2 A		

Optics summary

At 30 m	Monochromator: Si(111) cooled with LN2 Independent second crystal.
At 41 m	Mirror: 450 mm long. 3 regions depending on photon energy used: SiO$_2$, Ni coated,

	Pd coated
Beam size at sample	2 x 1 mm^2 unfocussed
Spectral range	min E = 2.5 keV; max E ~ 30 keV
Resolution in ΔE/E	10^{-4} and better
Flux at sample	~10^{13} ph s^{-1} at low energy (10^{-4} bw, 0.1A) ~10^{12} ph s^{-1} at high energy (10^{-4} bw, 0.1 A)

3.3.2. The principle of the XSW technique

When an X-ray hits a single crystal substrate and the Bragg scattering condition is fulfilled, the incident and scattered X-ray interfere to generate a standing wave field with a spatial modulation of the associated scatterer plane spacing d_H. The intensity of this standing wave field for a particular atom changes in a characteristic way with its location relative to the scatterer planes through the reflectivity range. The atomic absorption is proportional to that intensity profile, which reaches its maximum value when the atomic absorber lies on the antinodes of the standing wave field. This means one can measure the X-ray absorption profile at an adsorbate atom and obtain the height of this atom (D_H) relative to the substrate scatterer plane locations. Thus XSW has become a powerful tool which can be used to precisely determine the vertical position of atoms in the adsorbate. Usually it is difficult to monitor X-ray absorption, but the phenomena induced by adsorption such as photoemission and emission of an X-ray or an Auger electron can be monitored without considerable difficulties. In this work all the absorption profiles refer to the X-ray photoemission.

In order to obtain the vertical position of an atom on the sample substrate with X-ray standing wave, the phase of the standing wave need to be shifted by $\dfrac{d_H}{2}$. This can be realized by changing the energy or the incident angle of the X-ray. Due to the fact that the rocking curve (reflectivity vs. incident angle) width is generally narrow, extreme conditions such as highly collimated beam are necessary, and perfect sample crystals are needed if the measurement is executed by changing the incident angle. To overcome this limitation one can work at near-normal incidence (fixed incident angle) to the relative scatterer planes H = (hkl) for a particular Bragg condition, and scan through this condition by varying the X-ray wavelength, i.e. the photon energy. Because the Bragg condition has a turning point at normal incidence, the gradient of the Bragg condition with respect to incident angle is zero at this condition. The condition is found to be very insensitive to the exact incidence angle and thus to finite mosaicity.

The atomic absorption I(E) can be calculated with dynamical diffraction theory. One obtains the adsorption intensity with the following equation

$$I(E) = 1 + R + 2\sqrt{R}F^H \cos(\Phi + 2\pi P^H),$$ (3.33)

where R = R(E) is the reflectivity, $\Phi = \Phi$ (E) is the phase of the standing wave field, P^H equals (D^H modulo d^H), i.e, $\dfrac{D^H}{d^H}$ = n + P^H (n = 0, 1, 2…) is the coherent position and F^H the coherent fraction. The parameters which contain the structural information are P^H and F^H. After fitting the measured adsorption profile one obtains the values for P^H and F^H.

For a same element, D^H is the average distance between the atoms on the adsorption sites and the Bragg planes for the reflection H = (hkl), and F^H is the contrast of the interference term that corresponds to the incoherent average of the contribution of all atoms to the absorption yield. In the case of equivalent adsorption F^H equals unity.

The parameters F^H and P^H can also be considered as the amplitude and phase of the H-Fourier component of the spatial distribution of an adsorbate. This interpretation allows a simple possibility to calculate the coherent position and fraction from an atomic model with several inequivalent adsorption sites for the same type of atoms. Every atom k that contributes to the absorption profile has a coherent fraction of F_k^H = 1 and an individual position P_k^H. The signal measured for such a multisite adsorption system can be described by the structural parameters P^H and F^H, which are calculated by averaging all these complex numbers,

$$F^H \exp(i2\pi P^H) = \sum_{K=1}^{N} \frac{F_K^H}{N} \exp(i2\pi P_k^H)$$

It is often convenient to present this complex quantity in polar coordinates (Argand diagram), where the absolute value (length of the vector) is the coherent fraction and the phase (angle of the vector with respect to the real axis) is the coherent position, i.e., a phase of 2π corresponds to the distance d_H.

Usually the so-called dipole approximation is applied for photoemission, which assumes that the variation of the electromagnetic field of the incident radiation over the spatial extent of the photoemission initial state wave function is small. Generally non-dipole effects have been taken into account only when "hard" X-rays (photon energies around 20-40 keV) are used. However, it has been shown that in the case of photoemission-monitored NIXSW experiments at photon energies around 3 keV non-dipole effects can be very significant. This is because non-dipole effects can substantially change the photoemission angular dependence (and thus the angular derivative cross-section) at much lower energies. One important fact is that they introduce a forward-backward asymmetry into the angular dependence relative to the photon propagation direction. In this case magnetic dipole and electronic quadrupole contributions to the photoelectron yield should be taken into account. For this purpose

non-dipolar parameters Q, Δ and $\Psi = \tan^{-1}(Q\tan\Delta)$ are introduced, which change Equation 3.33 to

$$I(E) = 1 + \frac{1+Q}{1-Q}R + 2\sqrt{R}F^{H}\frac{(1+Q^2\tan^2\Delta)^{1/2}}{1-Q}\times\cos(\Phi - \Psi + 2\pi P^{H}),\qquad(3.34)$$

where Q is the asymmetry parameter, Δ is the difference between the partial phase shift of the emitter atom potential for the outgoing electron p- and d-state waves arising from the electric dipole and electric quadrupole transitions from the initial s-state.

When the adsorbate forms a mutilayer in which the atoms for a same element are nonequivalently adsorbed on the substrate surface, the coherent fraction vanishes thus only the first two terms remain in Equation 3.34, which turns to

$$I(E) = 1 + \frac{1+Q}{1-Q}R\qquad(3.35)$$

The asymmetry parameter Q can then be easily obtained by comparing the intensities of adsorption and reflectivity.

4. Experimental

4.1. The vacuum system

Figure 4-1 shows the ultra-high vacuum system used for this thesis. It is based on a Gammadata Scienta AB ESCA-200 photoelectron spectrometer and has been modified to meet the requirements of the specific experiments over the past years. The base pressure in this UHV system is in the low 1×10^{-10} mbar range. The apparatus is composed of two main chambers, namely the preparation chamber and the analysis chamber, which are separated by a gate valve. The analysis chamber is pumped with one turbo molecular pump, two ion getter pumps and two titanium sublimation pumps. It is equipped with an Al-K_α X-ray source (1486.6 eV) for X-ray photoelectron spectroscopy (XPS), an X-ray monochromator, a differentially pumped gas discharge lamp (UVL-HI, Fisons) for UV photoelectron spectroscopy, and a hemispherical energy analyzer (SES-200). There is also an ion gun (IQE 12/38, Specs) for low energy ion scattering (LEIS) experiments. The preparation chamber contains a manipulator with one fixed sample and one transferable sample, which can be transferred into the chamber through the loadlock, a sputter gun (ISS-2000-A, VSI Vacuum Science Instruments GmbH), a LEED optics (ErLEED-1000A, VSI Vacuum Science Instruments GmbH), a quartz microbalance (STM-100/MF, Sycon Instruments), a quadrupole mass spectrometer (QMA 400, Pfeiffer Vacuum), an electronic metal evaporator (EFM3, Focus) and a Knudsen cell evaporator. The preparation chamber is pumped with one turbo molecular pump and one titanium sublimation pump. Additionally, the rotary feed through (DPRF55 Omniax, Fisons) on the manipulator is pumped with an ion getter pump, the loadlock is pumped with a turbo molecular pump and the Knudsen cell is pumped with another turbo molecular pump, which enables changing the substance without breaking the vacuum in the preparation chamber.
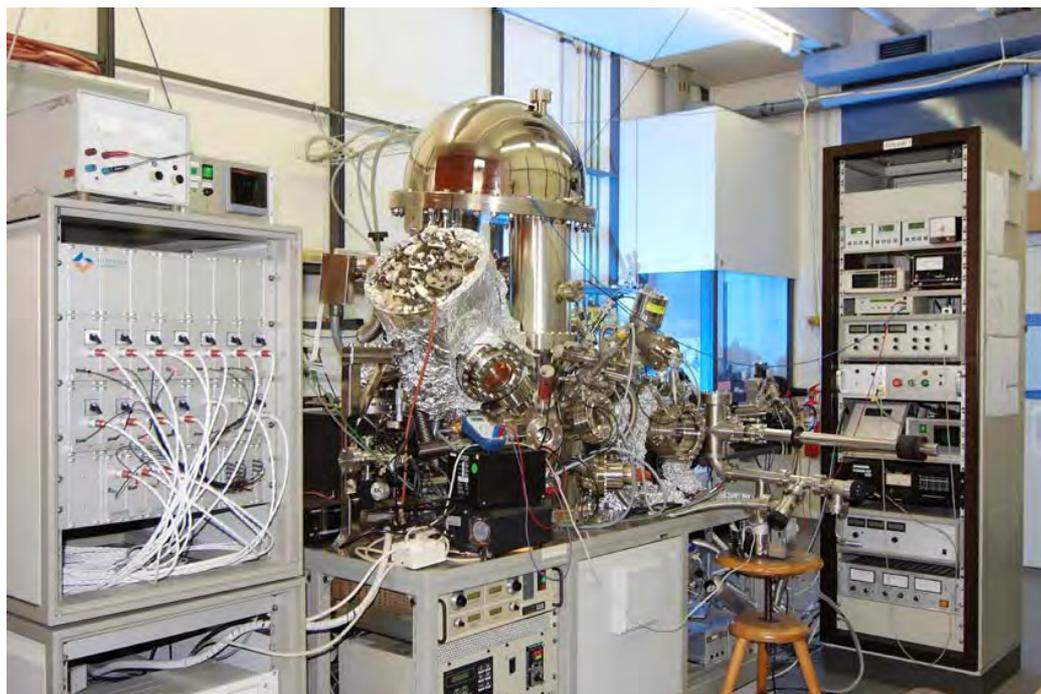
Figure 4-1. The ultra-high vacuum system used for the work in this thesis. In the middle is the hemispherical analyser with the analysis chamber beneath. Left to the analysis chamber is the X-ray monochromator, and right to the analysis chamber is the preparation chamber with the loadlock in front. The electronics on the right side are the control units of the sputter gun, metal evaporator, LEED optics, sample heater and turbo molecular pumps etc. The electronics on the left side are the control units of the hemispherical analyser.

4.2. Sample mounting

Permanently mounted samples, i.e., non-transferable Ag(111) and Au(111) single crystals in two different forms have been used. Figure 4-2 shows the two ways to mount the different samples on the manipulator. Figure 4-2 a) is the first sample which was embedded in a silver plated copper holder. The sample holder was fixed on the manipulator through the two molybdenum rods. A tungsten wire goes through the sample holder and works as filament for sample heating. Due to the large surface area and high heat capacity of the sample holder, this construction is less suitable for temperature programmed desorption (TPD) measurements. Figure 4-2 b) shows the second, later design in which the sample is also fixed on the manipulator with molybdenum rods. Two tungsten wires go through the sample and work as filaments for sample heating. This construction with very little material avoids disturbing desorption from the sample holder, thus is more suitable for TPD experiments. Cooling of the sample was realized with liquid nitrogen through the home-made cryostat, which is able to cool down the sample to temperatures below 120K.

a)

Side view

Horizontal cross section of the sample

Silver crystal with
(111) surface

sample

thermocouple

Tungsten wire

Silver plated copper

Tungsten wire

Molybdenum rod

b)

Tungsten wire

Polished surface

Molybdenum rod

Hole for thermocouple
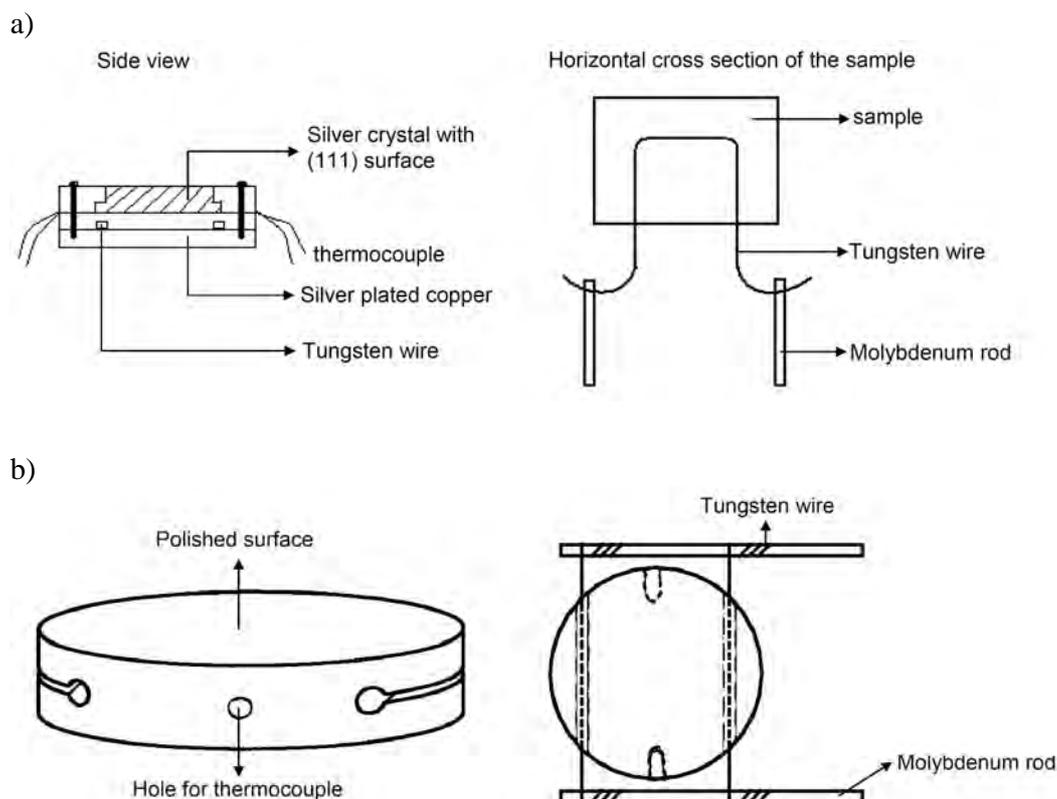
Figure 4-2. Side view and the horizontal cross Section of the fixed samples a) the first square sample, and b) the second round sample

4.3. Sample preparation

Sample preparation includes the cleaning of the substrate surface and the preparation of the adsorbed layers of the tetrapyrrole complexes (porphyrins and phthalocyanines). The preparation procedures will be explained in the following.

4.3.1. Cleaning of the substrates

The substrates used in the work are a Ag single crystal and a Au single crystal (purity > 99.999 %, purchased from *Surface Preparation Laboratory,* DE Zaandam, The Netherlands) with polished (111) surfaces, which are aligned to <0.1° with respect to the nominal orientation. Before preparation of the adsorbed tetrapyrrole layers, the substrate surface was cleaned to remove contaminations. This was realized by sputtering with Ar^+ ions in the preparation chamber with a voltage between 500-1000 V, for 30 to 60 min. During the sputtering process, the sample drain current is about - 2 to -3 µA. The sputtering process produces defects on the sample surface; therefore

after sputtering the sample is annealed for 5 min at 800 K for Ag(111), and 5 min at 850 K for Au(111) to recover the surface structure. After the sputtering and annealing process, sample cleanliness was checked with XPS, and formation of well-defined surface order was confirmed with LEED.

4.3.2. Preparation of the adsorbed thin layers of the tetrapyrrole complexes

In this work adsorbed thin layers of porphyrins and phthalocyanines have been investigated. The monolayers and multilayers of the tetrapyrrole complexes were prepared by physical vapour deposition (PVD) with a Knudsen cell. Except for Co-tetrakis(3,5-di-tert-butylphenyl)porphyrin (CoTTBPP), which was synthesized by PD Dr. Jux and co-workers, all the other porphyrins were purchased from the company *Porphyrin System*. All porphyrins have a specified purity of >98%. Phthalocyanine (2HPc), iron(II) phthalocyanine (FePc) and cobalt phthalocyanine were purchased from *Sigma-Aldrich*, and have specified purities of >99%, >90% and >97%, respectively. All porphyrins and phthalocyanines were degassed in vacuo by heating at 413 K for 24 h. Additionally phthalocyanines were degassed afterwards at 670 K for another 3 h.

Before evaporation, porphyrin or phthalocyanine molecules were heated to a certain temperature and kept at this temperature. Then the shutter on top of the Knudsen cell was opened, allowing porphyrin or phthalocyanine molecules to reach the substrate surface, which was held at room temperature. With different source temperatures and durations for the deposition, adsorbed organic layers with different thickness can be obtained. There is a linear relation between the layer thickness and the duration at a certain temperature.[FI07C] To obtain a monolayer, usually a multilayer was first prepared with a relative long evaporation time. Afterwards it was heated to a certain temperature to desorb the multilayer and leave a monolayer on the substrate. However in some special cases, monolayers were also prepared by controlling the exact evaporation time, which will be mentioned in the specific cases. The parameters for preparing different layers on different substrates are listed in Table 4-1.

Table 4-1. Evaportion parameters for preparing adsorbed thin layers of porphyrins and phthalocyanines

Substrate	Substance	$T_{knudsen\ cell}$ (K)	$t_{multilayer}$ (s)	$T_{desorption}$ (K)
Ag	2HTPP	638	180 (≈ 6 monolayers)	550
Ag	CoTPP	673	50 (≈ 2 monolayers)	530
Ag	ZnTPP	638	180 (≈ 3 monolayers)	550
Ag	CoTTBPP	638	600 (≈ 8 monolayers)	530
Ag	2HOEP	530	3600 (≈ 3 monolayers)	530
Ag	CoOEP	530	3600 (≈ 3 monolayers)	530
Ag	2HPc	670	3600 (≈ 10 monolayers)	530
Ag	FePc	680	3600 (≈ 10 monolayers)	530
Au	2HTPP	638	180 (≈ 6 monolayers)	540
Au	CoTPP	673	50 (≈ 2 monolayers)	530
Au	2HOEP	530	3600 (≈ 3 monolayers)	510
Au	CoOEP	530	3600 (≈ 3 monolayers)	500
Au	2HPc	670	3600 (≈ 10 monolayers)	560
Au	CoPc	720	3600 (≈ 5 monolayers)	600

4.3.3. Evaporation of the metallic Fe

An electron beam evaporator with an iron wire (purity > 99.99%) was used to deposit Fe. The amount of the deposited Fe was controlled by the ion flux of the partially ionized metal vapour. During the evaporation the voltage was about 800 V, the filament heating current was about 2.0 A, the filament emission was about 12 mA, and the ion flux was approximately 5.0 nA. The evaporation time and corresponding amount of Fe was taken from the PhD thesis of Dr. Ken Flechtner.[Fl2007C] The coverage θ of the tetrapyrrole monolayers on the metal substrate is defined as the number of adsorbed molecules per surface atom.

4.3.4. Dosing of small gas molecules

Oxygen and carbon monoxide molecules have been used as axial ligands for FeTPP monolayers on Ag(111). For this purpose a dosing system pumped with a turbo molecular pump and a rotary vane pump was used. Several laboratory mini cans with different gases are connected to a main gas line, which goes to the preparation chamber. The main gas line is separated from the preparation chamber with an electronically controlled valve. There is a leak valve between each mini can and the main gas line, which is used to regulate the gas flow during the dosing process. Oxygen and carbon monoxide used in this thesis are purchased from *Linde*, and have volumetric purities of 99.995% and 99.97%, respectively.

4.4. LEED measurements

As already mentioned in Section 4.1, the preparation chamber contains LEED optics for structural studies. In this work, it was used to determine the long range order of the substrate and the adsorbed tetrapyrrole layers. In order to obtain a better quality the samples were cooled down with liquid nitrogen to < 140 K. Kinetic energies around 170 V and 20 V were used for metal substrates and for tetrapyrrole layers, respectively. The LEED optics provides good quality within the energy range 50-500 eV. However, it is difficult to obtain sharp LEED spots below 50 eV, because the electron gun is difficult to focus below this energy. Thus the LEED pattern of the metal substrate usually has a much better quality than that of the tetrapyrrole layers. Usually prolonged adjustments of the lens voltages were necessary. This can lead to beam damage of the tetrapyrrole molecules since they are sensitive to the electron beam. Thus during a LEED measurement we first adjusted the lens voltages at one position on the sample, then moved the electron beam to another position to record the LEED pattern. In addition the low energy around 20 eV makes the electrons susceptible to magnetic fields, which also deteriorate the quality of the reflexes.

4.5. UPS measurements

In this work UPS was used to measure the work function and to obtain information about the the valence electronic structure of the samples. A helium discharging lamp was used as UV light source. The purity of the He gas is 99.999%. The pressure of He in the lamp was adjusted to give a high ratio of HeI_a UV light ($hv = 21.21$ eV) of the total UV light emission. As the gas pressure is reduced the lamp discharge will change color from the yellowish pink to greenish blue, indicating that a significant yield of He II ($hv = 40.8$ eV) is being obtained. During operation usually the gas pressure in the roughing line is about 0.1 mbar and the pressure in the chamber is about 2 to 3×10^{-9} mbar. During the measurement the sample was biased with -10 V to obtain clear secondary electron cut-off and better intensity of the electrons from the valence states. The binding energy scale of all spectra was corrected according to the clean metal substrate measured on the same day, whose Fermi edge was set to zero on the binding energy scale.

4.6. XPS measurements

The X-ray source used in this work is an aluminium X-ray anode from the company Gammadata Scienta AB (type: SA-100). A power of 300 Watt was chosen for the measurements. The Al K_α X-ray radiation was monochromatized before going into the analysis chamber. During the measurement the sample was usually held at a grazing emission position with the electron detection angle of 70° relative to the surface normal to increase the surface sensitivity. The measured regions and the corresponding parameters are listed in Table 4-2, where only the largest energy windows are listed. The resolution of XPS measurements is 0.3 eV for pass energy 150 V.

Table 4-2. Measured region and the parameters for XPS measurements

Region	Pass energy (eV)	Energy window (eV)	Step size (eV)	Time per Step (s)
Fermi edge	150	-2 – 2	0.05	0.02
Ag 3d	150	365 – 380	0.05	0.02
Au 4f	150	80-92	0.05	0.02
C 1s	150	282 – 293	0.05	0.02
N 1s	150	395 – 410	0.05	0.02
O 1s	150	527 – 547	0.05	0.02
Co 2p	300	776 – 806	0.05	0.02
Fe 2p	300	700 - 730	0.05	0.02

4.7. Data analysis for XPS and UPS

The analysis of the data was realized with the program IGOR Pro 6.04 and the macro file written by Dr. Jörg Pantförder, which was modified by Dr. Ken Flechtner for reading the data measured with the Scienta ESCA 200 spectrometer.

In order to compensate instrument-related shifts of the energy positions, which can for example be caused by small changes of the analyzer lens voltages with time, all the spectra were corrected according to the Fermi edge of the clean silver surface, where the binding energy equals zero. To compensate the intensity differences due to aging of the anode during the measurement, the intensities of the spectra were normalized with the intensity of a reference spectrum of the clean silver surface.

In addition to the elastically scattered photoelectrons, inelastic scattering also occurs, which forms the background. In order to obtain the actual signal the background was subtracted with the Shirley method[Sh72]. For the N 1s spectra, in addition to the inelastic scattered photoelectrons, excitation signals generated by plasmon or shake-

up satellites of the Ag 3d signals (at 399.2eV and 393.3eV) are also included in the background. This makes the subtraction of an additional background necessary. Similarly, for Fe $2p_{3/2}$ spectra in addition to the Shirley background, the Ag 3s signal at 718.9eV also contributes to the background. Therefore, background from the pure silver surface in this region was subtracted, taking into account the attenuation of the signal by the adsorbate.

The quantitative analysis of the XP spectra was carried out by line profile analysis according to the Least-Square method using χ-square-fitting. Usually Gaussian functions G and Lorentzian functions L are considered as model functions:

$$G(E, \omega, A) = \frac{A}{\omega} \sqrt{\frac{4 \ln 2}{\pi}} \cdot e^{-4 \ln 2 \left[\frac{(E-E_0)^2}{\omega^2} \right]}, \tag{4.1}$$

$$L(E, \omega, A) = \frac{2A}{\pi} \cdot \frac{\omega}{\omega^2 + 4(E-E_0)^2}. \tag{4.2}$$

Here ω represents the full width at half maximum, E the binding energy, E_0 and A the position and the amplitude of the line profile, respectively.

A mathematical convolution of both functions gives a Voigt function, which is usually used for the line profile fitting. To minimize computational complexity, however, the pseudo-Voigt function was used in this work, which essentially corresponds to a linear combination of Gaussian and Lorentzian function:

$$V_{PS}(E, \omega', A, m) = m \cdot L(E, \omega', A) + (1-m) \cdot G(E, \omega', A) \tag{4.3}$$

Here, m is the weighting factor, whereas ω' contains an additional factor α' for the asymmetry in the signal. The following equation describes the relationship:

$$\omega'(E, \omega, \alpha') = \omega + 2\alpha'(E - E_0) \tag{4.4}$$

4.8. X-ray standing wave (XSW) measurements

 XSW measurements were carried out at beamline ID32 of the European Synchrotron Radiation Facility (ESRF) in Grenoble, France. The UHV surface end-station of this beamline is equipped with a hemispherical electron analyzer (r = 150 mm), a low-energy electron diffraction (LEED) optics, and facilities for sample preparation. The angle between the synchrotron beam and the analyser axis was 45°. The base pressure of the chamber was below 5×10^{-10} mbar. The setup is shown in Figure 4-3.
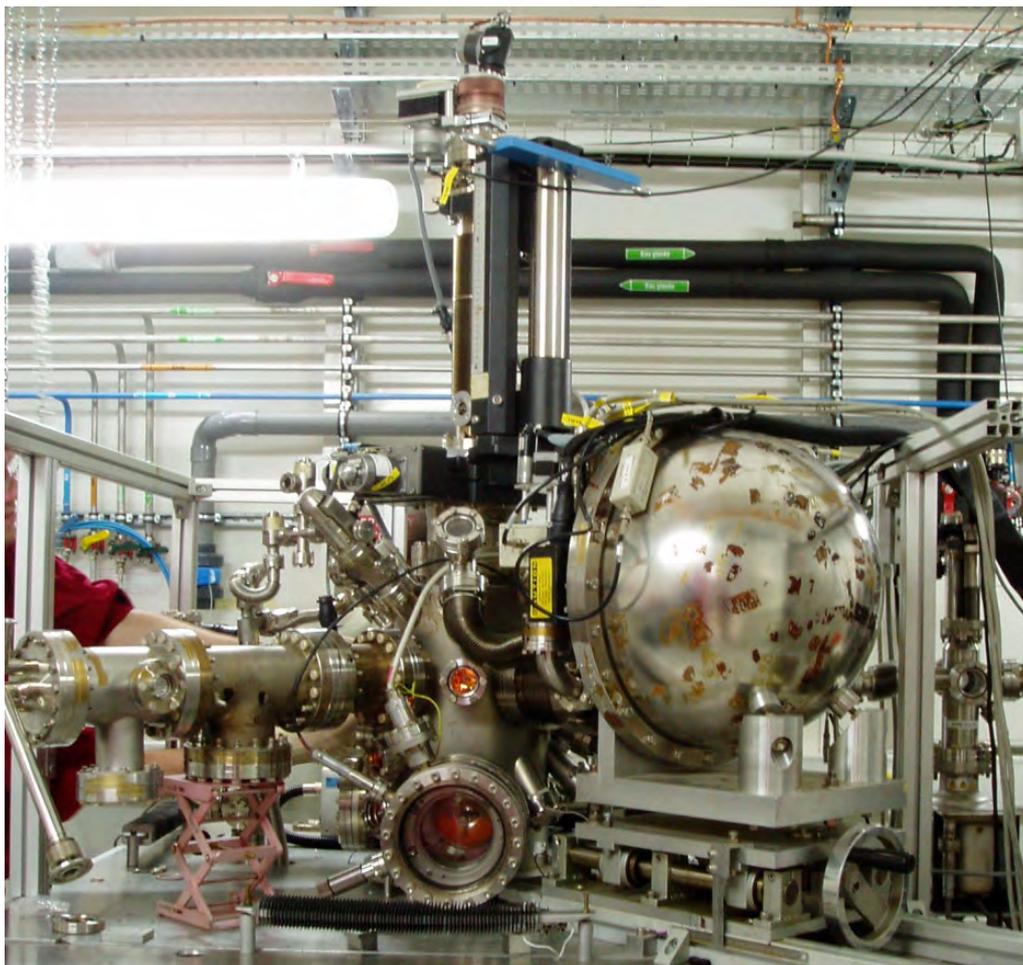
Figure 4-3. The front view of the set-up for XSW measurement. The hemispherical analyser is placed horizontally. Below the analyser, in the middle of the lower part of the system, is the positioning device to move the LEED optics. Above the analyser stands the sample manipulator.

The adjustable parameters of the sample position are shown as following in Figure 4-4. Two samples A and B are always measured in parallel.
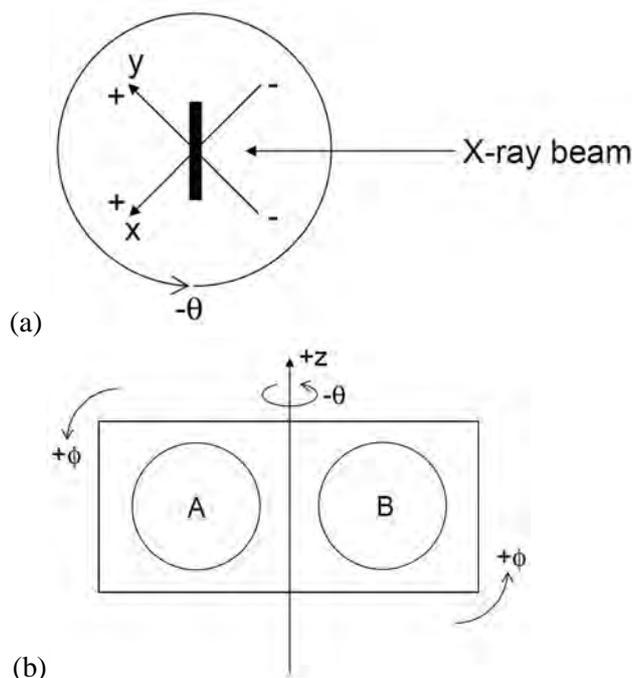
Figure 4-4. The adjustable parameters of the sample position for XSW measurements (a) View along the manipulator (along z axis in the direction -z); (b) View from the front side of the sample holder with two samples A and B.

4.8.1. Sample preparation

The substrate used for this investigation is a Ag single crystal with a polished (111) surface. The cleanliness and structural quality of the surface was checked by XPS, LEED and X-ray reflectivity tests. The sample surface was divided into many measuring spots, each having the size 1 mm × 1 mm. Firstly, a reflectivity vs. photon energy curve was acquired with intensity versus photon energy on every spot. The typical photon energy scan range is 8-10 eV around the energy of maximum reflectivity (2672 eV), with 50 or 60 intervals (i.e., 51 or 61 data points) every curve. Only those spots with FWHM of the reflectivity curve < 1.05 were considered suitable for the XSW measurements, because they have low mosaicity. Co(II)-tetraphenylporphyrin (CoTPP) and Zn(II)-tetraphenylporphyrin with specified purity >98 % were purchased from *Porphyrin Systems GbR*, and CoTTBPP was synthesized according to standard porphyrin synthesis protocols from commercially available 3,5-di-tert-butyl benzaldehyde (purity > 99%). All porphyrins were degassed in vacuo by heating to 420 K for 24 hours prior to the evaporation deposition.

The Ag(111) sample was sputtered and annealed as described in Section 4.3.1. Afterwards metalloporphyrin multilayers were prepared by vapour-deposition whilst the Ag crystal remained at ambient temperature. Sufficient thickness of the

multilayers was confirmed with XPS survey scans, in which no Ag3d signals could be detected. The corresponding monolayers were prepared by annealing the multilayers to 550 K.

4.8.2. Data acquisition and raw data treatment

For this investigation, first XP spectra of all elements present in the adsorbate except hydrogen were recorded, namely carbon, nitrogen and metals (Co and Zn). The XPS measurements were executed with varying photon energies around the Ag(111) Bragg energy 2627eV in small steps. The steps are identical to those used for measuring the corresponding reflectivity curve, which means 51 or 61 XPS measurements were carried out with corresponding photon energy. Co 2p, Zn 2p, N 1s and C 1s regions were chosen for the elements Co, Zn, N and C, respectively. The total 51 or 61 XPS measurements are considered as a XSW scan, and was completed within 10-30 min, and on each sample spot one to three XSW scans were carried out. The intensities of the incident and reflected beam as well as the sample current were monitored simultaneously. To check the beam damage XP spectra were acquired before and after each XSW scan. Typical XP spectra of Co 2p, Zn 2p and N1s regions are shown in Figure 4-5.
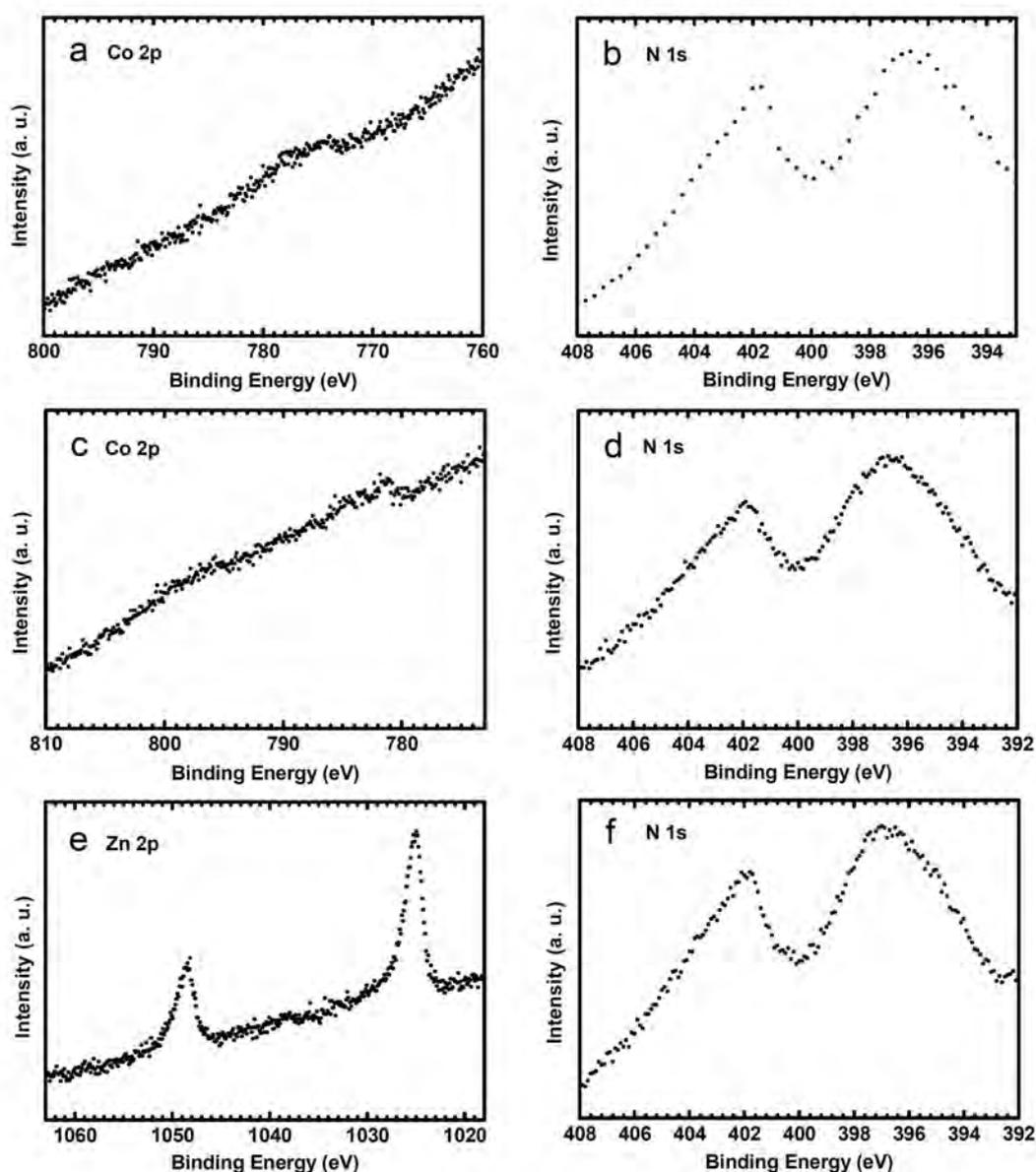
Figure 4-5. XP spectra for element Co, Zn and N in different metal porphyrin monolayers obtained during XSW measurements, acquired with photon energies around 2627 eV. (a) Co 2p XP spectrum of CoTPP, (b) N 1s XP spectrum of CoTPP, (c) Co 2p XP spectrum of CoTTBPP (d) N 1s XP spectrum of CoTTBPP, (e) Zn 2p XP spectrum of ZnTPP and (f) N 1s XP spectrum of ZnTPP.

After the raw data were obtained, the reflectivity curve was normalized to the incident beam intensity. The background of each XP spectrum in an XSW scan was subtracted and the area was integrated. The reflectivity (intensity vs. photon energy) and XSW absorption curves (absorption vs. photon energy) were obtained with this procedure. Then they were fitted according to equation (3). For Co 2p, Zn 2p and C 1s a linear background was adequate. However, Ag substrate gives rise to a curved background in the N 1s region, supposedly due to plasmon excitations[St06] or shake-up satellites of the Ag 3d signals[Po74] [Ma84]. Therefore, when subtracting background from N 1s

XP spectra, the background was fitted with a polynomial (following a procedure described in reference[St06]) and subtracted from the spectra. In this case, only the mean value of the XP spectra recorded with the same photon energy is used because the statistics of individual measurement is too poor. Typical absorption and reflectivity curves are shown in Figure 4-6.
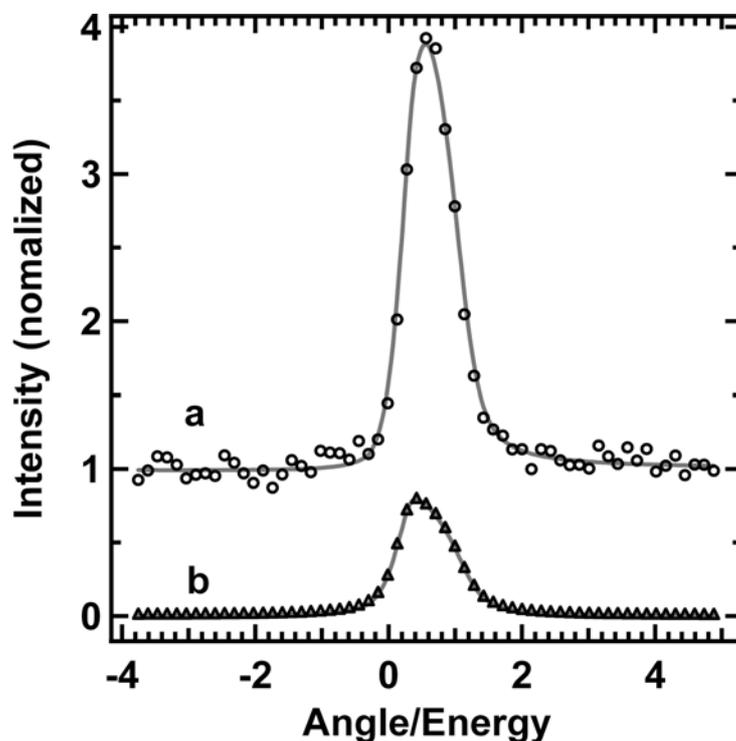
Figure 4-6. Typical absorption and reflectivity curves obtained during XSW measurements, Acquied from CoTPP monolayer on Ag(111) surface with photon energy 2.631 keV. (a) Absorption curve (b) Reflectivity curve. The circles present the original data points of the absorption curve and the hollow triangles present the original data of the reflectivity curve. The solid lines are the fitted curves according to Equation 3.34.

5. Adsorbed tetrapyrrole complexes on a Ag(111) surface

5.1. Adsorbed phthalocyanine thin films on Ag(111)

5.1.1. Adsorption of phthalocyanines

Multilayer desorption series

As described in Section 4.3.2, multilayers of Fe(II)Pc and the metal-free 2HPc were prepared by physical vapour deposition on a Ag(111) surface. During deposition, the temperature of the Knudsen cell was 670 K for 2HPc and 680 K for FePc, which led to a flux of approximately 0.016 monolayers per minute. Phthalocyanine monolayers were prepared by thermal desorption of the corresponding multilayers. In order to find out the desorption temperature, a thermal desorption series was carried out, in which the phthalocyanine multilayer was annealed at increasing temperatures. After each annealing step an XP spectrum in the C 1s region was taken. This procedure has been described for porphyrins in the dissertation of Dr. Ken Flechtner,[Fl07C] and is considered as a standard in our lab to obtain the desorption temperature for the preparation of phthalocyanine and porphyrin monolayers. Figure 5-1 shows the XP spectra of the thermal desorption series of 2HPc on the Ag(111) surface. The inset is the integrated peak area of the C 1s signal at different temperatures. Before reaching the temperature T_{des} at which the monolayer coverage is achieved, the C 1s signal slowly loses intensity. After annealing around 535 K, a sudden decrease of the C 1s signal intensity is observed, and the peak shifts to a lower binding energy position due to the more effective screening of the final core hole by the metal surface in the monolayer. Afterwards, when the annealing temperature is further increased, desorption of the monolayer can be observed, indicated by the decreased peak intensity. Usually for porphyrins, when the molecules are decomposed by annealing at high temperature, the signal shifts further to the lower binding energy side. Here in the 2HPc case, no further peak shift was visible; however, the C 1s spectrum changed its shape, indicating decomposition of the 2HPc molecules. It is worthwhile to mention that the multilayer in Figure 5-1 is relatively thin (between one and two monolayers), thus the difference of the peak intensity between multilayer and monolayer is small. However, in the inset the point of inflection can still be easily recognized and peak shift from multilayer to monolayer is about 0.25 eV towards lower binding energy. From the C 1s peak position and the peak area, 530 K was chosen to be the desorption temperature to obtain a 2HPc monolayer on Ag(111) surface.
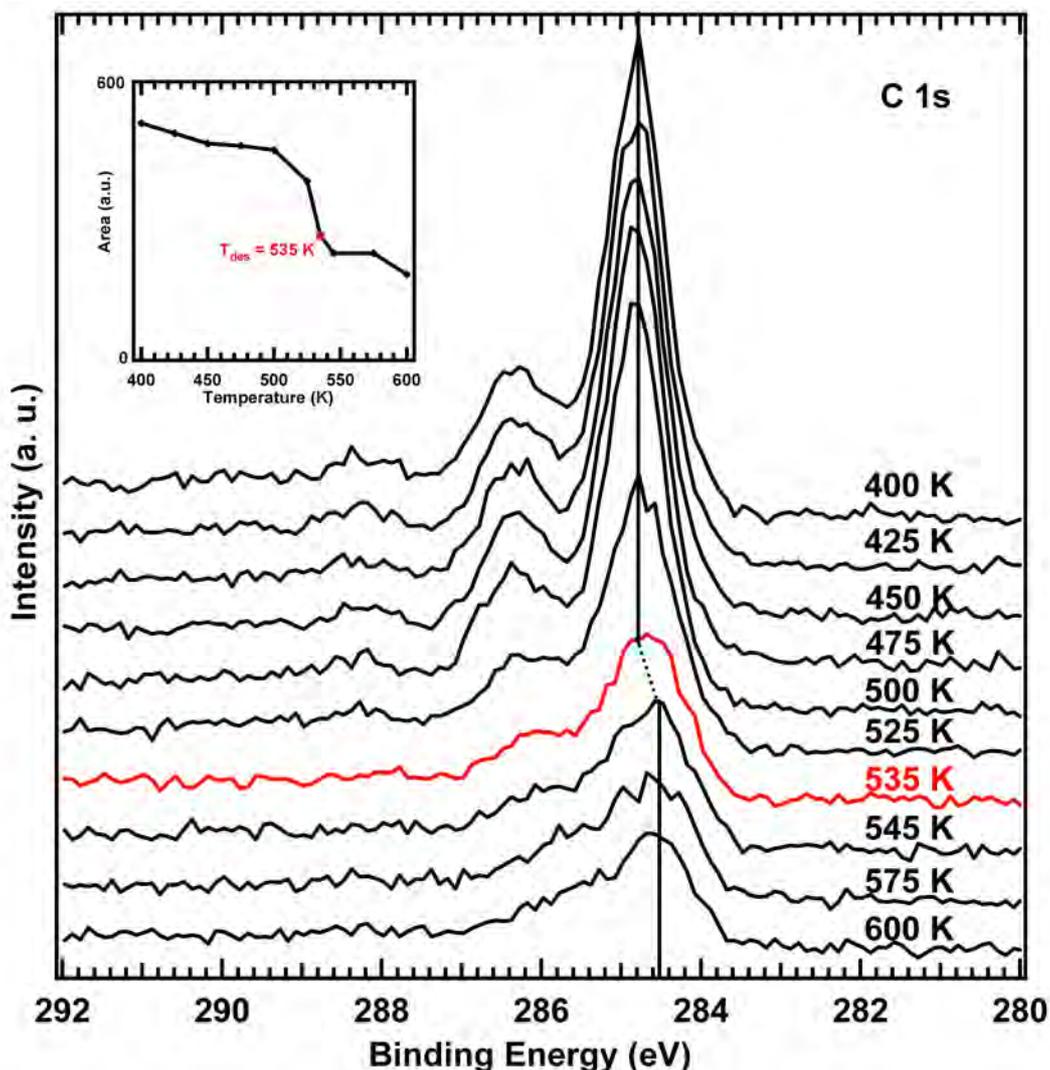
Figure 5-1. C 1s spectra taken after annealing of a 2HPc multilayer on the Ag(111) surface at the indicated temperatures. Inset: integrated peak areas of the spectra at different temperatures. The measurements were performed at room temperature with a detection angle of 70°.

Similarly Figure 5-2 shows the XP spectra of the evolution series of a FePc layer (between one and two layers). In this case the peak position shifted at 475 K by about 0.20 eV. The peak intensity remained relatively stable between 475 K and 530 K, and then started to decrease when the temperature increased. The peak position remained the same between 475 K and 550 K, suggesting that the FePc molecules are intact up to 575 K on Ag(111). After annealing at 600 K the peak shifted to lower binding energy side by about 0.20 eV, indicating decomposition of FePc molecules. From the C 1s peak intensity and position, 530 K was chosen as the temperature for multilayer desorption to obtain a FePc monolayer.
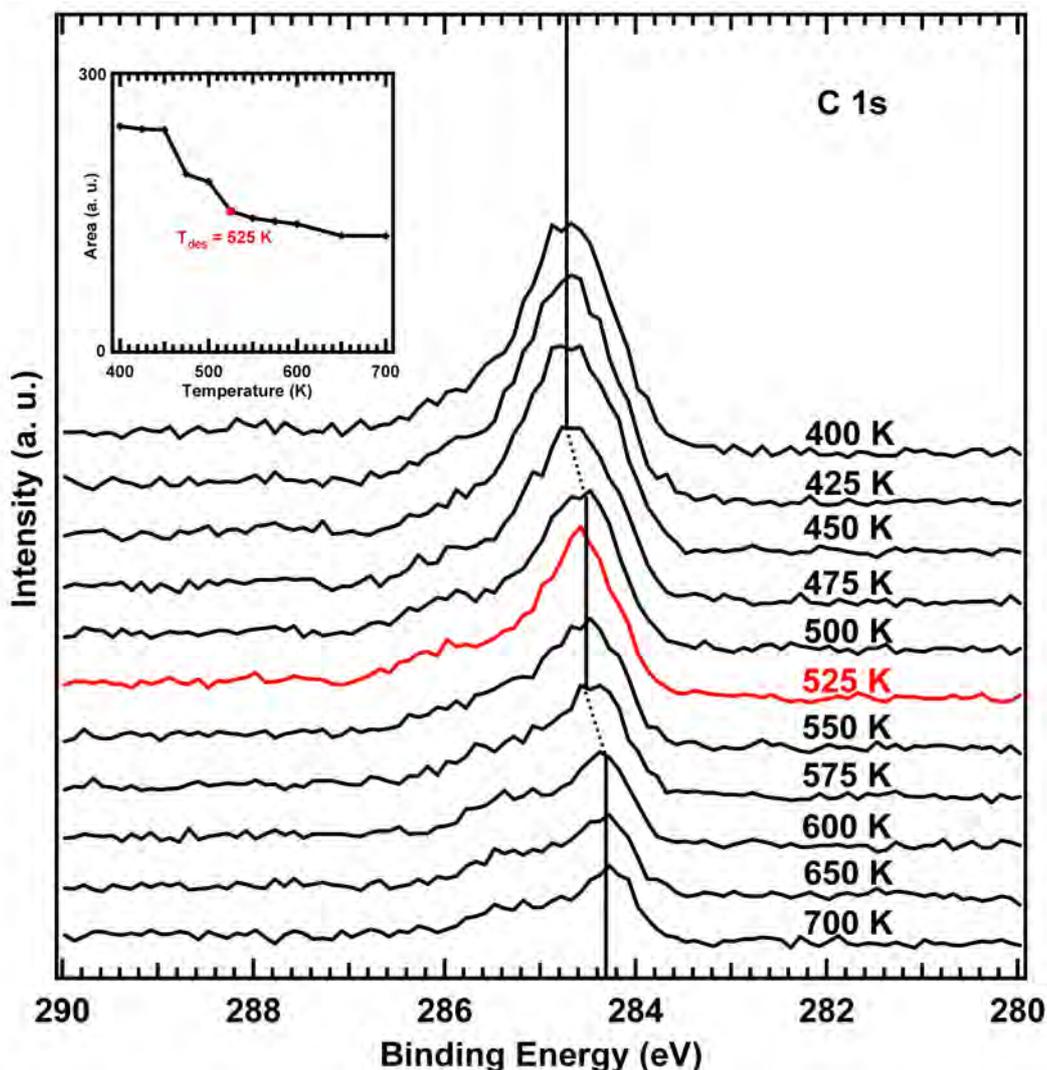
Figure 5-2. C 1s spectra taken after annealing of a FePc multilayer on the Ag(111) surface at the indicated temperatures. Inset: integrated peak areas of the spectra at different temperatures. The measurements were performed at room temperature with a detection angle of 70°.

The coverage θ of the phthalocyanine monolayers on the Ag substrate, defined as the number of adsorbed molecules per surface atom, was experimentally determined with STM and corresponded to θ = 0.037.[Ba08]

XP spectra of multilayer and monolayer of 2HPc and FePc on Ag(111) surface

Figure 5-3 shows XP spectra in C 1s region for 2HPc multilayer and monolayer on Ag(111) surface. The multilayer C 1s spectrum shows three peaks at 284.8 eV, 286.8 eV and 288.2 eV. According to the peak position and the relative ratio of the peak areas, the one at 286.8 eV is attributed to the hetero carbon atoms, which are directly connected to nitrogen atoms. And the most intensive peak at 284.8 eV is attributed to

the homo carbon atoms, which are only connected to other carbon atoms. The small signal at 288.2 eV presents the shake-up satellite feature of the C 1s photoelectrons of the 2HPc multilayer, which is typical for organic molecules with extended conjugated π systems [Sc04]. In the monolayer spectrum, this satellite feature vanishes. The C 1s peak position is shifted by 0.20 eV between multilayer and monolayer.
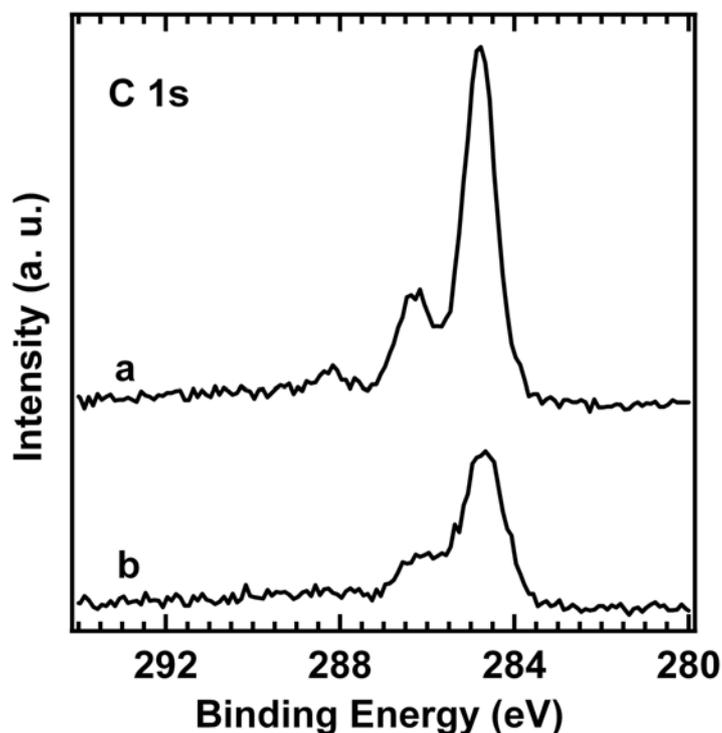
Figure 5-3. C 1s XP spectra for 2HPc multilayer (a) and monolayer (b) on Ag(111) surface.

Figure 5-4 shows N 1s XP spectra for 2HPc multilayer and monolayer on Ag(111). As can be seen from the molecular structure (Figure 2-4), the phthalocyanine molecule contains two chemically different types of nitrogen atoms, two pyrrolic (-NH-) and six iminic nitrogen atoms (=N-). Four of the iminic nitrogen atoms occupy the bridging meso-positions at the periphery of the molecule, while the other two are in the center along with the two pyrrolic nitrogen atoms. In the N 1s region of the XP spectrum for 2HPc monolayer, the respective signals appear at 400.2 eV (-NH-) and 398.5 eV (=N-), in line with previous XPS data[Al05A] [Al05B]. The ratio of the peak intensities after deconvolution is 1:3.05, in good agreement with the stoichiometry of the molecule. (The difference in the chemical shifts between the iminic nitrogen atoms in the peripheral meso-bridging positions and those in the center amounts to only 0.4 eV and is neglected in this discussion[Al05A] [Al05B].) The spectrum of the monolayer is shifted to lower binding energy by approximately 0.3 eV, which is attributed to the more efficient screening of the core whole of the photoion by the underlying Ag(111) surface.
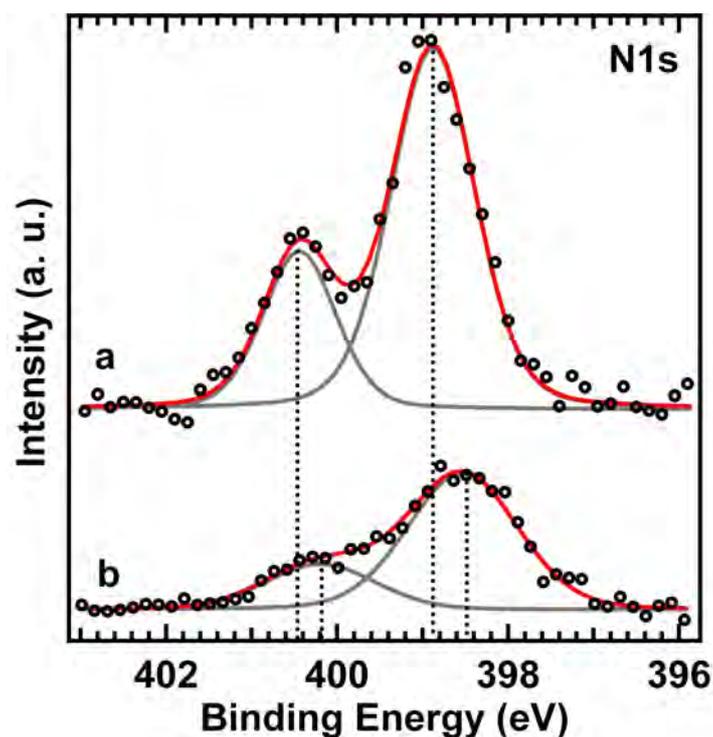
Figure 5-4. XP spectra in the N 1s region for 2HPc multilayer (a) and monolayer (b) on Ag(111). The black circles represent the original data, the solid gray lines are the peaks according to signal deconvolution, and the solid red line is the sum of these peaks.

Figure 5-5 shows C 1s XP spectra for FePc multilayer and monolayer on Ag(111), which are similar to those of 2HPc. Again one can observe a main peak composed of two signals (hetero and homo carbon atoms) and some satellite feature. Here the main C 1s peak of the FePc monolayer is shifted towards lower binding energy by about 0.2 eV in comparison to FePc multilayer.
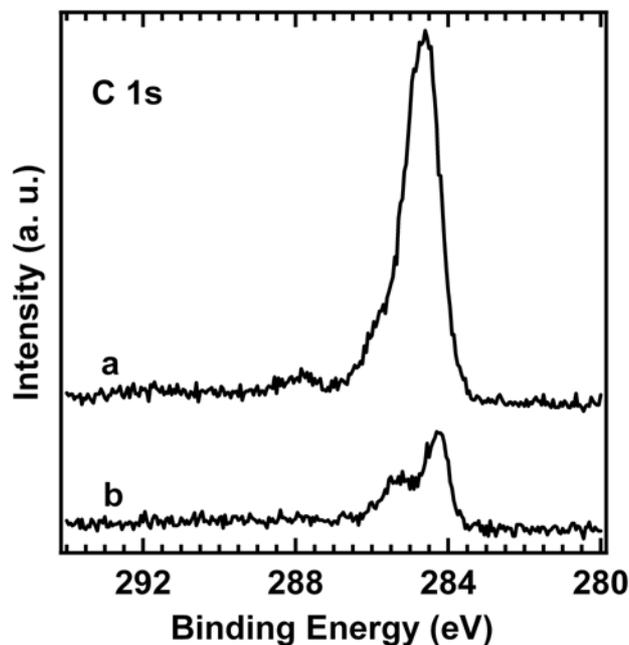
Figure 5-5. C 1s XP spectra for FePc multilayer (a) and monolayer (b) on Ag(111) surface.

Figure 5-6 shows N 1s XP spectra for FePc multilayer and monolayer on Ag(111) surface. Apparently all the nitrogen atoms in a FePc molecule are iminic, thus they show only one signal in the N 1s spectra.
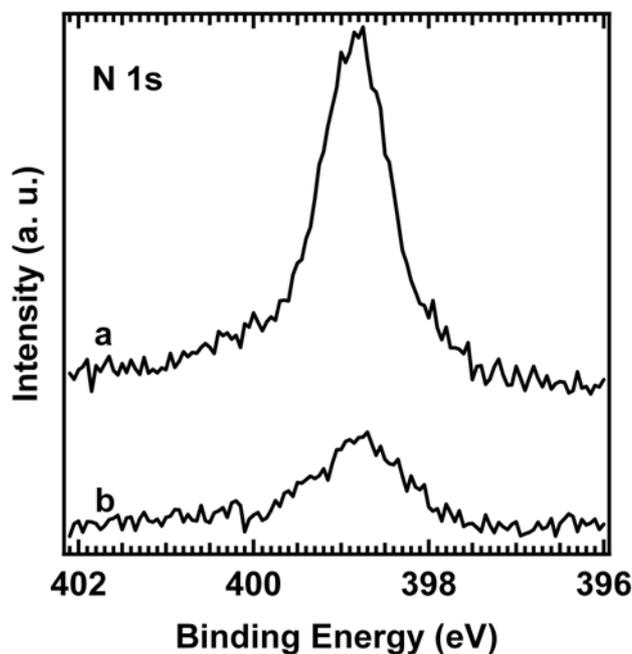
Figure 5-6. N 1s XP spectra for FePc multilayer (a) and monolayer (b) on Ag(111) surface.

Figure 5-7 shows Fe $2p_{3/2}$ XP spectra for FePc multilayer and monolayer on Ag(111). In the monolayer spectrum, the Fe $2p_{3/2}$ signal shows a main peak at 707.0 eV, which is accompanied by a weak satellite structure between 708 and 712 eV. A similar structure was obtained for the Co $2p_{3/2}$ signal of cobalt(II)-tetraphenylporphyrin (CoTPP) on Ag(111).[Lu07] In a detailed photoemission study of this system, the satellite structure was explained with the open-shell character of the metal ion, which results in final states of different spins and, thus, different energies. [Lu07] As an alternative model, a distribution of different efficiencies in the screening of the final core hole by the underlying metal surface can be assumed. According to this model, which was first suggested by Gunnarson and Schönhammer [Gu78], the main peak at 707 eV corresponds to most efficiently screened core holes, while the satellites at higher binding energies result from less efficiently screened core holes. Which of these two explanations is correct cannot be determined on the basis of our experimental data.

The Fe $2p_{3/2}$ spectrum of the FePc the multilayer is in good agreement with XPS data for FePc multilayers published previously[Åh06]. The broad and asymmetric shape of this signal has been attributed to the open-shell structure of the coordinated Fe ion, which leads to a coupling between the spin of the core hole and the spins in the valence shell. Compared to the monolayer spectrum, the maximum of the multilayer signal is shifted to higher binding energy, 708.6 eV. This is a typical value for Fe in the oxidation state +2, whereas the main signal of the monolayer spectrum at 707.0 eV is rather typical for Fe(0). A very similar difference in the peak positions of multilayer and monolayer has been described for the Co $2p_{3/2}$ signal of CoTPP on Ag(111).[Lu07] A detailed investigation with X-ray and UV photoelectron spectroscopy revealed that the Co ions in the CoTPP monolayer interact strongly with the Ag surface, which transfers electron density to the Co ion. Thus, the observed peak shift results to a large extent from a partial reduction of the Co ion.[Lu07] It is likely that a similar effect causes the different positions of the Fe $2p_{3/2}$ signal for multilayers and monolayers of FePc. Because of the planar geometry of the molecule, the distance between the Fe ion and the Ag surface is probably shorter than the Co-Ag distance of adsorbed CoTPP, making the Fe-Ag interaction possibly even more effective.
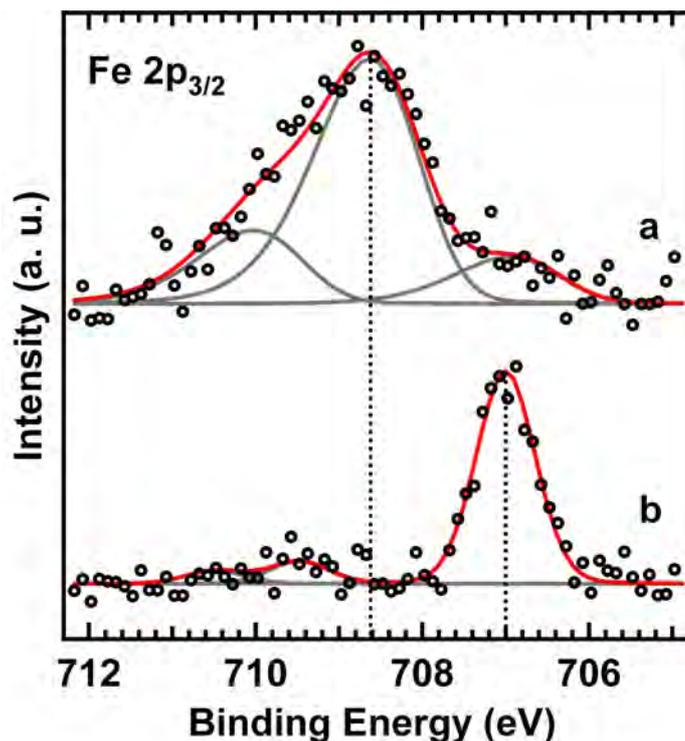
Figure 5-7. Fe $2p_{3/2}$ XP spectra for FePc multilayer (a) and monolayer (b) on a Ag(111) surface. The black circles represent the original data, the solid gray lines are the peaks according to signal deconvolution, and the solid red line is the sum of these peaks.

5.1.2. Metalation of metal-free phthalocyanine (2HTPP) on a Ag(111) surface

Previous studies have shown that adsorbed metalloporphyrins can be synthesized directly on a surface by metalation of the adsorbed porphyrins with vapour-deposited metal atoms, for example Fe, Co, and Zn.[Bu07B] [Go06] [Fl07A] [Au07A] According to gas phase DFT calculations[Sh07], the metalation reaction starts with the coordination of the neutral metal atom by the nitrogen atoms of the intact porphyrin. Thereafter, the pyrrolic hydrogen atoms migrate to the metal center, where they complete the reaction by desorbing as H_2. The *in situ* metalation of porphyrin monolayers under ultrahigh vacuum conditions provides clean and uniform metalloporphyrin monolayers with very high degrees of metalation, typically > 90%.

For practical applications, phthalocyanines are more suitable than porphyrins because of their higher stability and lower price. Thus, the question arises whether the direct metalation reaction can also be employed for the *in situ* synthesis of metallophthalocyanine monolayers. Naively, one may assume that the reactivity of phthalocyanine toward metal atoms is similar to the reactivity of porphyrins, because both provide the same coordination environment. However, the phthalocyanine molecule also contains four peripheral iminic nitrogen atoms which could coordinate

coadsorbed metal atoms and thus give rise to an unwanted side reaction. The fact that such a side reaction is theoretically possible has been demonstrated in a study of the interaction of tetrapyridylporphyrin (2HTPyP) with Fe on Cu(111). In this study, it was found that the iminic nitrogen atoms of the pyridyl groups strongly attract the coadsorbed Fe atoms.[Au07B] Phthalocyanine may react in an analogous way because the peripheral meso-bridging nitrogen atoms should show a reactivity similar to that of the nitrogen atoms of the pyridyl groups of 2HTPyP. Another difficulty may arise from the fact that the metal atoms, which are vapor-deposited on the complete monolayer of the ligand molecules, need to diffuse to find a vacant coordination site. In the case of a monolayer of tetraphenylporphyrin (2HTPP), it was found that Fe and Co atoms are sufficiently mobile on the densely packed 2HTPP monolayer for an almost complete metalation at room temperature.

However, the phthalocyanine monolayer may allow less mobility of the metal atoms because their tetrapyrrole macrocyles are in direct contact to the surface. In contrast, the peripheral phenyl groups of 2HTPP (which are rotated out of the porphyrin plane) act as spacers and create a gap between the porphyrin macrocycle and the surface.[Lu07] It appears likely that the coadsorbed metal atoms are able to diffuse in this gap with lower activation energy than between a phthalocyanine molecule and the surface. Alternatively, diffusion of the metal atoms on the molecular layer or between the molecules may be possible, but both mechanisms seem energetically unfavorable. In the first case, the bond between the metal atom and the surface must be broken, whereas in the second case the molecules in the densely packed layer must be laterally displaced. For these reasons, metalation of a phthalocyanine monolayer may be slow or require an excess of the metal.

Despite these potential complications, we have found that the metalation of well-ordered monolayers of phthalocyanine on an Ag(111) surface proceeds rapidly at room temperature and leads to almost complete metalation. In addition, the process appears to be highly selective; that is, no indications of side reactions were found.

XPS results

In this thesis, the coverage θ of the phthalocyanine or porphyrin monolayers on the metal substrate is defined as the number of adsorbed molecules per surface atom. Figure 5-8 shows the N 1s XP spectra during the metalation course and a monolayer of directly deposited commercial FePc as a reference. Deposition of a sub-stoichiometric amount of Fe atoms ($\theta_{Fe} = 0.027$) on the 2HPc monolayer at room temperature leads to significant changes in the N 1s signal. The two components of adsorbed 2HPc lose intensity, while another signal appears at 398.7 eV (Figure 5-8 b). With a slight excess of Fe atoms ($\theta_{Fe} = 0.044$), the two signals from 2HPc vanish completely and give way to a single peak at 398.7 eV (Figure 5-8 c). Apparently, the

four central nitrogen atoms are now in a chemically identical (or very similar) state. To clarify the question of whether the coordination of the Fe atoms results in the formation of iron(II)-phthalocyanine (FePc), a monolayer of this commercially available complex was measured. The corresponding XP spectrum, displayed in Figure 5-8 d, is virtually identical to the spectrum in Figure 5-8 c for the metalated 2HPc. The agreement between these two spectra provides strong evidence that the reaction of adsorbed 2HPc with coadsorbed Fe atoms leads to the formation of iron(II)-phthalocyanine. This conclusion is further supported by XP signals of the coordinated metal.
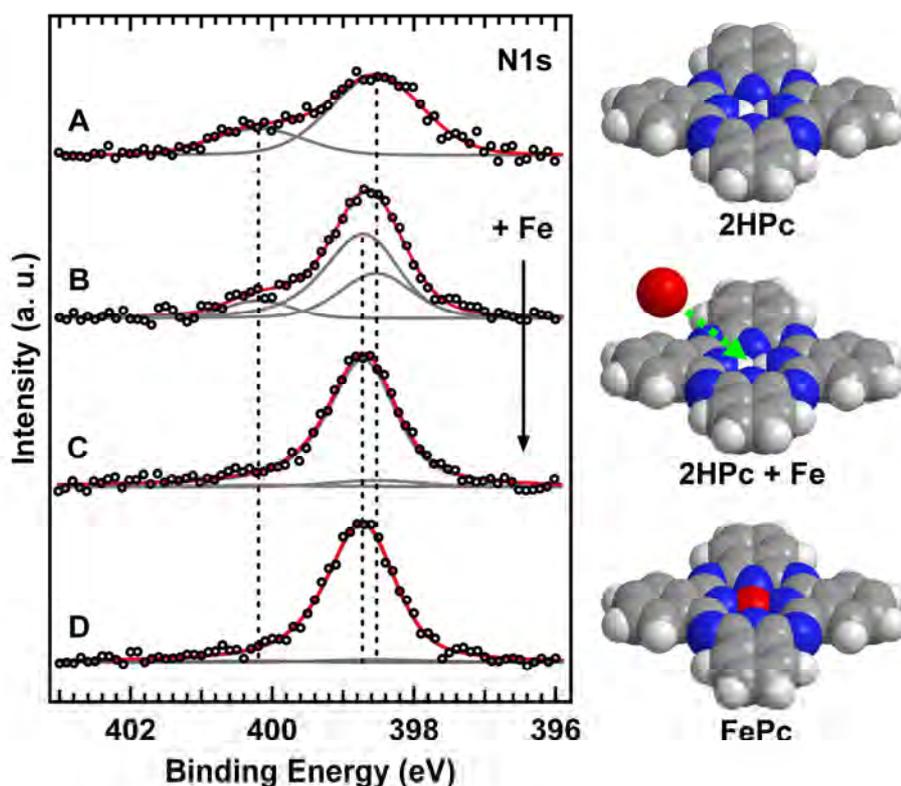
Figure 5-8. N 1s XP spectra of (a) a monolayer of 2HPc, (b) a monolayer of 2HPc after the deposition of increasing amounts of iron with $\theta_{Fe} = 0.027$, (c) with $\theta_{Fe} = 0.044$ and (d) a monolayer of directly deposited commercial FePc as a reference. The fit neglects the small binding energy difference of 0.4 eV[Al05A] [Al05B] between the iminic nitrogen atoms in the peripheral meso-positions and in the center, for both 2HPc with 6 and FePc with 8 iminic nitrogen atoms. The black circles represent the original data, the solid gray and blue lines are the peaks according to the signal deconvolution (of which gray lines stand for the components from 2HPc and the blue line represents FePc), and the solid red line is the sum of these peaks.

49

Figure 5-9 a shows the Fe $2p_{3/2}$ signal after deposition of a substoichiometric amount of Fe (θ_{Fe} = 0.027) on the 2HPc monolayer. This spectrum corresponds to the same state as the N 1s spectrum in Figure 5-8 b. The Fe $2p_{3/2}$ signal shows a main peak at 707.2 eV, which is accompanied by a satellite structure between 708 and 712 eV.

Deposition of a slight excess of Fe (θ_{Fe} = 0.044, Figure 5-9 b) causes only minor changes in the spectrum compared to the spectrum for stoichiometric Fe deficiency (Figure 5-9 a). The main signal at 707.2 eV grows relative to the satellites because its position coincides with the position for uncoordinated Fe(0). (The reasons for this deviation from the typical peak position for Fe(II) have been discussed in the previous section for the directly deposited FePc monolayer on Ag(111) surface.) For comparison, the Fe $2p_{3/2}$ signal of a directly deposited monolayer of commercial FePc is displayed in Figure 5-9 c, which is almost identical to Figure 5-9 b and confirms the formation of FePc by direct metalation.
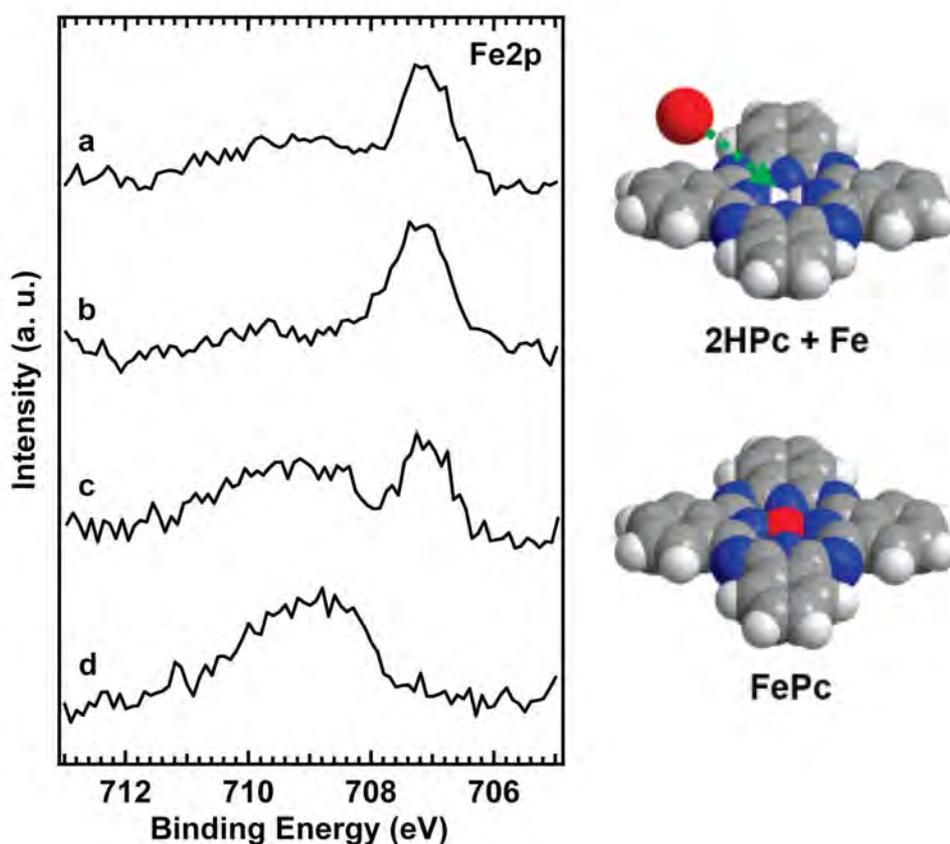
Figure 5-9. Fe $2p_{3/2}$ XP spectra of a monolayer of 2HPc after the deposition of increasing amounts of iron, (a) θ_{Fe} = 0.027 and (b) θ_{Fe} = 0.044; (c)a monolayer of directly deposited commercial FePc as a reference, and (D) FePc multilayers ($\approx$2 monolayers).

Conclusions

The XP spectra in both the Fe 2p and the N 1s region prove that monolayers of iron(II)-phthalocyanine on an Ag(111) surface can be obtained by direct metalation of phthalocyanine monolayers with the stoichiometric amount of vapour deposited Fe atoms. The adsorbed iron(II)-phthalocyanine (FePc) prepared *in situ* is chemically identical to directly deposited FePc. The reaction proceeds rapidly at room temperature and leads to high degree of metalation of the phthalocyanine molecules (95%). The fact that all deposited Fe atoms up to the stoichiometric amount find a coordination site indicates that the Fe atoms are sufficiently mobile on the surface even in the presence of the densely packed phthalocyanine monolayer. The additional STM investigations[Ba08] reveal that the Fe atoms are exclusively coordinated by the central nitrogen atoms of the phthalocyanine molecules; no competing coordination on the peripheral meso-bridging nitrogen atoms was observed. In general, the ultrahigh vacuum environment with its very low concentration of contaminants provides excellent conditions for the *in situ* preparation of such reactive metal complexes. Therefore, the procedure described here may also be applied successfully for the synthesis of monolayers of M(II)-phthalocyanines with metal ions that are usually not stable in the +2 oxidation state. The presence of the substrate surface may have an additional stabilizing influence on such unusual oxidation states.

5.2. Adsorbed porphyrin thin films on Ag(111) surface

Adsorbed porphyrin layers on a Ag(111) surface, including 2HTPP, 2HOEP, CoTPP, CoTTBPP, CoOEP, ZnTPP and FeTPP, have been studied. In the following sections the results from structural investigation, in-situ metalation and surface coordination will be presented and discussed.

5.2.1. NIXSW measurements

Previous XPS and UPS studies by Lukasczyk et al. revealed the existence of an electronic interaction between the Co ion in CoTPP monolayer as well as in CoTTBPP monolayer and the underlying Ag(111) surface.[Lu07] According to their interpretation of the UPS data, this interaction is slightly stronger for CoTPP monolayer on Ag(111) compared with CoTTBPP monolayer. This interpretation was based on the assumption that the distance between the Co ion and the substrate is smaller in the CoTPP monolayer than in the CoTTBPP monolayer. These distances were estimated using Van der Waals radii; however, no measurements were carried out to verify these estimates. To solve this problem, near normal incident X-ray standing wave measurements (NI-XSW) were carried out, as described in Section 4.8,

to measure the distance between the Co ion to the underlying Ag(111) surface in the CoTPP and the CoTTBPP monolayers. As a comparison the Zn-Ag(111) distance was measured for a ZnTPP monolayer, since no interaction between Zn ion and the underlying Ag(111) surface was observed[Fl07C]. Distances between the other atoms (C and N) in the porphyrin monolayers and the Ag(111) surface were also measured for better understanding of the molecular conformation of the porphyrin molecules.

Multilayers of metalloporphyrin

NI-XSW measurements of metalloporphyrin multilayers were carried out for determining the asymmetry parameter Q for the Co 2p and Zn 2p levels. Q values for N 1s and C 1s used in this work are taken from literature[St06]. When the layer is sufficiently thick, the asymmetry parameter Q can easily be obtained using Euation 3.35 with the measured photoelectron intensity and reflectivity values. The measured Q values for Co 2p and Zn 2p are listed in Table 5-1 along with the literature values for N 1s and C 1s. Apparently all Q values are high, meaning that the dipole approximation for photoemission process no longer holds, and the multipole corrections are indeed necessary.

Table 5-1. Values of the asymmetry parameter Q for different core levels

	Co 2p	Zn 2p	N 1s	C 1s
Q	0.19	0.12	0.22(2)	0.24(2)

Monolayers of metalloporphyrin

With the NI-XSW technique, monolayers of CoTPP, ZnTPP and CoTTBPP have been investigated. For one XSW measurement, 51 or 61 XP spectra were taken, each with a different photon energy around the normal incidence Bragg energy of Ag(111). Afterwards the intensity of the spectra were plotted versus the photon energy, and the curve was fitted to obtain the coherent position P^H and coherent fraction F^H according to Euation 3.34. For each element several XSW measurements were carried out, the number of which depends on the intensity of the corresponding XP spectra. Usually for carbon, the XSW measurement was repeated three to four times, and for nitrogen and the metals 20 to 30 times. Figure 5-10 shows the typical XSW absorption and reflectivity curves for CoTPP, CoTTBPP and ZnTPP, along with the fits. The mean values of P^H and F^H of the atoms relative to Ag(111) Bragg planes are listed in Table 5-2.
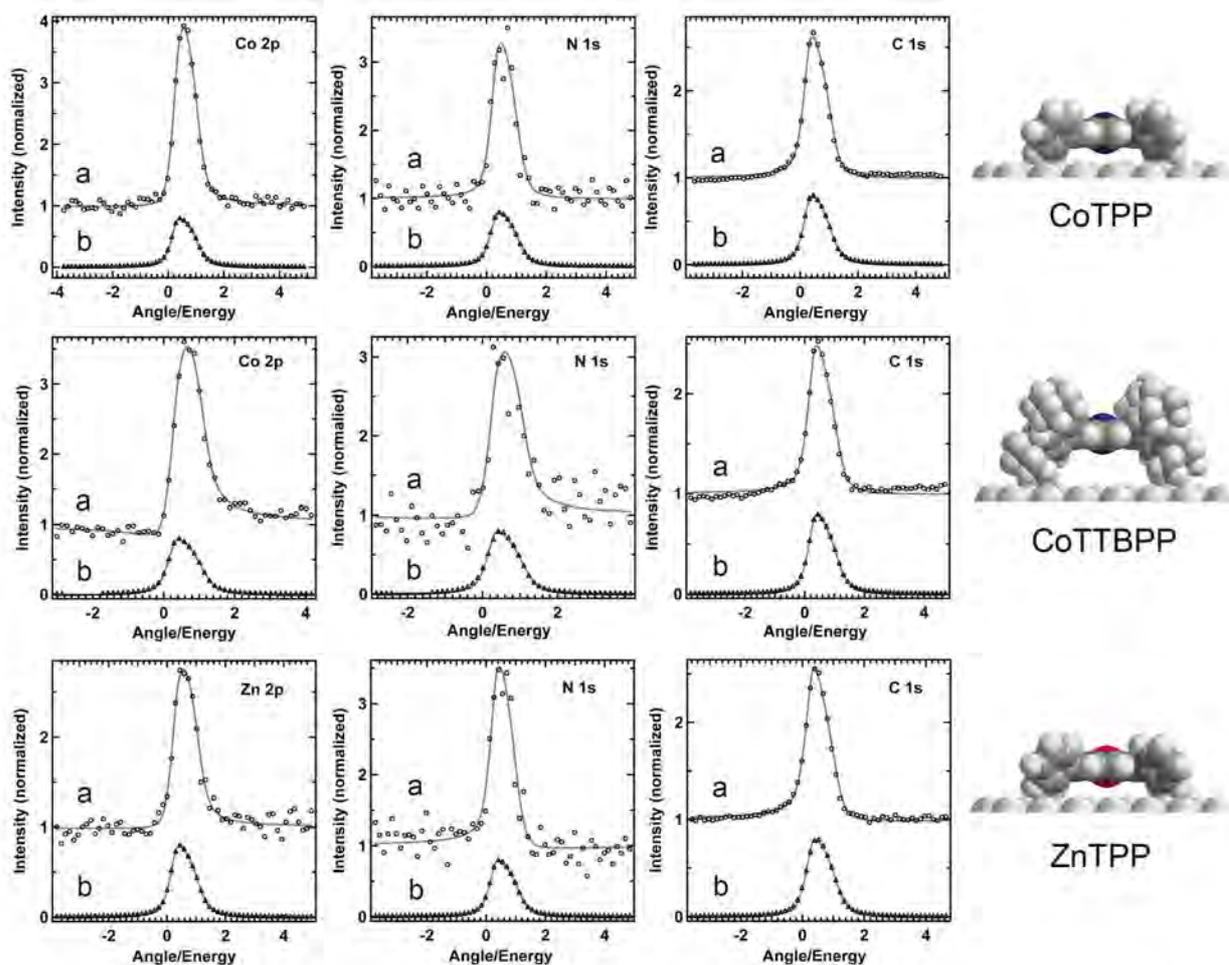
Figure 5-10. Typical XSW absorption and reflectivity curves and the corresponding fits. From top to bottom: CoTPP, CoTTBPP and ZnTPP. (a) absorption curves (b) reflectivity curves.

Table 5-2. Coherent position and coherent fraction of the atoms relative to Ag(111) Bragg planes

	Metal 2p region		N 1s		C 1s	
	P^H	F^H	P^H	F^H	P^H	F^H
CoTPP	0.236±0.024	0.861±0.164	0.227±0.059	0.600±0.222	0.319±0.177	0.177±0.028
CoTTBPP	0.188±0.049	0.987±0.320	0.092±0.049	0.584±0.151	0.345±0.074	0.091±0.058
ZnTPP	0.238±0.015	0.537±0.112	0.273±0.034	0.342±0.099	0.393±0.019	0.202±0.041

The results are also been presented in Argand diagrams in Figures 5-11. In the Argand diagram the length of the vector corresponds to the coherent fraction and the phase angle of the vector with respect to the real axis presents the coherent position.

(a)

(b)

(c)
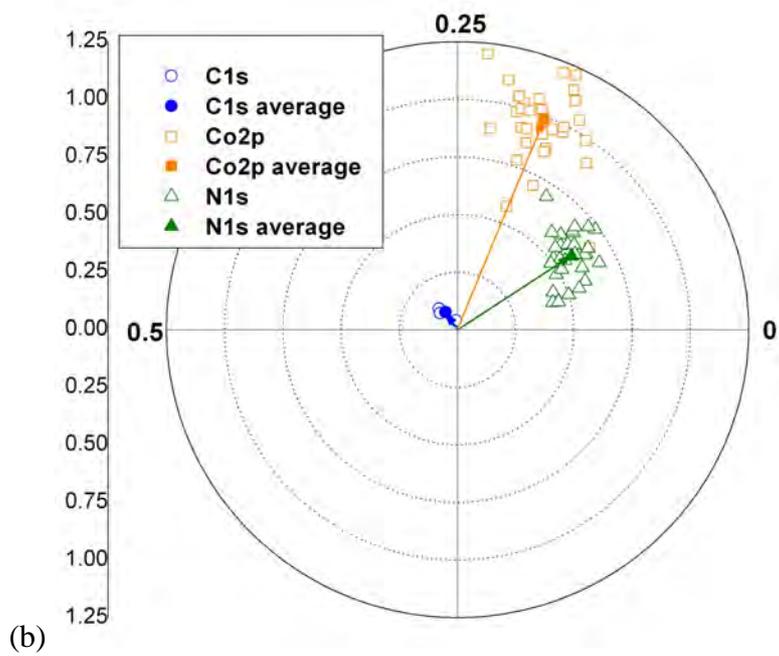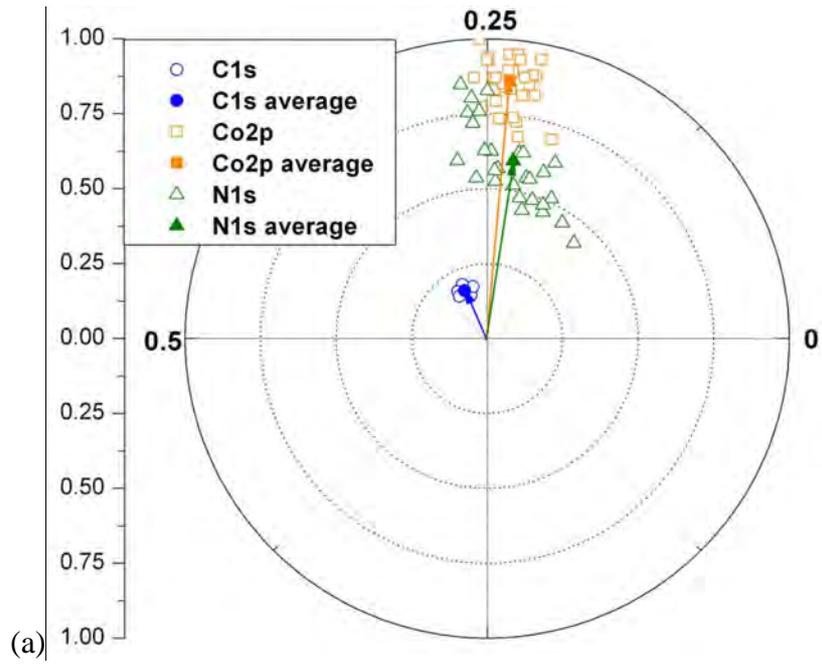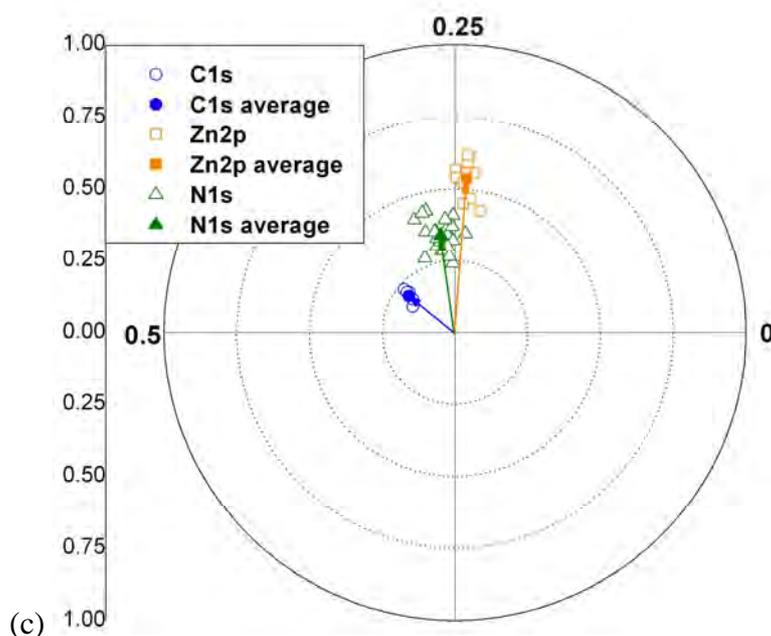
Figure 5-11. Argand diagrams showing XSW results for different elements (a) CoTPP monolayer, (b) CoTTBPP monolayer, and (c) ZnTPP monolayer, all at room temperature. Each data point presents an individual XSW measurement, in which 51 or 61 XP Spectra were taken with different photon energies. The final values for P^H and F^H in Table 5-2 were obtained by averaging over the results of these individual measurements.

From the results of the CoTPP monolayer on Ag(111) two possible distances D^H between the elements and the substrate surface can be derived, because the measured coherent position P^H is the distance D^H modulo the distance between two adjacent Bragg planes of the substrate, d^H. With the definition $\frac{D^H}{d^H} = n + P^H$ (n = 1, 2, 3…), and considering the atomic van der Waals radii of the elements, the possible values of D^H are shown in Table 5-3.

Table 5-3. Possible values of D^H for different elements in CoTPP, CoTTBPP and ZnTPP monolayers.

	$D^H_{Metal\ Atoms}$ (Å)		$D^H_{Nitrogen}$ (Å)		D^H_{Carbon} (Å)	
CoTPP	2.91±0.06	5.27±0.06	2.89±0.14	5.25±0.14	3.11±0.09	5.47±0.09
CoTTBPP	5.16±0.12	7.52±0.12	4.93±0.11	7.29±0.11	5.53±0.17	7.89±0.17
ZnTPP	2.92±0.04	5.28±0.04	3.00±0.08	5.36±0.08	3.28±0.04	5.64±0.04

Discussion

As the carbon atoms in all three metalloporphyrins necessarily occupy different vertical positions relative to the Ag(111) surface, the measured coherent fraction F^H is low in all three cases. The relatively low coherent fraction for N 1s suggests different vertical positions of N atoms in the porphyrin molecules. This may be a result from different orientations of the porphyrin molecules on Ag(111), or due to the tilt of the porphyrin molecules, or due to the saddle-shaped distortion of the molecules[We08A] [We08B]. Previous STM images showed that at monolayer coverage, all three porphyrin molecules lie on Ag(111) with the porphyrin framework parallel to the surface, and the porphyrin frame work also undergoes saddle-shaped distortion[Bu07A] [Bu09]. This rules out the possibility of tilt of the porphyrin molecules. Thus most likely the different vertical positions for N atoms are due to the saddle shaped distortion of the porphyrin molecules. The NI-XSW results for each porphyrin will be discussed in detail in following sections.

a. CoTPP monolayer on Ag(111)

As shown in Table 5-3, the average distance between the Co ions and the Ag(111) surface is almost identical to that between N atoms and the substrate, while the average of carbon atoms is at a slightly higher position. This may be related to the interaction between the Co ion and the underlying surface. The Co-Ag(111) interaction is basically composed of three components, which are the attractive coulomb interaction between the Co ion and its image in the metal, the attractive van der Waals force, and the possibly repulsive covalent interaction (as proposed in reference [Lu07]). The XSW results show that the overall interaction is attractive, which attracts the Co ion towards the Ag(111) surface, leading to a deformation of the porphyrin framework. According to literature, the deformation is induced by intramolecular repulsion between the peripheral phenyl groups and the porphyrin ring, which enclose a dihedral angle of only 35°.[We08A] [We08B] For the free CoTPP molecule, it was shown that angles below 60° lead to a deformation of the porphyrin macrocycle and that a dihedral angle of 35° causes a substantial increase of the total energy of the molecule (between 73.7 kJ/mol at 40° and 136.8 kJ/mol at 30°).[Wö08] There is a balance between the attraction to the surface and the intramolecular steric repulsion, which leads the CoTPP molecule to a curved form, with the Co ion and the average distance of N atoms closer to the surface than the average distance of C atoms.

For Co ions in the CoTPP monolayer on the Ag(111) surface, an F^H value of 0.861±0.164 suggests high homogeneity of the prepared monolayer. A P^H_{cobalt} value of 0.236±0.024 was obtained, which gives two possible D^H_{cobalt} values, 2.91±0.06 Å and 5.27±0.06 Å. Considering the atomic van der Waals radii of the elements, the shorter distance 2.91±0.06 Å would only be possible if the CoTPP molecules lie

totally flat on the surface, which would imply that the peripheral phenyl goups are in plane with the porphyrin macrocycle. However, the phenyl groups cannot be in plane with the macrocycle for steric reasons[Wö08]. STM images for CoTPP monolayers prepared with the same procedure[Ba09] also show that the molecules lie on Ag(111) surface with the porphin ring out of the substrate surface due to the presence of the peripheral phenyl groups, which excludes the D^H_{cobalt} value of 2.91±0.06 Å. Another argument against 2.91±0.06 Å is the distance between Cu atoms in an adsorbed CuPc monolayer and the underlying Ag(111) surface. CuPc molecules in a monolayer lie flat on the Ag(111) surface, while CoTPP molecules are distorted on Ag(111), and the Cu^{2+} ion is smaller than the Co^{2+} ion. These facts indicates that D^H_{cobalt} for CoTPP monolayer on Ag(111) should not be shorter than D^H_{copper} for CuPc monolayer on Ag(111).[Ku10] The measured D^H_{copper} is around 3.04 Å for a CuPc monolayer on Ag(111) at room temperature,[Ku10] hich is larger than 2.91±0.06 Å. From this point of view, 2.91±0.06 Å is also not a possible value. The larger value 5.27±0.06 Å gives an immediate impression that the distance is too large for the Co ion to have an covalent interaction with the underlying Ag(111) surface, as has been observed previously[Lu07]. However, with XSW technique the measure distance is the distance between the atoms in the adsorbate and the Bragg planes of the substrate, rather than a local distance between the atoms of the adsorbate and an individual atom of the substrate. Thus for the surprisingly high value 5.27±0.06 Å, our suggestion is that an Ag atom is trapped within the space between the Co ion and the underlying Ag(111) surface, and interacts with the Co ion. This reduces the local Ag-Co distance by approximately 2.36 Å (the distance between two adjacent Ag(111) planes), and leads to a distance of about 2.91 Å, which is a reasonable covalent type bond length, and agrees with results of DFT calculations.[Hi10]

b. CoTTBPP monolayer on Ag(111)

For a CoTTBPP monolayer on Ag(111) an F^H value of 0.987±0.320 again indicates high vertical homogeneity of the prepared monolayer. A P^H_{cobalt} value of 0.188±0.049 was obtained, which corresponds to a D^H value of 2.80±0.12Å, 5.16 ±0.12Å or 7.52±0.12 Å for n =1, 2 or 3 in $\frac{D^H}{d^H} = n + P^H$, respectively. When one calculates with the atomic van der Waals radii, the value 2.80±0.12Å is too small for the 3, 5-di-tert-butylphenyl groups to be possible. On the contrary the distance 7.52±0.12 Å is too long (even if the spacer groups are completely perpendicular to the silver surface, this distance is below 7 Å). Previous studies show that XP and UP spectra for CoTPP and CoTTBPP monolayers are very similar. [Lu07] [Fl07B] Since for CoTPP only 5.27±0.06 Å is the possible distance, most likely the distance for CoTPP is also in that range. Thus 5.16±0.12Å remains as the only possible value. This distance matches rather well with the STM results from literature[Bu07A], which gives a D^H_{cobalt} value of 5.2 Å. Similar to the CoTPP case, the only plausible explanation for the interaction between

Co ion and the underlying substrate surface despite the large distance is that an Ag atom is trapped in the space under the porphyrin molecule and interacts with Co atom above it. reduces the local Ag-Co distance by approximately 2.36 Å and leads to a local Ag-Co distance of 2.80 Å, which is a reasonable length of a covalent type bond. Unlike expected, D^H_{cobalt} is smaller in CoTTBPP case than in CoTPP case, because the larger peripheral substituents in CoTTBPP lead to stronger van der Waals attraction to the substrate and consequently smaller dihedral angle.

A $P^H_{nitrogen}$ value of 0.092±0.049Å gives an average distance of 4.93±0.11Å between the nitrogen atoms on a CoTTBPP monolayer and the underlying Ag(111) surface. Taking the errors into account, this distance is the same as the average distance between the Co ions and the underlying substrate surface, while it is much smaller than the average distance between the carbon atoms and the Ag(111) surface (5.53±0.17Å). Again we interpret that the difference is caused by the interaction between the Co ion and the Ag(111) surface, in which the periphery of the porphyrin framework is bent upwards while the cobalt and nitrogen atoms in the center are closer to the substrate surface.

c. ZnTPP monolayer on Ag(111)

A ZnTPP monolayer on the Ag(111) surface was studied as a comparison to CoTPP, since the Zn atoms in the ZnTPP monolayer do not show covalent interaction with the underlying substrate surface. On the one hand, the peak shift on Zn $2p_{3/2}$ XP spectra between ZnTPP monolayer and multilayer is only 0.25 eV[Kr07], suggesting no covalent interaction between Zn ion and the underlying surface. On the other hand, the UP spectrum of ZnTPP monolayer on Ag(111) in the range of 0-1.5 eV below E_F is identical to that of a 2HTPP monolayer, as demonstrated in Figure 5-12 [Fl07C], which also shows no covalent interaction between Zn ion and Ag(111). In the ZnTPP case, a D^H_{zink} value different from D^H_{cobalt} was expected. Surprisingly the distances are almost identical. The N atoms are at the same average height as the Zn ion, silimar to that in the CoTPP case. In the ZnTPP monolayer the average distance between carbon atoms and the Ag(111) surface (3.28±0.04Å) is higher than that for a CoTPP monolayer (3.11±0.09Å), indicating stronger deformation of the porphyrin framework. The measured F^H_{zinc} for ZnTPP monolayer on Ag(111) is 0.537±0.1120, which is much lower than the measured F^H_{cobalt} for CoTPP monolayer (0.861±0.164). This indicates that, on Ag(111) the ZnTPP monolayer is less homogenous than the CoTPP monolayer. For example, there may exist different conformations of ZnTPP molecules on Ag(111).
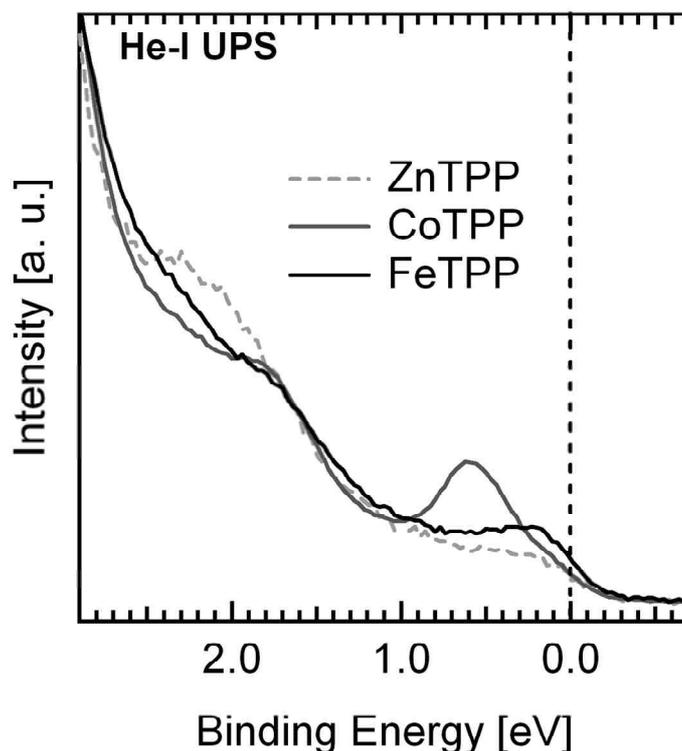
Figure 5-12. UP spectra of CoTPP, FeTPP and ZnTPP monolayers on Ag(111) in the region near the Fermi edge.[Fl07C] The interaction-induced signal between 0 and 1 eV can be observed for CoTPP and FeTPP monolayer, but not for ZnTPP monolayer.

Conclusion

With the XSW technique, the vertical distances between the Ag(111) surface and the atoms in the CoTPP, CoTTBPP and ZnTPP monolayers have been measured. The results show that in both CoTPP and CoTTBPP monolayers, the N atoms have the same average distance to the surface as the Co atoms, while the C atoms have a higher average position. This is probably caused by the deformation of the porphyrin framework due to the attractive interaction between porphyrin core and the underlying Ag(111) surface. F^H_{cobalt} for both Co porphyrin monolayers is high, indicating high homogeneity of the monolayers. The effects of the covalent interaction between Co ions and Ag(111) seen in the photoemission spectra is proposed by the possible trapping of a Ag atom in the space between Co ions and the underlying Ag(111) surface. In the CoTPP and ZnTPP monolayers Co and Zn ions are at the same height in spite of the fact that XPS and UPS indicate very different interactions between the metal ions and the underlying Ag(111) surface. F^H_{zink} is rather low, indicating that there might exist different conformations of ZnTPP molecules in the monolayer.

5.2.2. Metalation of 2HTPP with Fe: Reversed order of deposition

Usually in our lab a metalloporphyrin layer is prepared by vacuum thermal deposition of the corresponding metalloporphyrin molecules, which are synthesized ex-situ with wet chemistry methods. In the ex-situ synthesis both the starting materials and the products have direct contact with the solution and the atmosphere, which leads to difficulties in the preparation of metalloporphyrins sensitive to the solution or to the air. For example, Fe(II)-porphyrins are extremely sensitive to oxygen, thus it is difficult to obtain pure Fe(II)-porphyrins with the conventional methods. Therefore, the commonly employed vacuum thermal deposition of ex-situ synthesized metalloporphyrin molecules was ruled out as a way to prepare Fe(II)-porphyrin layers. Instead, in-situ metalation of monolayers and multilayers of 2H-tetraphenylporphyrin (2HTPP) with Fe atoms on Ag(111) has been developed. It has been studied with scanning tunneling microscopy (STM) and X-ray photoelectron spectroscopy (XPS).[Bu07B] [Au07A] [Fl07C] [Bu08] This surface confined coordination reaction results in the formation of adsorbed iron(II)- tetraphenylporphyrin (FeTPP). It is demonstrated that metalation of 2HTPP can be achieved by depositing iron atoms onto a monolayer of 2HTPP at room temperature, which we call the metalation of the normal order. The following results show that by depositing 2HTPP onto a Ag(111) surface with pre-deposited iron, the metalation of 2HTPP is also feasible (reversed order). However, the latter route requires elevated temperatures, indicating that this reaction includes at least one step with an activation barrier. The XPS results are described in detail in the following section.

XPS Results

The evidence of the formation of iron(II)-tetraphenylporphyrin (FeTPP) is provided by X-ray photoelectron spectra, which show characteristic changes in the N 1s (Figure 5-13) and Fe 2p (Figure 5-14) regions in the course of the metalation reaction.[Fl07C] [Bu08]

First, 0.1 ML Fe was deposited on the Ag surface, followed by a monolayer (equivalent to $\theta = 0.037$) of 2HTPP. The N 1s XP signal of the resulting layer (Figure 5-13 a) shows the two characteristic peaks of a 2HTPP monolayer, indicating that no reaction between Fe and 2HTPP occurs at room temperature. After heating to 550 K, an additional component at 398.7 eV appears in the spectrum (Figure 5-13 b). In line with the STM data and the N 1s spectra in the literature[Fl07C] [Bu08], this component is attributed to FeTPP. If the same procedure is performed with a thin multilayer of 2HTPP deposited on 0.1 ML Fe/Ag(111), the yield of FeTPP is slightly higher (Figure 5-13 c). This suggests that the pre-deposited Fe atoms partly diffuse into the 2HTPP multilayer and form FeTPP there. The heating step causes desorption of the

excess of 2HTPP, whereas the FeTPP molecules remain on the surface because of their increased interaction with the Ag surface.
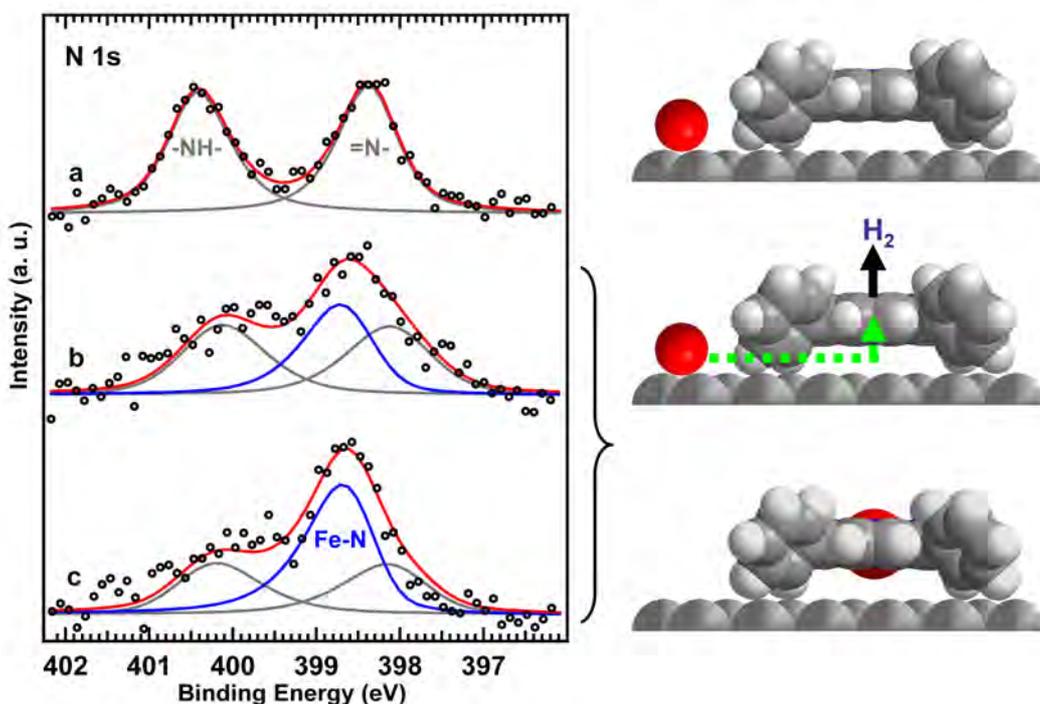
Figure 5-13. N 1s XP spectra of the metalation of tetraphenylporphyrin (2HTPP) with pre deposited Fe atoms. (a) 2HTPP monolayer on Fe/Ag(111) with 0.1 ML Fe, (b) after heating to 550 K. In (c), a thin multilayer of 2HTPP (ca. 1.5 monolayers) was deposited on Fe/Ag(111) with 0.1 ML Fe before the sample was heated to 550 K (intensity normalized for better comparison with monolayer spectra).

Fe $2p_{3/2}$ XP spectra in Figure 5-14 are the additional proof for the metalation of 2HTPP with pre-deposited Fe atoms. Spectrum 5-14 b was directly taken after the deposition of a 2HTPP monolayer on pre-deposited Fe atoms. The Fe 2p3/2 peak is at the same position of as in the case of pre-deposited Fe atoms, indicating no change of the chemical status of the Fe atoms. The peak intensity is decreased as a result of the damping by the 2HTPP monolayer. After heating to 550K for 30s (Figure 5-14 c), the peak position is slightly shifted to higher binding energy by about 0.2 eV and the intensity increased, which indicates the diffusion of Fe atoms to the central coordination cavity in 2HTPP monolayer and the formation of FeTPP. After a thin multilayer (about 1.5 monolayers) of 2HTPP was evaporated on the pre-deposited Fe atoms followed by heating at 550 K, spectrum 5-14 d was obtained. The peak position is shifted further to the higher binding energy side by about 0.25 eV and the intensity is about 10% higher than in spectrum 5-14 c which indicates that the excessive Fe atoms diffuse into bulk silver after metalation, and the degree of metalation of the 2HTPP multilayer is higher than that of the monolayer. Although the peak position in spectrum 5-14 c is higher than that of the free Fe atoms in spectrum 5-14 a, the

difference is rather small. Similar to the Fe $2p_{3/2}$ spectra in the FePc case in Figure 5-7 and 5-9, the small difference of the peak positions between 5-14 a and 5-14 c is possibly due to the transfer of electron density from the Ag(111) substrate to the Fe ions. This is in good agreement with previous study.[Lu07] [Ba08] [Bu08]
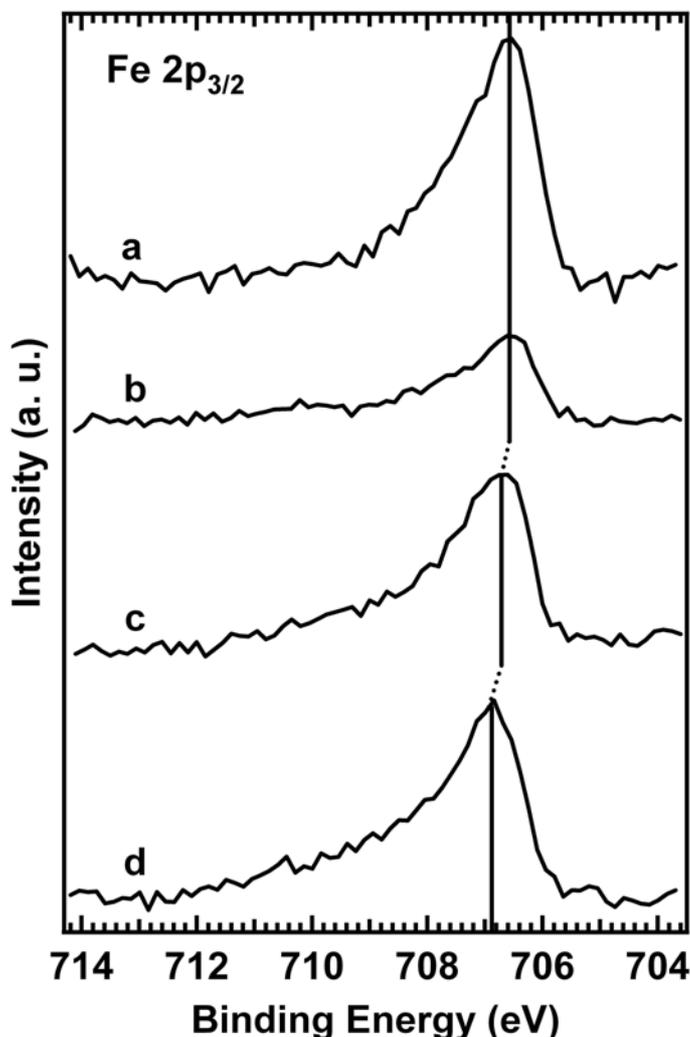
Figure 5-14. Fe $2p_{3/2}$ XP spectra for (a) Fe atoms on Ag(111) surface, (b) 2HTPP monolayer on pre-deposited Fe atoms on Ag(111), (c) 2HTPP monolayer on pre-deposited Fe atoms on Ag(111) after heating to 550 K, and (d) 2HTPP multilayer on pre-deposited Fe atoms on Ag(111) after heating to 550 K.

Discussion

Previous gas-phase density functional theory (DFT) calculations on the metalation of porphyrin molecules with Fe atoms have shown that the reaction would proceed without activation barriers in the gas phase, whereas for other metals, such as Co, Ni, Cu, and Zn, partly substantial barriers were predicted.[Sh07] According to these calculations, the neutral metal atom is first coordinated by the four nitrogen atoms of

the intact porphyrin. Subsequently, the two pyrrolic hydrogen atoms migrate to the metal center, where they recombine and desorb as dihydrogen (H_2). In the course of these H transfer steps, the metal atom is oxidized to the dication.

In the case of the metalation of 2HTPP monolayers with pre-adsorbed Fe atoms, however, the situation is different, since the reaction is extremely slow at room temperature, but more rapid at 550 K. This indicates the presence of a substantial activation barrier (between ~75 and ~140 kJ/mol), in disagreement with the barrierless reaction path predicted for the gas phase. This difference shows that, unsurprisingly, the surface has an important influence on the metalation in the monolayer range. On the other hand, if the Fe atoms are deposited on a 2HTPP monolayer, the reaction is rapid at room temperature, suggesting that the activation barrier observed in the case of pre-deposited iron is related to the formation of Fe clusters at the step edges. As shown in STM images, at the steps and in the clusters, the Fe atoms are relatively strongly bound compared to sites at the terraces.[Bu08] In this situation, the rate-limiting factor for the metalation is probably the two-dimensional (2D) phase equilibrium between the Fe clusters and Fe atoms diffusing across the surface, because only the latter can directly react with the porphyrin molecules. The 2D vapor pressure of iron may be too low at room temperature to observe a reaction on the timescale of several days, but increases exponentially with temperature, resulting in a rapid reaction at 550 K.

The rapid room-temperature reaction in the case of Fe *post*-adsorption indicates that the metalation reaction is fast enough to successfully compete with the diffusion of the Fe atoms to the steps and the formation of island there. In this context, it is important to note that the diffusion may be hindered by the porphyrin layer. In addition, the step sites are already occupied by 2HTPP, which means that the total energy gain resulting from the decoration of the steps with iron atoms or clusters is reduced by the binding energy of the molecules to the step sites. Both effects facilitate the metalation reaction and disfavour island formation at the steps. Another factor that may influence the reaction rate and may be responsible for the difference in reactivity for pre- and post-adsorption of Fe atoms is the metalation step itself. Although barrierless in the gas phase, on the surface this step includes cleavage of the bond between the Fe atom and the surface, which makes the occurrence of an activation barrier likely. In the case of Fe post-adsorption, the additional kinetic energy of the Fe atoms (gained by release of the adsorption energy) may help to surmount this activation barrier. This is an alternative explanation for the observation that the reaction proceeds rapidly already at room temperature. On the other hand, it should be mentioned that the electronic interaction between the surface and the iron atom is not completely suppressed when the latter is coordinated by the porphyrin.[Lu07] [Kr07] Although it has not been possible to quantify the strength of this

residual interaction yet, it is likely that it reduces, if attractive, the activation barrier for the coordination of the adsorbed Fe atom.

Similar to the results of the present study, the reaction of pre-deposited Zn atoms with 2HTPP on Ag(111) was found to be very slow at room temperature, but rapid at 550 K.[Kr07] However, metalation with Zn also requires elevated temperatures when the metal is post-deposited on the porphyrin monolayer. This is in agreement with the calculated gas phase mechanism, which predicts an activation barrier of 137 kJ /mol for the transfer of the first pyrrolic hydrogen atom to the Zn atom; this value is in good agreement with the experimentally determined overall activation energy (130 kJ /mol). Thus, the rate of the metalation with Zn may actually be controlled by an intramolecular reaction step, whereas the reaction of pre-deposited Fe with 2HTPP is controlled by a step in which the surface is involved. It is obvious that in Figure 5-13 b the metalation reaction for 2HTPP with Fe is not complete, although excessive amount of Fe was used. For metalation of 2HTPP with pre-deposited Fe, the Fe atoms first forms clusters on Ag(111), and the Fe atoms need to diffuse from the clusters to the porphyrin molecules to form FeTPP. The presence of porphyrin molecules may hinder the diffusion of Fe atoms to some extend, thus cause the incomplete metalation of 2HTPP.

Comparison with results from the literature

The reaction between terephthalic acid (TPA) and post-adsorbed Fe atoms on Cu(100) was studied by Tait et al. with STM, XPS, and low-energy electron diffraction (LEED).[Ta08] Supramolecular coordination interactions between Fe and TPA result in the formation of 2D metal-organic networks, whose structure depends on the Fe/TPA ratio. Upon coordination of the Fe atoms by the deprotonated TPA, the Fe 3p XP signal shifts to higher binding energy by 2.1 eV, which indicates that the Fe-TPA network contains cationic iron. This result contrasts the findings for FeTPP on Ag(111) in this study, but also previous XPS data for FePc[Ba08] and CoTPP on Ag(111)[Lu07] [Kr07], where the coordinated Fe and Co ions (with a nominal +2 oxidation state) show the same binding energies as adsorbed, but uncoordinated Fe and Co atoms. As was mentioned, this effect was attributed to electron transfer from the surface to the coordinated metal ions, which reduces the effective oxidation state of these ions. The fact that the TPA coordinated Fe ions are clearly cationic despite the presence of the surface is possibly related to the coordinating oxygen atoms, which have a higher electron negativity than the nitrogen atoms in porphyrin and phthalocyanine. In addition, differences in the valence electronic structure between Cu(100) and Ag(111) may play a role.

The interaction of pre-deposited cobalt on Au(111) with TPA on Au(111) was investigated by Clair et al.[Cl06]. It was shown that the TPA molecules are involved in

two competing processes: the formation of TPA islands (which are stabilized by pair wise dimerization, mediated by the carboxylic groups) and the reaction with the Co clusters, which leads to the dissolution of the clusters and the formation of a Co-TPA metal-organic network. (In this case, both the Co atoms and the TPA molecules need to be mobile to allow for formation of the metal-organic network.) Interestingly, the authors discuss the possibility of an equilibrium state between these two processes, although the fact that formation of Co terephthalate includes release of dihydrogen and its removal from the system implies that no thermodynamic equilibrium state can be reached. Instead, the reaction should proceed until either the TPA islands or the Co clusters have been completely consumed, depending on which species is in the minority. In this respect, the situation is very similar to that for Fe/2HTPP, which is also an irreversible reaction because of the release of H_2. If the reaction is found to be incomplete (as in the case of the metalation of 2HTPP multilayers), the reason is most likely related to kinetic hindrance rather than thermodynamic equilibrium.

Conclusion

Tetraphenylporphyrin (2HTPP) reacts with pre-deposited iron on Ag(111) surface under formation of iron(II)-tetraphenylporphyrin (FeTPP). The related STM results show that iron first forms clusters which decorate the steps on the Ag(111) surface.[Bu08] At room temperature, these Fe clusters do not react with 2HTPP, but the reaction is fast at 550 K, indicating a reaction barrier.

5.2.3. Adsorbed CoOEP and 2HOEP layers on Ag(111) surface

The metal centers of many M(II)-porphyrins and M(II)-phthalocyanines possess no axial ligands and therefore represent coordinatively unsaturated sites with potential catalytic or sensor functionality. In the adsorbed state, the underlying metal surface can occupy one of the axial sites and, as an additional ligand, influence the electronic structure of the metal center. There have been various studies of this phenomenon. [Sc00] [Sc01] [Ba04] [Lu07] For example, as already mentioned in Section 5.2, the UPS study of CoTPP monolayer on Ag(111) revealed the existence of a valence state at 0.6 eV below the Fermi energy (E_F), which is absent in the multilayer UP spectrum of CoTPP and the monolayer spectrum of metal-free 2HTPP on Ag(111)[Lu07]. The observation indicates that on the one hand the signal is induced by the interaction between the molecule and the substrate, on the other hand the signal is related to the presence of the Co ion [Lu07] [Go09].

The here outlined interpretation[Lu07] [Fl07C] [Go09], however, has been challenged by a combined STM and NEXAFS study of CoTPP on Cu(111), which focuses on the interplay between molecular conformation and electronic structure. Using NEXAFS,

it was shown that the CoTPP molecules undergo a surface-induced distortion and acquire a saddle-shaped conformation in the adsorbed state.[We08A] [We08B] In this geometry, two opposing pyrrole rings of the porphyrin macrocycle are bent towards the surface by 20° relative to the surface plane, while the other two pyrrole rings are bent away from the surface. As already mentioned in Section 5.2, for the free CoTPP molecule, it was shown that angles below 60° lead to a deformation of the porphyrin macrocycle and that a dihedral angle of 35° causes a substantial increase of the total energy of the molecule (between 73.7 kJ/mol at 40° and 136.8 kJ/mol at 30°).[Wö08] The averaged tunnelling spectrum of the thus distorted CoTPP molecule on Cu(111) shows an electronic state at 0.6 eV below E_F [We08A] [We08B], similar to the previous observations for CoTPP on Au(111) (with STS) [Ba04] and CoTPP on Ag(111) (with UPS)[Lu07], where this state was attributed to the interaction between the Co ion and the metal substrate. However, visualization of the frontier orbitals of CoTPP on Cu(111) by tunnelling spectroscopy mapping (dI/dV mapping) revealed that this state is not localized on the central Co ion. Instead, the maximum orbital coefficients appear at two opposing pyrrole units of the deformed porphyrin ligand. [We08A] [We08B] These findings cast doubts on the previous interpretation[Lu07] [Fl07B] of the adsorption-induced valence signal at 0.6 eV: If this signal is related to the Co-substrate interaction, one should expect that the Co ion (rather than the pyrrole units of the ligand) appears as a bright protrusion when the bias voltage is adjusted so as to allow for tunnelling from this state. Instead, the dI/dV mappings suggest an alternative explanation for the changes in the valence electronic structure: The occurrence of the state at 0.6 eV may be directly related to the deformation, which lifts the degeneracy of electronic states (occupied and unoccupied) and thereby also influences the surface chemical bond of the ligand. Accordingly, the new signal could arise from the ligand-surface interaction (for example, occupation of the former LUMO by electrons from the substrate, as has been observed for other aromatic molecules such as NTCDA and PTCDA on Ag(111)[Lu07] [Be07]) rather than from the interaction between metal center and surface. The lack of an adsorption-induced new valence state in the case of the 2HTPP monolayer could be explained with a different degree of deformation of the metal-free ligand. (Note that STM and NEXAFS studies of the structurally similar 2H-tetrapyridylporphyrin on Cu(111) suggest that the adsorbed metal-free macrocycle is more distorted than the corresponding metal complex.[Au07B] [Kl08])

To discriminate between the effects of molecular deformation and surface interaction on the electronic structure and to clarify the origin of the state at 0.6 eV below E_F, we studied cobalt octaethylporphyrin (CoOEP) monolayers on Ag(111) with XPS, UPS and STM. In CoOEP, the Co ion is exposed to the same coordination environment as in CoTPP, but the molecules adsorb in a flat, undistorted conformation, as shown in the STM image (Figure 5-18). This is to be expected based on its molecular structure and is in line with previous STM investigations of NiOEP on Au(111)[Sc02] [Yo06] [Pa06] NiOEP on Cu(111), Ag(001) and Ag(111)[Ra06], NiOEP on graphite[Og06] [Sc07], and

CoOEP on Au(111)[Yo04]. The here observed surface-induced changes in the valence electronic structure of CoOEP on Ag(111), however, are virtually identical to those reported for CoTPP, proving that they are predominately caused by the interaction between the metal center and the substrate, and not by molecular distortions. For comparison, 2HOEP was also investigated with XPS and UPS. Figure 5-15 shows the molecular structure of CoOEP and 2HOEP molecules.
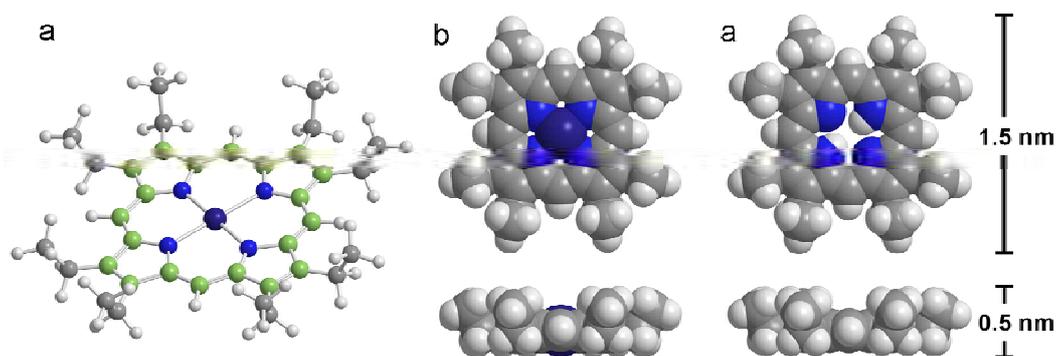
Figure 5-15. (a) Ball-and-stick model of cobalt octaethylporphyrin (CoOEP). For clarity, the carbon atoms of the conjugated porphyrin cycle are shown in green color, those of the ethyl groups in grey. Space-filling models of (b) CoOEP and (c) 2H-octaethylporphyrin (2HOEP) in top and side view.

Multilayer desorption series of 2HOEP and CoOEP on Ag(111) surface

Similar to phthalocyanine monolayers, porphyrin monolayers in this thesis are usually prepared by thermal desorption of an adsorbed multilayer on Ag(111) surface. Figures 5-16 and 5-17 show the XP spectra of the multilayer desorption temperature series for 2HOEP and CoOEP on Ag(111) surface, respectively. For 2HOEP multilayer, after annealing at 525 K, a shift of the C 1s XP signal of about 0.8 eV can be observed, while no sudden decrease of the signal intensity can be seen. The small decrease of the C 1s signal intensity is again due to the small thickness of the multilayer (bilayer) and the detection at grazing emission, as already mentioned in Section 5.1.1. For CoOEP multilayer, after annealing the C 1s peak position remains the same until 575 K, while a sudden decrease of the intensity happens after annealing at 525 K. Thus from the C 1s peak position and intensity, 525 K was chosen for both 2HOEP and CoOEP as the temperature of the thermal desorption to prepare a corresponding porphyrin monolayer, referring to the peak positions and peak intensities.
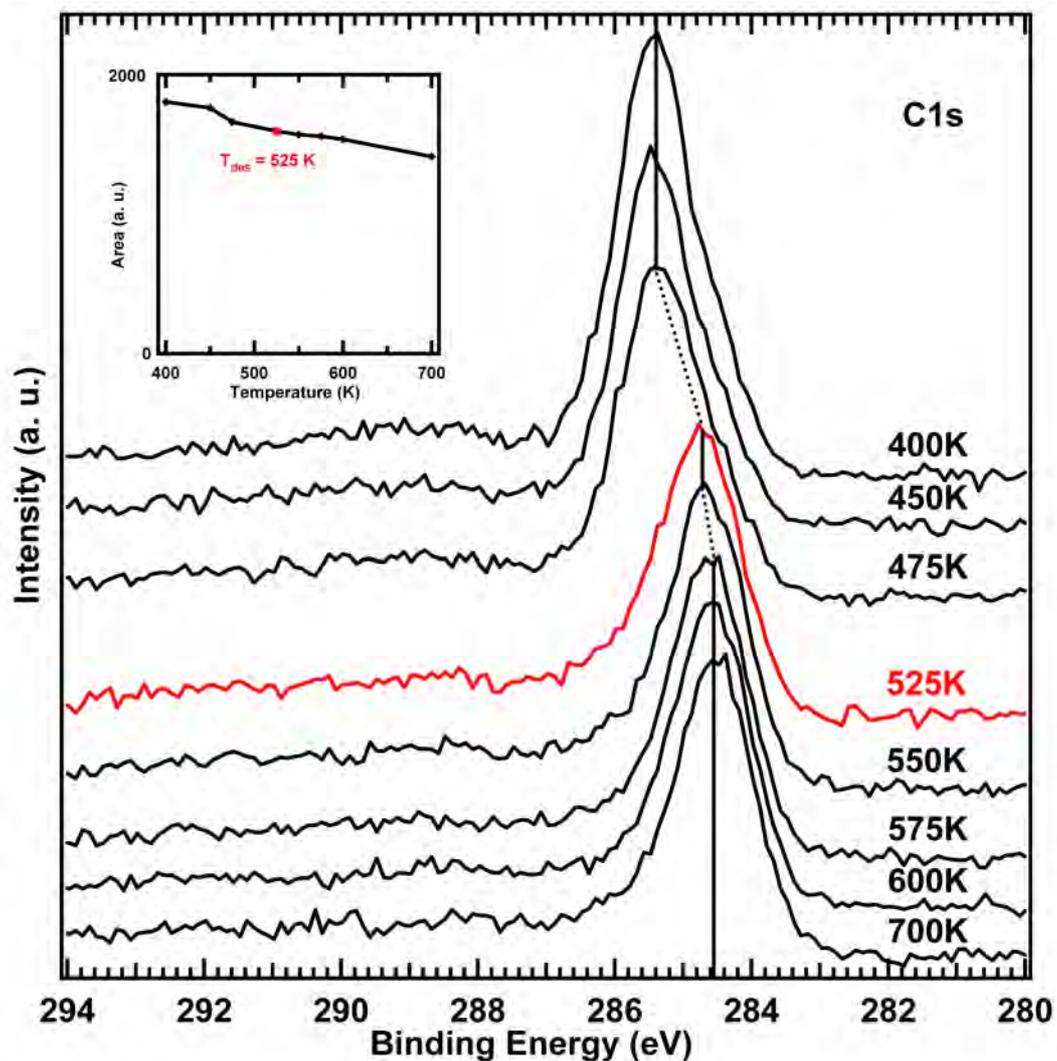
Figure 5-16. C 1s spectra taken after annealing of a 2HOEP multilayer on Ag(111) at the indicated temperatures. Inset: integrated peak areas after annealing for 30 s at different temperatures. The measurements were performed at room temperature with a detection angle of 70°.
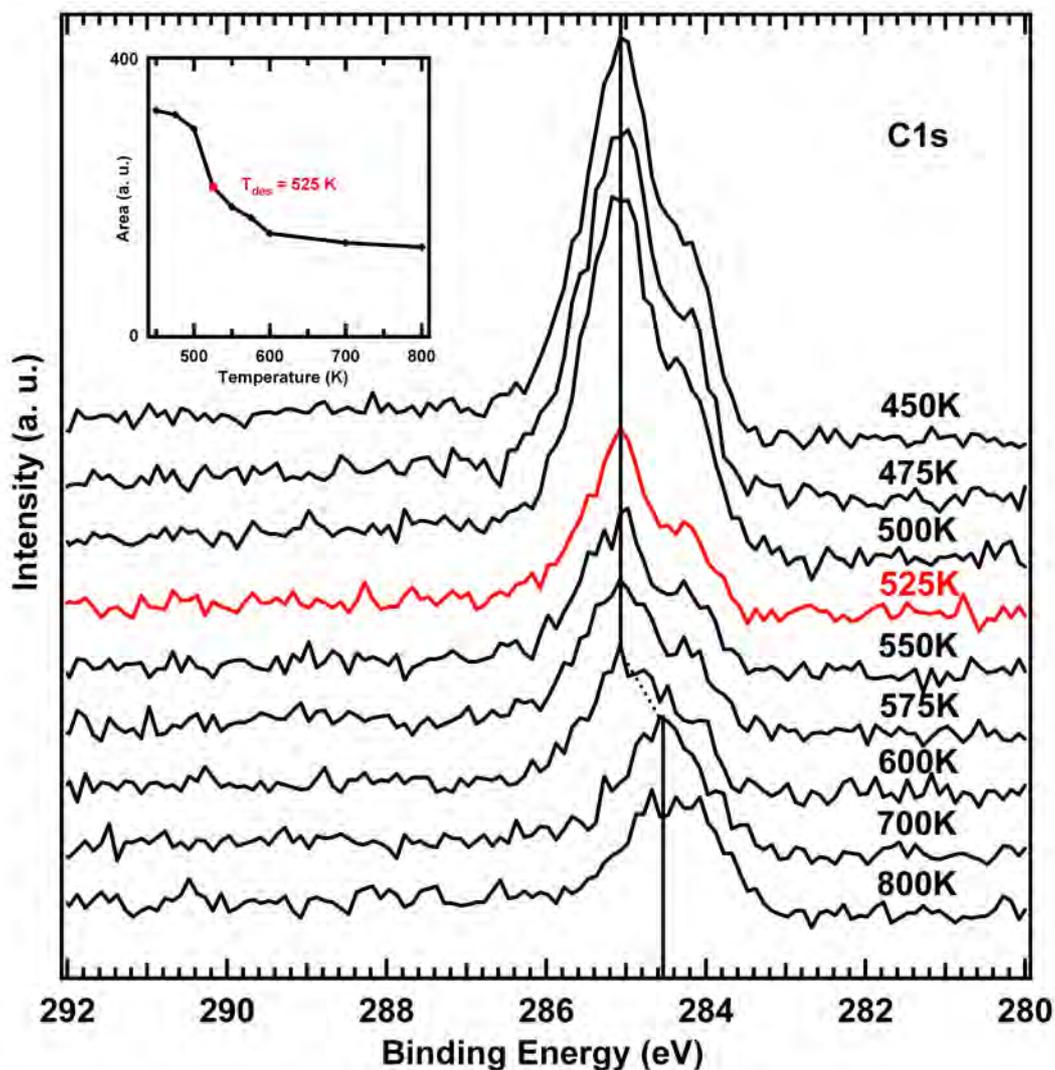
Figure 5-17. C 1s spectra taken after annealing of a CoOEP multilayer on Ag(111) at the indicated temperatures. Inset: integrated peak areas after annealing for 30 s at different temperatures. The measurements were performed at room temperature with a detection angle of 70°.

Structural study with LEED

Figure 5-18 shows the LEED pattern of a CoOEP monolayer on Ag(111) taken with electron energy of 22 V. By comparison to the LEED pattern for the clean Ag(111) surface (not shown), the structure and lattice constant of the CoOEP monolayer has been determined with the method described in Section 3.3.2. CoOEP forms a hexagonal structure on Ag(111) with a lattice constant 1.45 nm. This is in good agreement with an STM study of a CoOEP monolayer on Ag(111) surface by F. Buchner et al., as shown in Figure 5-19.[Ba09] With STM the structure is determined to be an oblique (but almost hexagonal) arrangement with lattice constants of $a = 1.550 \pm 10$ nm and $b = 1.45 \pm 0.10$ nm and an enclosed angle $\alpha = 60° \pm 3°$.[Ba09]
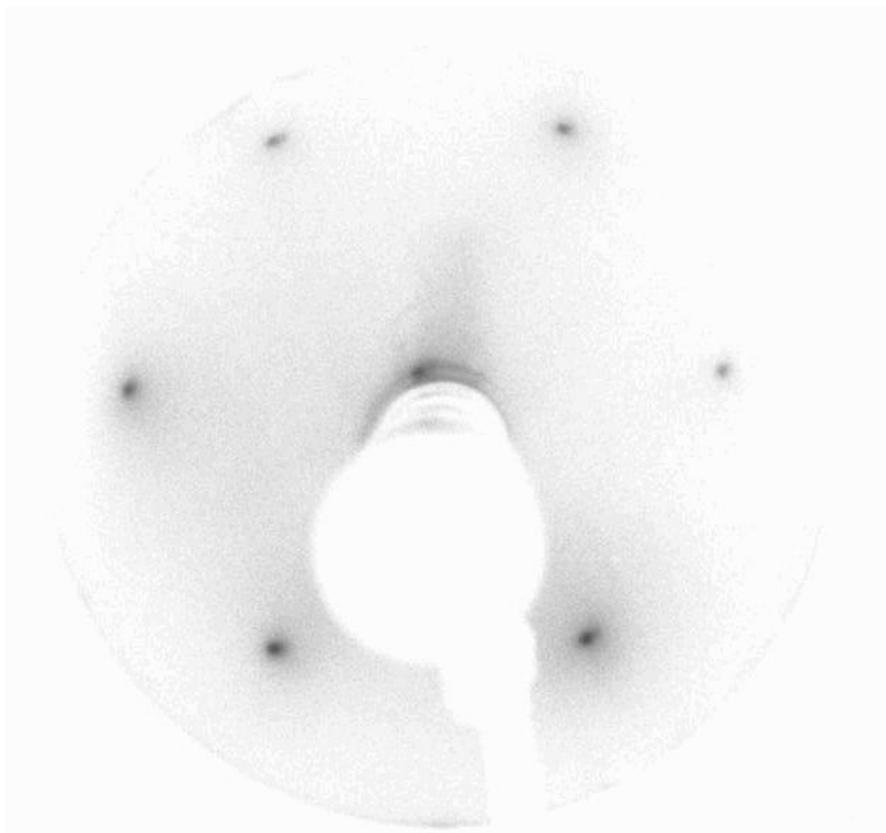
Figure 5-18. LEED pattern of CoOEP monolayer (with electron energy 22 eV) on Ag(111). Note that the 00-reflex is not in the center of the phosphor screen, probably because of the sample adjustment problem, e.g., the sample surface is not perpendicular to the electron beam.
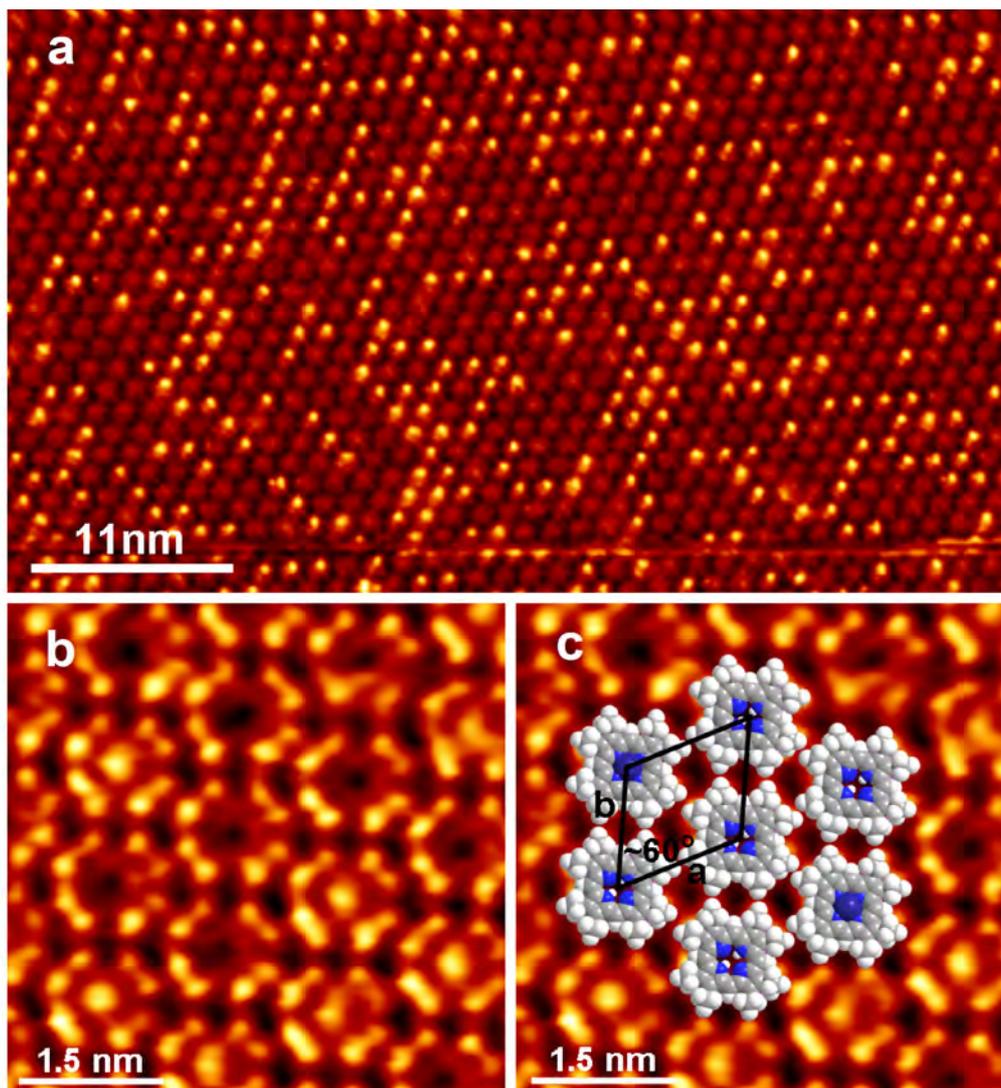
Figure 5-19. (a) STM micrograph of an intermixed 2HOEP/CoOEP layer prepared by vapor deposition of a nominal 2:1 mixture of the respective species onto the Ag(111) surface. Counting over large areas results in 34% protrusions, which can be identified with CoOEP molecules. Tunneling parameters: I_{set} = 31 pA, U_{gap} = −1.17 V. (b, c) STM micrograph of a self-assembled intermixed 2HOEP/CoOEP layer on Ag(111). Tunneling parameters: I_{set} = 37 pA, U_{gap} = −0.20 V. In (c), the micrograph is superimposed by scaled models of the corresponding OEP molecules and the unit cell is indicated (a = 1.55±0.10 nm, b = 1.45±0.10 nm).[Ba09]

XPS study of adsorbed 2HOEP and CoOEP layers on a Ag(111) surface

Figure 5-20 shows the Co $2p_{3/2}$ XP spectra of the CoOEP multilayer and monolayer on the Ag(111) surface. The main peak for the CoOEP multilayer is located at 780.6 eV, which is a typical position for cobalt(II) compounds[Wa79] [Ki75], and thus in agreement with the formal oxidation state of the cobalt ion in CoOEP. The signal shows a complex multiplet structure, which results most likely from the open-shell

character of the Co ion (d^7) and which is in agreement with previous measurements on CoTPP and cobalt(II) tetrakis-(3,5-bis-(tert-butylphenyl) porphyrin (CoTTBPP).[Lu07] [Sc00] In the XP spectrum of the CoOEP monolayer, the main peak appears at a much lower binding energy of 778.9 eV, which is typical of Co(0). Again, the signal shows a satellite structure that is attributed to the paramagnetic character of the Co center. Direction and magnitude of the surface-induced chemical shift of the Co 2p signal are very similar to the shifts observed previously for CoTPP and CoTTBPP on Ag(111). The absolute Co $2p_{3/2}$ binding energies of CoOEP multilayers and monolayers, however, are approximately 0.6-0.7 eV higher than those for CoTPP and CoTTBPP. [Lu07]
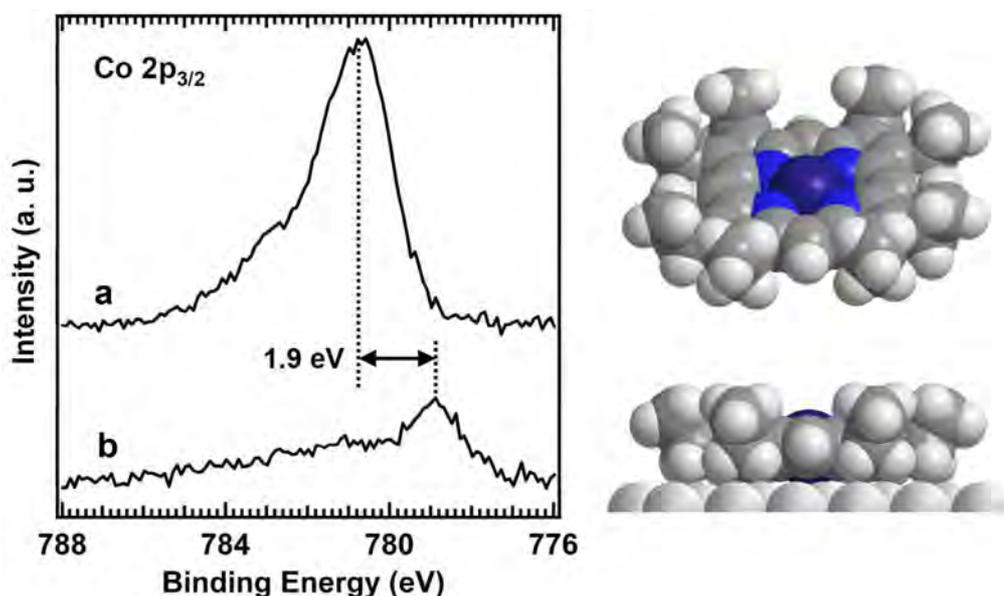
Figure 5-20. Co $2p_{3/2}$ XP spectra of CoOEP on Ag(111). (a) CoOEP multilayer (~10 monolayers), (b) CoOEP monolayer.

The strong shift of the Co 2p signal (-1.9 eV, also listed in Table 5-3), suggests a direct electronic interaction of the Co ion with the underlying Ag surface. If initial state effects are taken into account, the direction of the shift can be interpreted as a partial reduction of the Co ion by electrons from the silver surface, as has been proposed for CoTPP on Ag(111).[Lu07] In addition, final state effects such as charge-transfer screening, which would also indicate a substantial electronic interaction between the Co ion and the Ag surface, could contribute to the shift.

Figures 5-21 and 5-22 present the XP spectra in the N 1s and C 1s regions for CoOEP and 2HOEP layers. Contrary to the substantial shift of the Co $2p_{3/2}$ signal, the C 1s signals of CoOEP multilayer and monolayer differ by only 0.6 eV, while no significant shift is observed for the N 1s signal (also listed in Table 5-4). The shift of the C 1s signal towards lower binding energy can be attributed to final state effects,

especially a more effective screening of the final core hole by the metal surface as compared to the weaker dielectric screening in the multilayer. The larger shift of the C 1s signal of CoOEP as compared to that of CoTPP (see Table 5-4) most likely reflects the shorter average distance of the C atoms to the substrate for CoOEP and the resulting more efficient screening. The negligibly small shift of the N 1s signal suggests that the relaxation shift is compensated by a concomitant chemical shift to higher binding energies. This shift possibly results from a chemical bond between the N atoms and the Ag surface, which leads to a transfer of electron density to the substrate. Similar interactions of the porphyrin nitrogen atoms and the substrate have previously been reported for FeOEP on a Co film.[We07] The bonding mechanism of CoOEP on Ag(111) can thus be described by a bonding-backbonding synergism, in which electron density is transferred from the substrate to the Co ion and partially returned to the substrate via the nitrogen atoms. The C 1s peak of CoOEP multilayer shows at least two components. This can be attributed to the aromatic carbon atoms (20 carbon atoms) and the carbon atoms of the ethyl groups (18 carbon atoms). The carbon atoms of the ethyl groups can be further divided to carbon directly (8 carbon atoms) and not directly (8 carbon atoms) connected to the aromatic ring. This makes the C 1s peak contain three components, with the ratio 5 : 2 : 2 from higher to lower binding energy side.
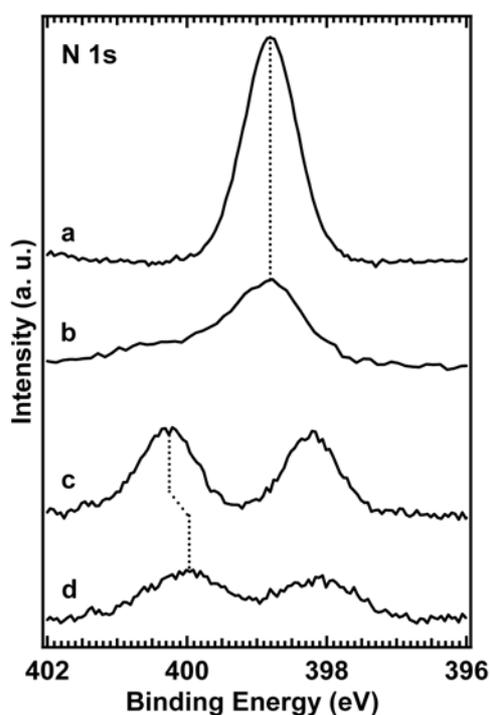
Figure 5-21. N 1s XP spectra of (a) CoOEP multilayers, (b) CoOEP monolayer, (c) 2HOEP multilayers, and (d) 2HOEP monolayer.
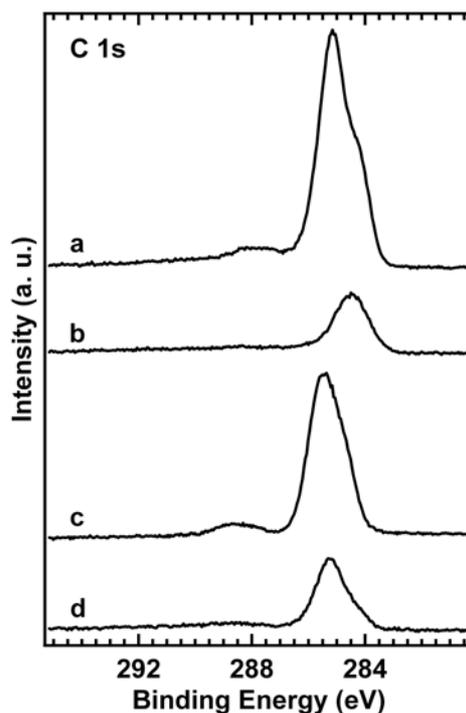
Figure 5-22. C 1s XP spectra of (a) CoOEP multilayers, (b) CoOEP monolayer, (c) 2HOEP multilayers, and (d) 2HOEP monolayer.

Table 5-4. XPS core level shifts (in eV) between multilayer and monolayer coverages of various porphyrins on Ag(111). All signals shift towards lower binding energy in the monolayer. Data for CoTPP taken from ref. [Lu07]

	CoOEP	2HOEP	CoTPP	2HTPP
Co 2p	1.9	-	1.8	-
C 1s	0.6	0.2	0.2	0.3
N 1s	0	0.3	0.3	0.1

UV Photoelectron Spectra and Work Function Changes

Figure 5-23 shows UV photoelectron spectra of CoOEP multilayer, CoOEP monolayer, 2HOEP monolayer, and clean Ag(111). The multilayer spectrum (top) features an intense signal centered at 1.9 eV below E_F. This signal is attributed to the highest occupied molecular orbital of the complex, possibly a singly occupied orbital (SOMO). In the monolayer spectrum (second from top), this peak is shifted to 1.7 eV, most likely due to the more efficient screening of the hole by the metal surface (relaxation shift). Apart from this signal, the monolayer spectrum shows an additional peak at 0.6 eV, which is absent in the multilayer spectrum and therefore related to the interaction of the CoOEP molecule with the Ag(111) surface. In order to clarify the role of the cobalt ion in this interaction, comparison with a monolayer of the metal-free ligand, 2H-octaethylporphyrin (2HOEP) was made. In the respective UP

74

spectrum (third from top), the additional peak is absent, indicating that the cobalt ion is indeed involved in the interaction. In fact, the 2HOEP monolayer spectrum completely lacks adsorbate-induced contributions in the energy range (or they have very low intensity). Thus, the SOMO related signal that appears in the CoOEP spectra is probably also related to the presence of the Co ion and probably corresponds to orbitals with predominant Co 3d character. Comparison with the UP spectra of CoTPP on Ag(111)[Lu07] show that the SOMO related signal appears at 2.3 eV in the monolayer spectrum and at 1.8 eV in the monolayer, i.e., at slightly higher binding energies than in the case of CoOEP. The interaction induced signal at 0.6 eV, however, has the same position for CoTPP and CoOEP.
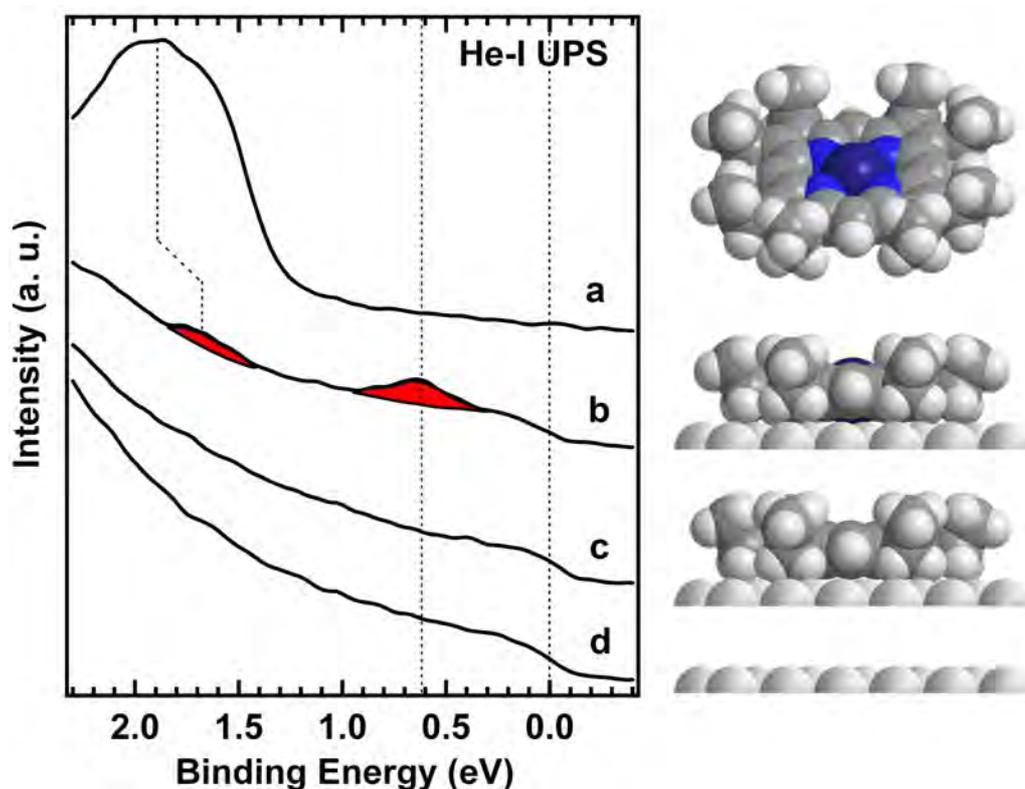
Figure 5-23. He-I UP spectra of CoOEP multilayer (~five monolayers), CoOEP monolayer, 2HOEP monolayer, and the clean Ag(111) surface (from top to bottom).

Additional information about the nature of the molecule-substrate interaction was obtained from the adsorbate-induced work function changes (or vacuum level shifts), which were extracted from the UP spectra as described in Section 3.1.4. The full range UP spectrum is shown in Figure 5-24, and the changes of the work function are listed in Table 5-5. CoOEP and 2HTPP monolayers lower the work function of the Ag(111) surface by 0.84 eV and 0.44 eV, respectively. Reductions of the work function by organic molecules have frequently been observed and have been attributed to the Pauli repulsion between the electrons of the molecule and those of the metal. This "cushion effect" leads to a depletion of charge between the molecule

and the metal and is thus responsible for the formation of the adsorption-induced dipole layer, which causes the work function change.[Wi05] The difference in $\Delta\Phi$ between the monolayers of CoOEP and 2HOEP may be attributed to the presence of the Co ion and its electronic interaction with the Ag surface. In Table 5-5, the work function changes caused by CoOEP and 2HOEP are compared to the respective data for CoTPP and 2HTPP on Ag(111), as were reported in ref. [Lu07]. CoOEP induces a larger work function change than CoTPP, while 2HOEP has less influence on the work function than 2HTPP. Table 5-5 also shows the positions of the highest occupied molecular levels; these values equal the barrier heights for hole injection at the organic/metal interface. [Is99] All data in Table 5-5 refer to monolayer coverage. The energy of the highest occupied level for 2HOEP could not be determined with certainty, because the intensity of the levels close to the Fermi energy is obviously too low. The first clearly visible signal at 4.1 eV below E_F is probably not derived from the HOMO state.
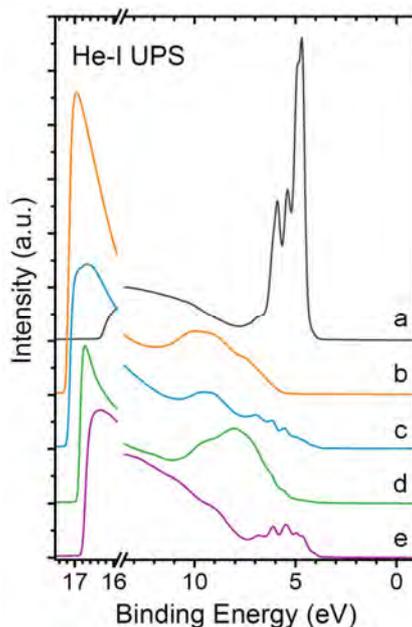
Figure 5-24. He-I UP spectra of (a) the clean Ag(111) surface, (b) CoOEP multilayer, (c) CoOEP monolayer, (d) 2HOEP multilayer and (e) 2HOEP monolayer.

Table 5-5. Work function changes $\Delta\Phi$, and energies of the highest occupied molecular levels with respect E_F (in eV). Data for CoTPP and 2HTPP from ref. [Lu07]

	CoOEP	2HOEP	CoTPP	2HTPP
$\Delta\Phi$	-0.84	-0.44	-0.72	-0.84
ε_F^V	-0.60	(-4.1)	-0.62	-2.4

A schematic energy diagram of the CoOEP/Ag(111) interface at monolayer coverage is presented in Figure 5-25. It was derived from UPS data within the approximation of Koopmans' theorem[Ko34] and is in line with the work of Seki et al.[Yo96] [Is99] about porphyrin/metal interfaces, in which the energy levels of the porphyrins are fixed to the vacuum level of the metal with a finite energy shift at the interface (work function or vacuum level shift).
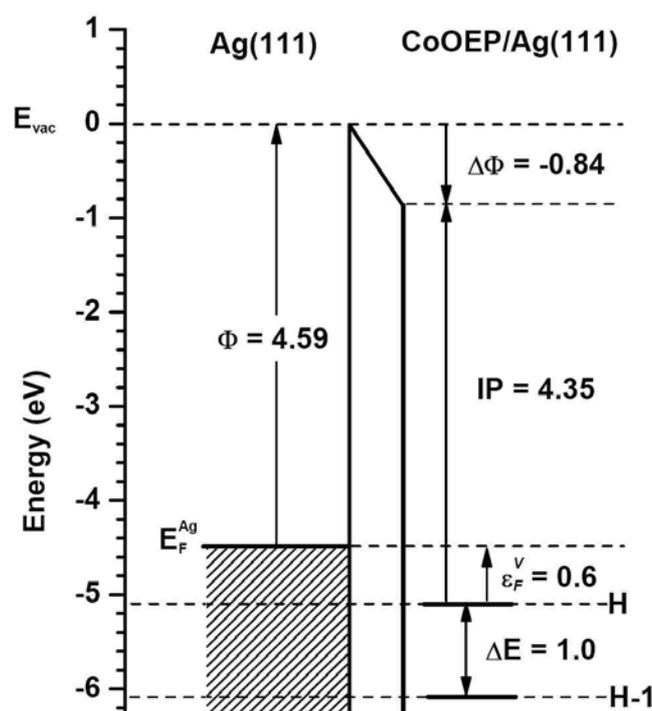
Figure 5-25. Schematic diagram of the electronic levels at the CoOEP/Ag(111) interface at monolayer coverage. Φ is the work function of clean Ag(111) and $\Delta\Phi$ the adsorbate-induced work function shift or shift of the vacuum level. IP denotes the ionization potential of the adsorbed CoOEP. ε_F^V is the position of the highest occupied molecular level with respect to E_F and equals the barrier height for the hole injection at the organic/metal interface. H is the highest adsorbate-related level, induced by the interaction between the Co ion and the substrate. H-1 is the former highest occupied level of the CoOEP molecule.

Conclusions

Despite the undistorted conformation of the molecule, the monolayer UP spectrum of CoOEP shows the same signal at 0.6 eV as was found for the distorted CoTPP molecule. This is clear proof that the 0.6 eV state is directly related to the interaction of the Co porphyrin with the surface and not caused by molecular distortion. The fact that the state is not found in the monolayer spectrum of the metal-free 2HOEP indicates that the Co ion plays the decisive role in this interaction.

5.2.4 Attachment of small gas molecules to a porphyrin monolayer adsorbed on a Ag(111) surface

As a central component of the hemoglobin subunits, iron porphyrin (heme) plays an important role in the oxygen transport process in the blood of mammals. Analogouses processes have potential applications in the field of sensors[Sc05], organic solar cells[Ra00] and catalysis[Hu07], since metalloporphyrins contain a metal center which is not coordinatively saturated. Therefore, related experiments have been conducted by coordinating oxygen molecules on a FeTPP monolayer. The FeTPP monolayer was firstly synthesized *in situ* in the UHV chamber by depositing Fe atoms to a 2HTPP monolayer on Ag(111), which is described in the dissertation of Dr. Flechtner.[Fl07C] Compared to the amount needed for the complete metalation of 2HTPP monolayer (0.037 ML), only 0.025 ML Fe was used in this experiment to avoid excessive atomic Fe, as adsorbed Fe is expected to react readily with oxygen, which may potentially lead to erroneous results of the experiment. After metalation, oxygen molecules were introduced into the chamber as described in Section 4.3.4. Oxygen was dosed for 90 min with a partial pressure of 8×10^{-7} mbar, which equals a dosage of 3250 L. The sample was held at room temperature during the dosing process. XPS measurements were carried out before and after oxygen dosing.

Figure 5-26 shows the XP spectra in the Fe $2p_{3/2}$ region before and after oxygen dosing. The Fe $2p_{3/2}$ spectrum taken before oxygen coordination contains a main signal and some satellite structures. The main signal at 707.2 eV is near a typical Fe(0) position. After oxygen attachment the main signal is shifted to 709.3 eV, while a small signal remains at a Fe(0) position. The apparent change of the Fe $2p_{3/2}$ spectra indicates that oxygen molecules have coordinated to the FeTPP molecules and lead to the change of electron density on Fe. The change of electron density on Fe may be the result of different effects. Firstly, it can come from the direct transfer of electron density from Fe to O_2, which leads to the formation of superoxide (O_2^-) or peroxide (O_2^{2-}). Secondly, as already observed for NO coordination on CoTPP and FeTPP,[Fl07B] [Fl07C] the coordination of O_2 on FeTPP may also suppress the electronic interaction between the Fe ion and the underlying substrate. This would also reduce the electron density transferred from the substrate to the Fe ion.
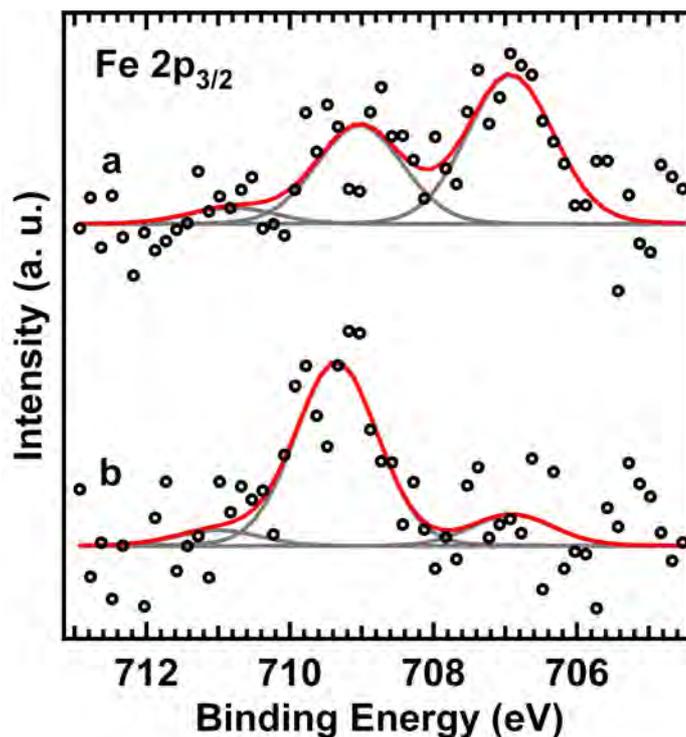
Figure 5-26. XP spectra in the Fe $2p_{3/2}$ region before (a) and after (b) oxygen coordination.

Figure 5-27 shows the O 1s spectrum measured on the FeTPP monolayer after dosing of oxygen. The oxygen spectrum can be fitted with two components centered at 530.6 eV and 529.3 eV. The two components have equal intensity, indicating two different oxygen species with the ratio 1:1. This is probably due to the end-on binding of an oxygen molecule to the Fe atom in the center of a FeTPP molecule, which forms a superoxide complex, as opposed to a peroxide complex for side-on coordination. A simplified sketch of the end-on and side-on coordination modes is shown in Figure 5-28.
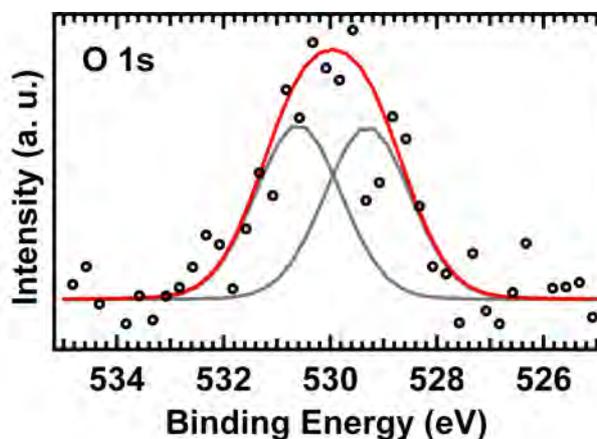
Figure 5-27. XP spectra in the O 1s region after oxygen dosing
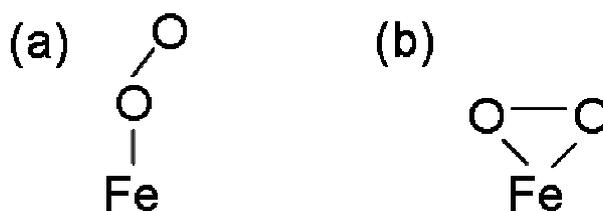
Figure 5-28 Simplified sketch of the end-on (a) and side-on (b) coordination modes of O_2 on the Fe center of a FeTPP molecule.

The changes in the Fe $2p_{3/2}$ spectra and the O 1s spectrum show that oxygen molecules can coordinate to the FeTPP molecules on the central Fe atoms, most likely in form of an end-on binding mode. Table 5-6 shows the results of unpublished DFT calculations[Sh10] for the binding energies of small molecules on the central metal atoms of different metalloporphyrins. It is obvious that the bond energy of CO on Fe(II)TPP is much higher than that of O_2 on Fe(II)TPP. With a bond energy of -36.58 kJ/mol for O_2 on Fe(II)(P), the Fe(II)(P)-O_2 complex should not be formed at room temperature, which is contradictory to our experimental result. Possibly there is influence from the Ag(111) surface in the experiment, which makes the result different from the gas phase calculation. Furthermore, the gas phase DFT calculation may be of limited accuracy.

Table 5-6 Results of gas phase DFT calculations of the binding energies (in kJ/mol) of small molecules on the central metal atoms of different metalloporphyrins[Sh10]

Porphyrin	DFT	NO	CO	CN	O_2	NH$_2$	H$_2$O
Zn(P)	B3LYP	-7.83	-16.62	-290.9	-	-66.12	-54.92
	PW91	-1.00	-10.46			-56.05	-45.04
Ni(P)	B3LYP	-7.91	-6.66			-6.91	-20.18
	PW91	-31.06					-17.66
Co(P)	B3LYP	-15.91	-20.43	-341.0	-	-51.32	-42.95
	PW91	-115.7	-50.73				-43.24
^{1}Fe(II)(P)	B3LYP	-166.9	-170.3	-279.2	-36.58	-149.2	-110.4
^{3}Fe(II)(P)	B3LYP	-51.19	-54.54	-163.7		-32.73	-

In order to clarify if CO molecules can replace O_2 molecules in the FeTPP-O_2 complex, an exchange experiment has been conducted by dosing CO molecules onto the monolayer of adsorbed FeTPP-O_2 complexes. CO was dosed at room temperature for 60 min with the partial pressure of 1 x 10^{-6} mbar, which equals a dosage of 2700 L. However, as shown in Figure 5-29, no significant changes have been observed in the Fe $2p_{3/2}$ and O 1s XP spectra.
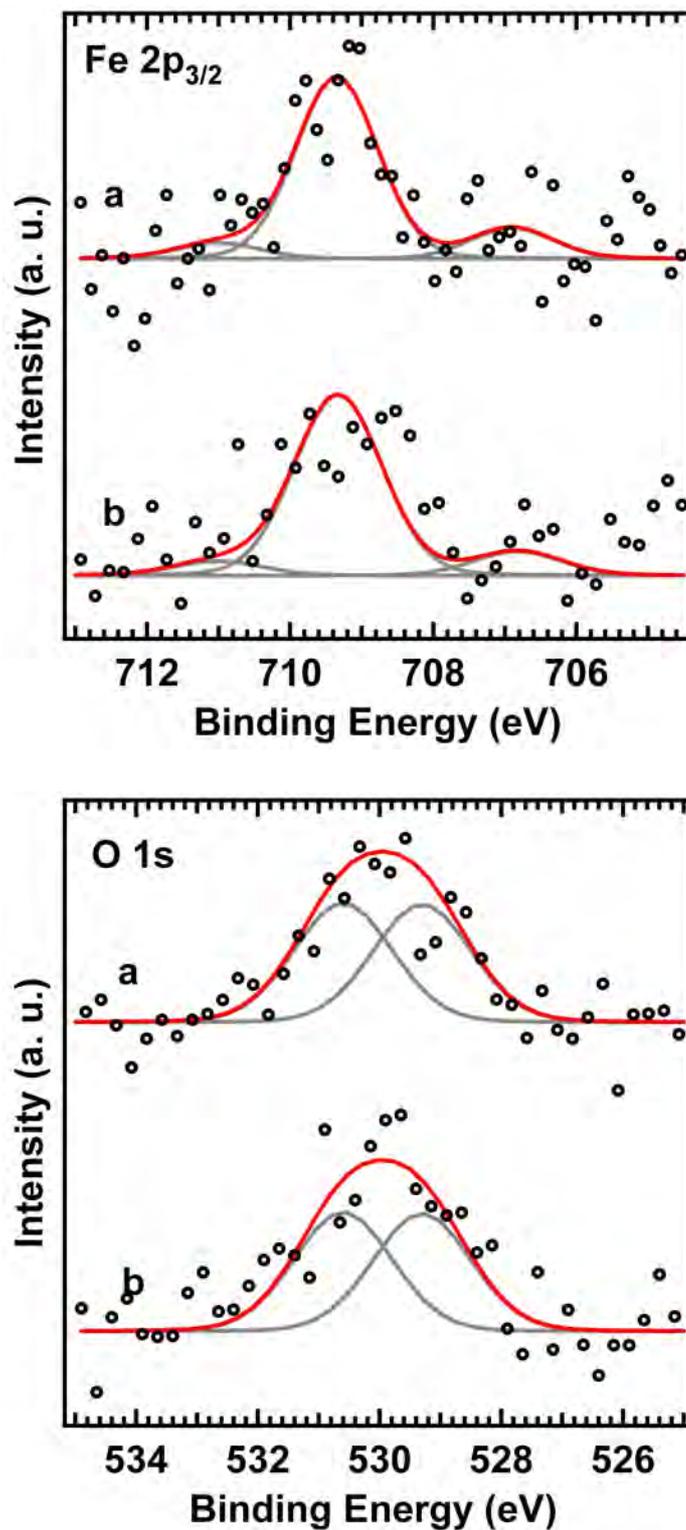
Figure 5-29. XP spectra in Fe $2p_{3/2}$ and O 1s regions. (a) FeTPP-O_2 complex, (b) FeTPP-O_2 complex after exposed in 2700 L CO at 300 K.

From the above results we conclude that O_2 in the FeTPP-O_2 complex can not be exchanged by CO under the here applied conditions. Since the exchange of O_2 by CO

in the FeTPP-O_2 complex contains at least two steps, i.e., firstly breaking of the bond between FeTPP and O_2, secondly formation of the bond between FeTPP and CO, this reaction may have an activation barrier. This would explain why no exchange occured by simply introducing CO into the chamber at room temperature. In order to examine whether the exchange occurs at higher temperatures, further experiment need to be executed.

One can see that the signal to noise ratio of the XP spectra in the gas dosing experiments is low, which limits the significance of the study. After the upgrade of the Scienta system in January 2009, the signal to noise ratio has been increased, this enables us to obtain more reliable results for the corresponding experiments in the successive PhD studies.

6. Adsorbed tetrapyrrole complexes on a Au(111) surface

Previous studies of ZnTPP, CoTPP, FeTPP, CoOEP, FePc, and SnPc have shown that on Ag(111) the electronic interaction between the metal ion and the underlying substrate depends strongly on the nature of the tetrapyrrole metal center, and the conformation of the tetrapyrrole molecules depends on both the metal ion and the tetrapyrrole framework.[St06] [Fl07C] [Lu07] [Ba08] [Ba09] A related question concerns the influence of the different substrates on the electronic interaction between the metal ion and the substrate, and on the conformation of the tetrapyrrole complex. Here, we chose Au(111) as the substrate to study this question, and the porphyrin molecules we used are CoTPP, 2HTPP, CoOEP and 2HOEP, which have been extensively studied on Ag(111). For a comparison between porphyrin and phthalocyanine, CoPc and 2HPc have also been studied on Au(111). This combination seemed a logical choice, since the interaction of Co porphyrin with the homologous Ag(111) surface is presently the best understood system of this class. Both substrates are similar in that they belong to the face centered cubic (fcc) noble metals with a fully occupied d band. However, the (111) surfaces have different structure despite having the same nominal orientation, because Au(111) reconstructs,[Ha85] [Wö89] [Ba90] while Ag(111) does not. Moreover, there has been extensive investigation of the structural properties of porphyrin and phthalocyanine monolayers on Au(111), which allows us to focus here on their electronic properties.

6.1. Adsorbed porphyrins on a Au(111) surface

2HTPP, CoTPP, 2HOEP and CoOEP thin films (multilayers and monolayers) were prepared on Au(111) surface using the method describe in Section 4.3.2. Their properties and the interaction with the underlying Au(111) substrates were investigated with XPS and UPS.

6.1.1. Multilayer desorption series

To determine the temperature for monolayer preparation, multilayer desorption series were executed. For 2HTPP, 2HOEP and CoOEP, it was routinely realized with XPS. The spectra were shown in Figure 6-1, 6-3 and 6-4. For CoTPP with UPS an alternative approach was used. Since UPS spectra of CoTPP monolayer and multilayer show different signals, presenting different valence band structures, the temperature series measured with UPS can also be used to determine the multilayer desorption temperature.

Figure 6-1 shows the multilayer desorption temperature series for 2HTPP. As already described in Section 5.1.1, with the C 1s peak position and peak intensity, a temperature in the range from 520 K to 575 K can be chosen as the multilayer desorption temperature. Thus 540 K, which is in the middle of this temperature range, was chosen to prepare a 2HTPP monolayer. It is worth mentioning that the experiments of the multilayer thermal desorption series were all carried out at grazing emission with detection angle 70°, which caused the experiments to be very surface sensitive and decreased the difference in intensity between multilayer and monolayer coverage. In order to obtain more reliable results, the multilayer desorption measurements should be done under normal emission in the future, and TPD measurements should also be carried to obtain complementary results.
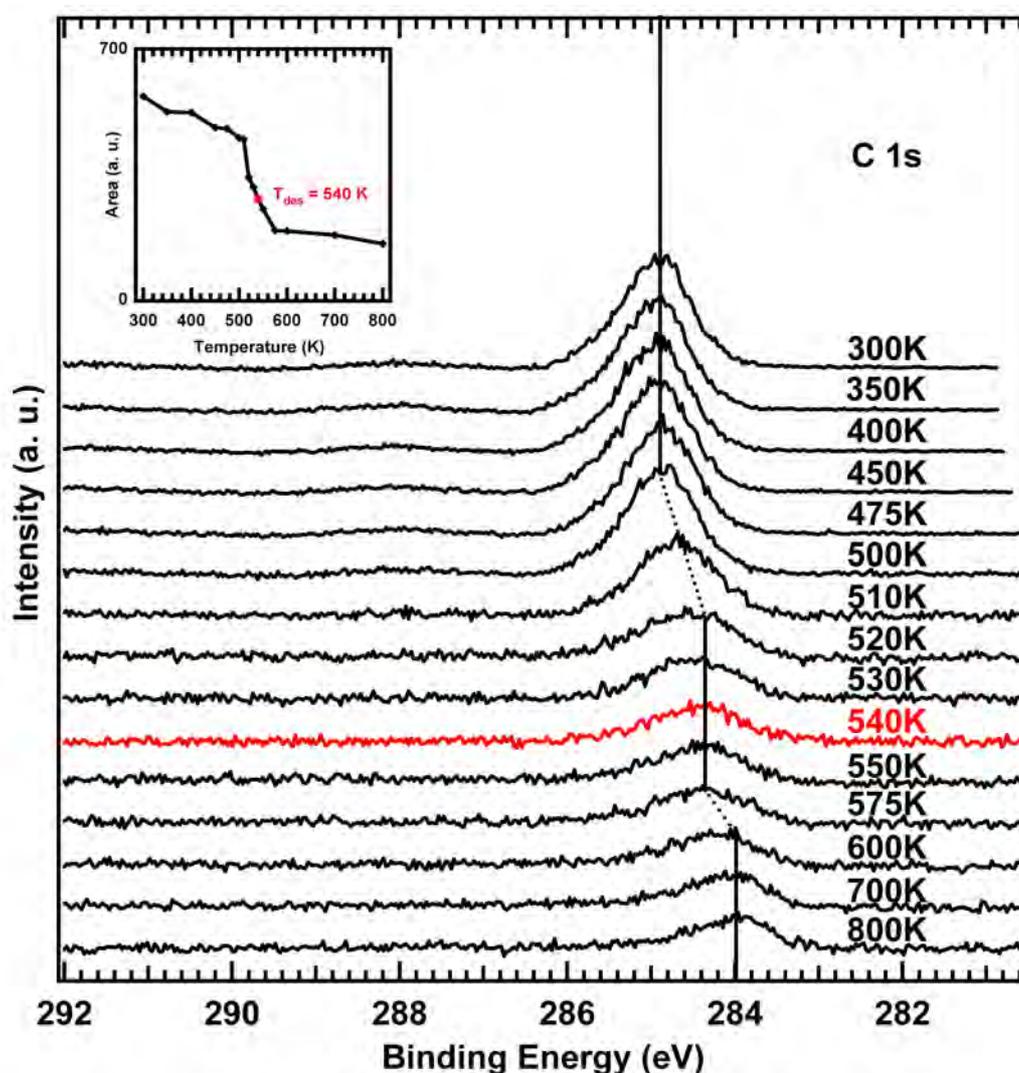
Figure 6-1. C 1s spectra taken after annealing of a 2HTPP multilayer (~ 5 monolayers) on the Au(111) surface at the indicated temperatures for 30 s. Inset: integrated peak areas of the spectra at different temperatures. The measurements were performed at room temperature with a detection angle of 70°.

The thermal evolution series of a CoTPP multilayer is shown in Figure 6-2. When the CoTPP film is a thick multilayer, only the electronic structure of the CoTPP multilayer appears in the UPS spectrum and no feature from the Au(111) substrate should be seen. As the temperature increases the thickness of film decreases due to desorption and the feature of the Au(111) surface together with that of the CoTPP monolayer can gradually be observed. At a certain temperature the spectrum presents a unique shape much different from the CoTPP multilayer on Au(111) surface, indicating the formation of a CoTPP monolayer. When the temperature is further increased the spectrum keeps its shape until the CoTPP monolayer is destroyed by the high temperature. 530 K was chosen to prepare a CoTPP monolayer from a multilayer.
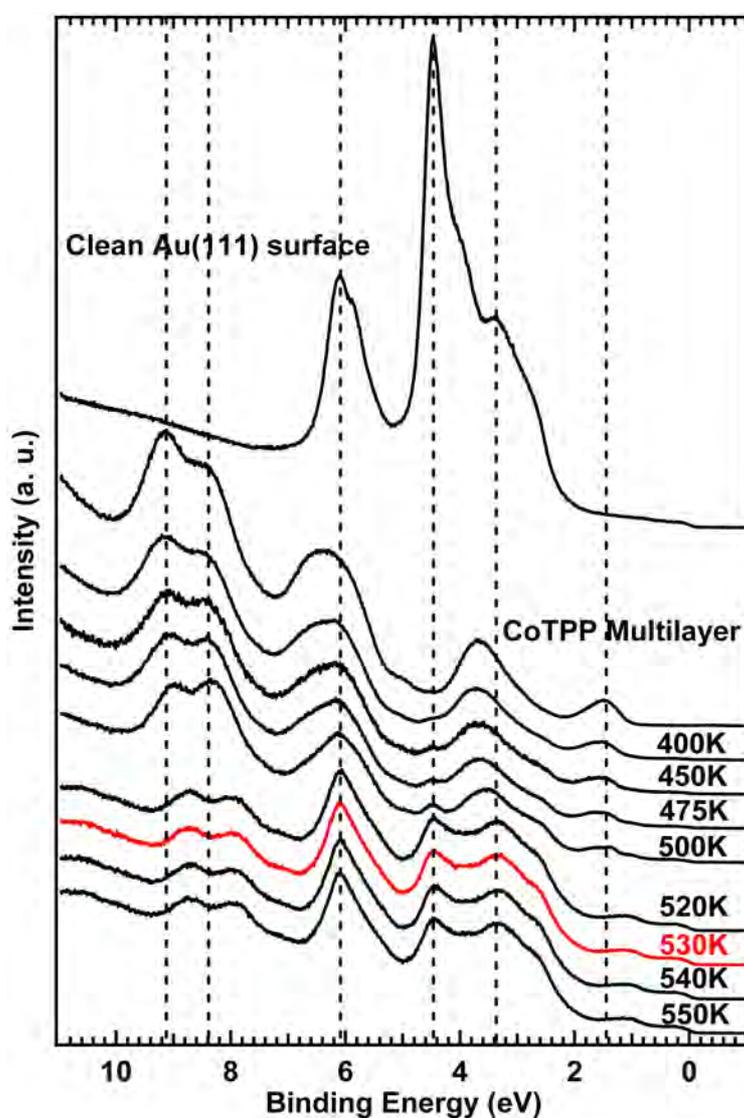
Figure 6-2. UPS spectra taken after annealing of a CoTPP multilayer (~ 5 monolayers) on the Au(111) surface at the indicated temperatures for 30 s. The measurements were performed at room temperature with a detection angle of 0°.

Similar to the multilayer desorption series of 2HTPP, the series for 2HOEP is shown in Figure 6-3. One can see that on Au(111) the thermal desorption of the 2HOEP multilayer happens at a lower temperature compared with 2HTPP, which is the same on Ag(111) surface. From the intensity and position of the C 1s signal the temperature for the preparation of 2HOEP monolayer was chosen as 500 K.
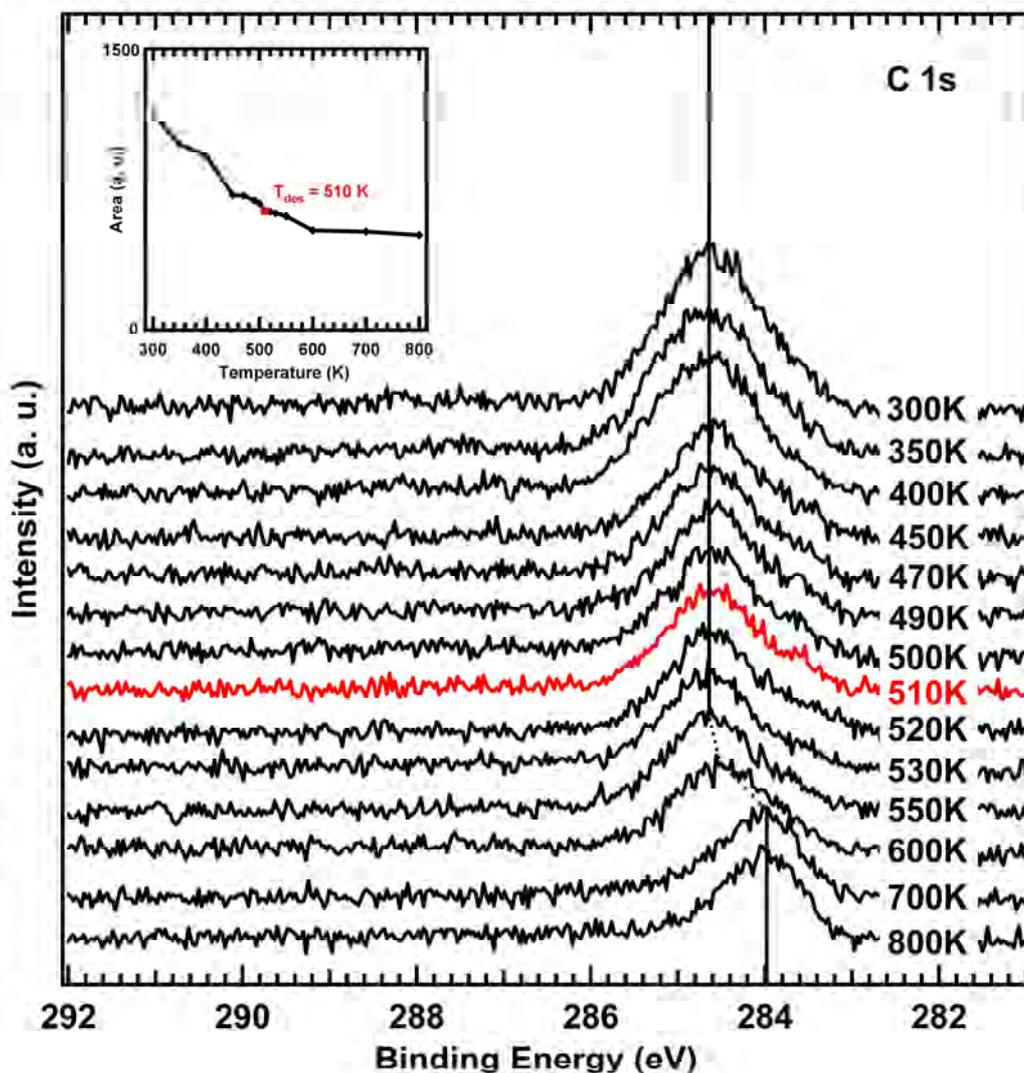
Figure 6-3. C 1s spectra taken after annealing of a 2HOEP multilayer (~ 3 monolayers) on the Au(111) surface at the indicated temperatures for 30 s. Inset: integrated peak areas of the spectra at different temperatures. The measurements were performed at room temperature with a detection angle of 70°

The same measurement was carried out for CoOEP and is shown in Figure 6-4. As the multilayer desorbs, the C 1s peak intensity decreases but the position remains the same until 550 K, which is different from the 2HOEP case. Considering the peak intensity and the multilayer desorption temperature of 2HOEP, the temperature for the preparation of CoOEP monolayer was chosen as 510 K. Since no peak shift could

be observed up to 550 K, a question arises whether 600 K is the real multilayer desorption temperature. This will be discussed further in Section 6.1.3, which provides the evidence that after annealing at 510 K, the CoOEP multilayer has already desorbed to leave a monolayer on the Au(111). Why there is no shift of the C 1s signal between multilayer and monolayer is so far still unclear. However, the same has been observed for the N 1s signal of CoOEP on Ag(111), where it was assumed that the relaxation shift is compensated by a concomitant chemical shift to higher binding energies.[Ba09]
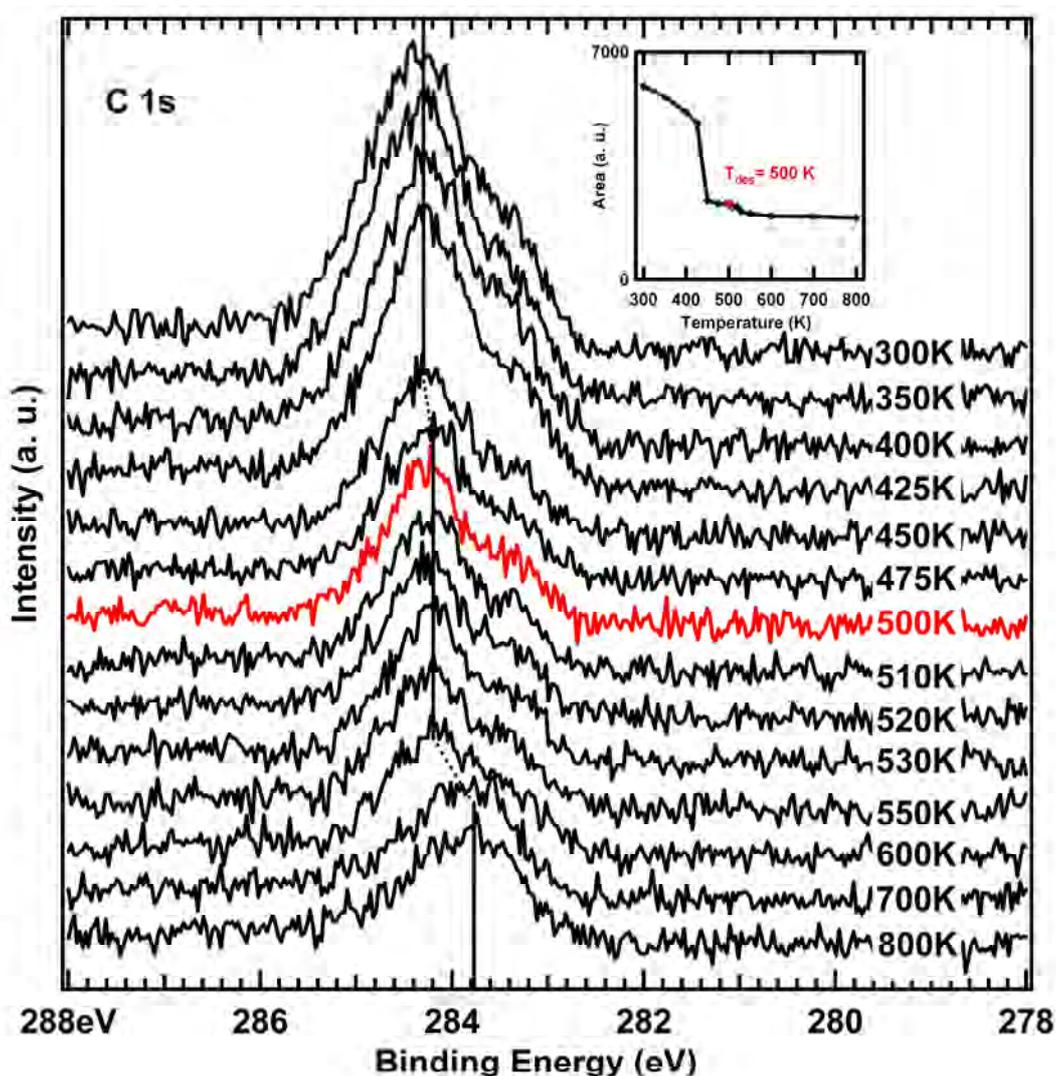
Figure 6-4. C 1s spectra taken after annealing of a CoOEP multilayer (~ 2 monolayers) on the Ag(111) surface at the indicated temperatures for 30 s. Inset: integrated peak areas of the spectra at different temperatures. The measurements were performed at room temperature with a detection angle of 70°

6.1.2. XP spectra in C 1s and N 1s regions of adsorbed porphyrin layers

Figure 6-5 shows XP spectra in the C 1s and N 1s regions for the metal-free 2HTPP and 2HOEP monolayers and multilayers. In the C 1s spectra for 2HTPP and 2HOEP multilayers (Figure 6-5 a and b), the shake-up satellite structure can be clearly seen, which is typical for organic molecules with extended conjugated π systems[Sc04]. Compared with 2HOEP, this feature is more obvious for the 2HTPP multilayer. Since the metal free porphyrins contain two types of nitrogen atoms, namely pyrrolic (-NH-) and iminic nitrogen atoms (=N-), the N 1s spectra show two peaks (Figure 6-5 c and d). In both metal free porphyrins the ratio of pyrrolic and iminic nitrogen atoms is 1:1. However in all N 1s spectra the apparent intensity of the peak at higher binding energy (to simplify, it is called N $1s^a$) is higher than that of the peak at lower binding energy (N $1s^b$ peak), except for 2HTPP multilayer (So far therer is no explanation for the different appearance of the N 1s spectrum of 2HTPP multilayer.). Both N 1s signals have satellite structures at higher binding energies. The satellite structure of N $1s^b$ lies under N $1s^a$, which makes N $1s^a$ appear higher than N $1s^b$. The satellite structure of N $1s^a$ cannot be very well recognized due to the background subtraction. For both C 1s and N 1s regions, the peak of a monolayer shifted to lower binding energy position relative to the multilayer peak, due to the more effective core hole shielding by the metal substrate.
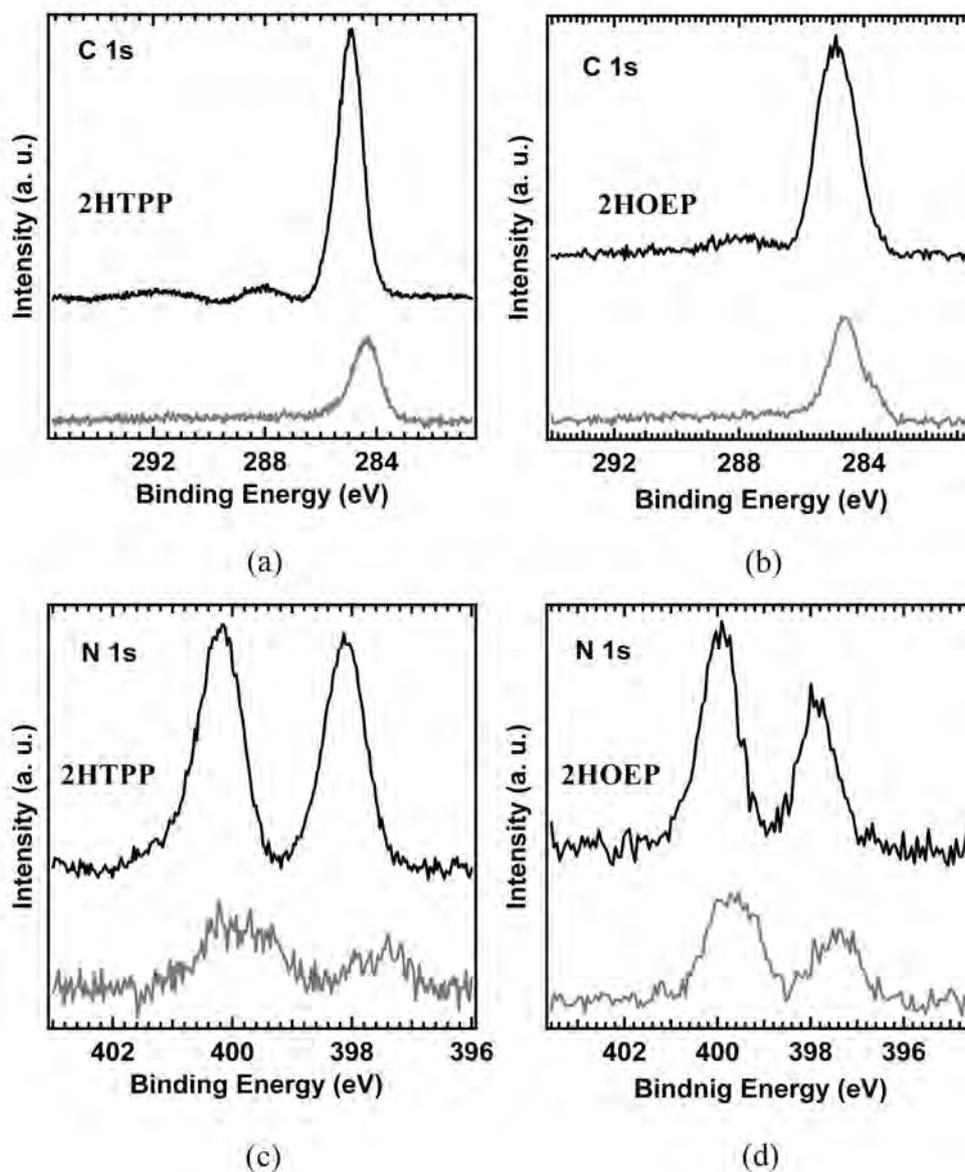
Figure 6-5. XP spectra in the C 1s and N 1s regions for 2HTPP and 2HOEP monolayers (grey) and multilayers (black) on a Au(111) surface.

Similar XP spectra in C 1s and N 1s regions were obtained for monolayers and multilayers of CoTPP and CoOEP and are shown in Figure 6-6. Again, in the C 1s spectra the satellite feature can be observed for CoTPP and CoOEP multilayers and is more pronounce for the CoTPP multilayer. Unlike the C 1s peak of the 2HOEP multilayer and monolayer, where only a sharp signal can be observed, the C 1s peaks of both CoOEP multilayer and monolayer show at least two components. The same has been observed and discussed in Section 5.2.3 for CoOEP multilayer on Ag(111). Similar to the C 1s peak of the CoOEP multilayer on Ag(111), the C is peaks of the CoOEP multilayer and monolayer on Au(111) can also be attributed to the aromatic carbon atoms (20 carbon atoms) and the ethyl carbon atoms directly (8 carbon atoms)

and not directly (8 carbon atoms) connected to the aromatic ring, which makes the C 1s peak contain three components, with the ratio 5 : 2 : 2 from higher to lower binding energy side. Since in CoTPP and CoOEP molecules there is only one type of nitrogen atoms, the N 1s spectra show only one peak. Different to the metal-free 2HOEP, the peak positions in both C 1s and N 1s spectra for the CoOEP monolayer remain the same as the peak positions for the CoOEP multilayer. The reason remains unclear, however, one suggestion is that the relaxation shift is compensated by a concomitant chemical shift.[Ba09]
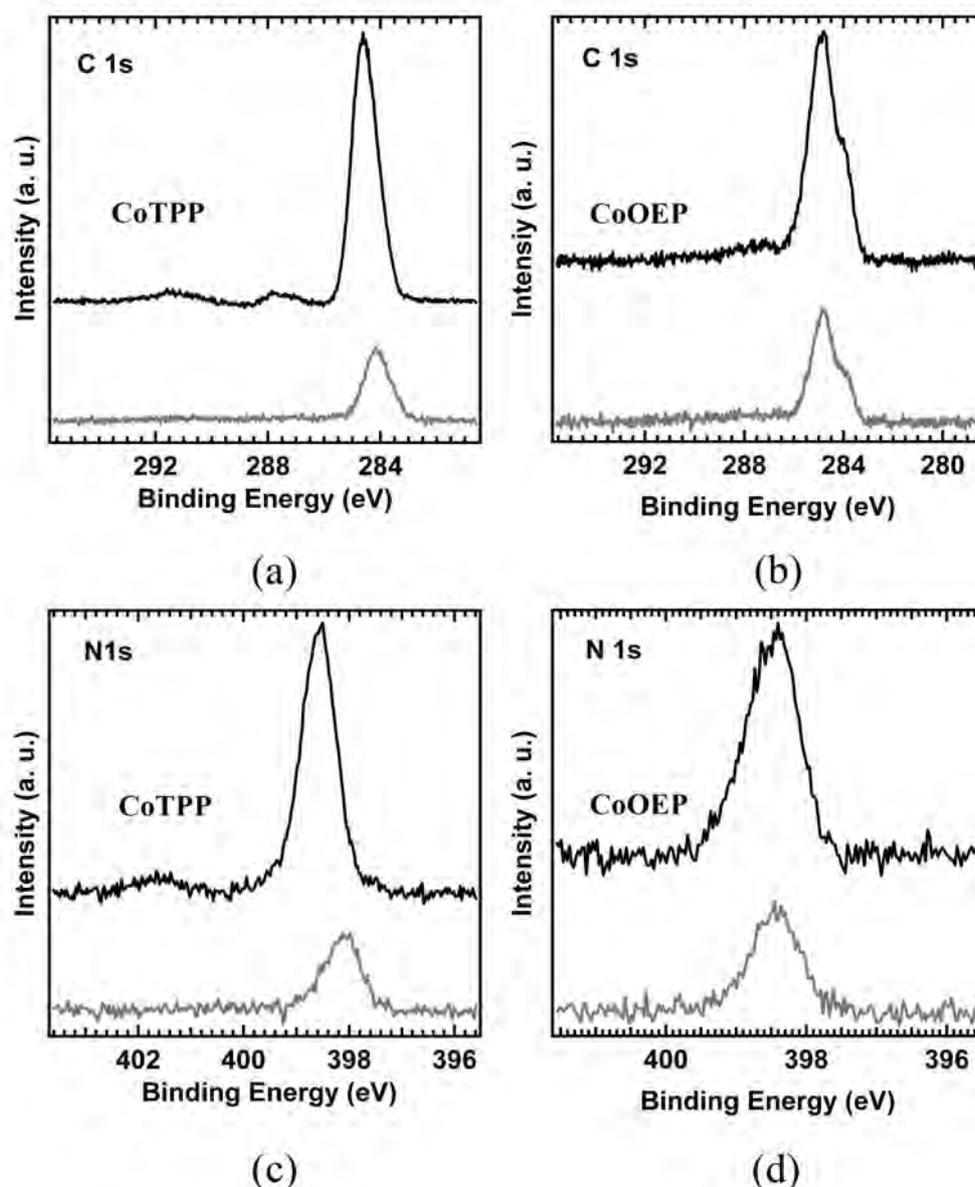
Figure 6-6. XP spectra in the C 1s and N 1s regions for CoTPP and CoOEP monolayers (grey) and multilayers (black) on the Au(111) surface.

6.1.3. Study of the interaction between adsorbed Co(II) porphyrin molecules and the underlying Au(111) surface

Similar to the study on the Ag(111) surface, the interaction between adsorbed cobalt porphyrin molecules and the underlying Au(111) surface has also been studied with XPS and UPS in this thesis. Because there has been extensive investigation of the structural properties of porphyrin monolayers on Au(111), we can focus here on their electronic properties. Previous studies with scanning tunnelling microscopy (STM) and calculations with density functional theory (DFT) have shown that on Au(111) CoTPP forms a well ordered monolayer with a rectangular unit cell, at both room temperature and low temperatures.[Sc00] [Sc01] [Ba04] [Br09]. Thereby, the CoTPP molecules undergo a saddle-shaped distortion[Br09], similar as on Ag(111)[Ba09] and Cu(111) [We08A]. This conformational adaption in the adsorbed state is driven by intramolecular steric repulsion between the ortho hydrogen atoms of the peripheral phenyl groups and the porphyrin core. The repulsive forces set in when the dihedral angle between porphyrin and phenyl rings is below $60°$[Wö08] and lead to an increasing saddle-shaped distortion of the porphyrin core. In the adsorbed complex, the degree of deformation is determined by a balance between the molecule-surface attraction, which forces the phenyl rings towards small dihedral angles, and the energy costs for the deformation.[Wö08], [We08] The typical $(22 \times \sqrt{3})$ herring bone reconstruction of Au(111)[Ha85] [Wö89] [Ba90] is not lifted upon adsorption of CoTPP.[Sc00] [Sc01] [Sc02] [Ba04] CoOEP forms highly ordered, incommensurate monolayers on Au(111) in which the molecules lie parallel to the surface, according to STM investigations at the liquid/Au(111) interface.[Yo04] Similar observations were made by STM on NiOEP/Au(111) under ultrahigh-vacuum (UHV) conditions, where a strongly distorted quasi-hexagonal lattice was found, in which the molecules have alternately different orientations in adjacent molecular rows.[Sc02] In contrast, CoOEP on Ag(111) forms a hexagonal lattice in which all molecules have the same orientation.[Ba09] These structural differences between CoOEP on Au(111) and Ag(111) are presumably related to the surface reconstruction of Au(111), which is not lifted by the adsorbates. Unlike CoTPP, CoOEP adsorbs in a flat, undistorted geometry on Ag(111) and Au(111).[Sc02] [Ba09] This is possible because the peripheral ethyl groups of CoOEP can rotate such that all terminal -CH_3 groups point away from the surface. In this conformation, the porphyrin core and the eight -CH_2- groups bound to the periphery are in the same, undistorted plane.[Ba09] It is therefore expected that the Co ions in CoOEP are closer to the substrate than in CoTPP and consequently interact more strongly with the surface.

In the following, a detailed XPS/UPS investigation of CoTPP and CoOEP monolayers and multilayers on Au(111) will be presented, in particular with respect to the interaction between the Co ion in the monolayers and the underlying Au

surface. For this purpose, we also compare with the respective metal-free ligand molecules 2HTPP and 2HOEP.

XPS measurements

Figure 6-7 shows the Co $2p_{3/2}$ XP spectra of a CoTPP multilayer (a) and a monolayer (b) on Au(111). The multilayer spectrum features a main peak at 779.9 eV and satellite structures at higher binding energy positions. The satellite structure has been attributed to the open-shell character of the Co(II) ion with its d^7 electron configuration.[Lu07] In the monolayer spectrum, the main peak is shifted by about 0.5 eV toward lower binding energy and at the same time an additional minor component appears at 777.9 eV (-2.0 eV relative to the multilayer signal). The satellite structures at higher binding energies are also present in the monolayer spectrum. The integrals of the peaks in the deconvoluted CoTPP monolayer spectrum have the following ratios (from low to high binding energies): 1 : 2 : 1.1 : 0.77 : 0.79. The ratio of the integrals of the strongly shifted component at 777.9 eV to the remaining part of the spectrum, including all satellites, is thus 1 : 4.6. Since part of the satellite intensity may be associated with the component at 777.9 eV, its total contribution to the Co $2p_{3/2}$ signal is probably larger than suggested by this ratio.
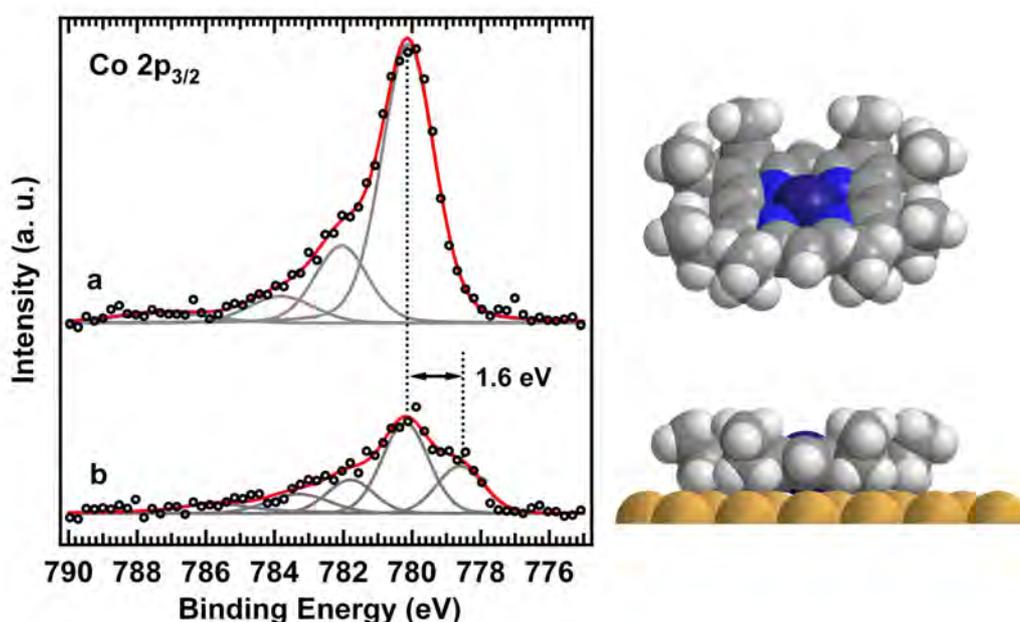
Figure 6-7. Co $2p_{3/2}$ XP spectra of CoTPP on Au(111). (a) CoTPP multilayer (~ 10 monolayers), (b) CoTPP monolayer. The black circles represent the original data, the solid gray lines are the peaks according to signal deconvolution, and the solid red line is the sum of these peaks. Note that the deconvolution does not necessarily represent the full complexity of the satellite structure at higher binding energies, which is due to the unpaired electrons at the Co ion.

The respective Co $2p_{3/2}$ spectra for the CoOEP monolayer and multilayer are shown in Figure 6-8. The main signal of the multilayer spectrum (a) is located at 780.2 eV and is accompanied by a satellite structure that extends towards higher binding energies. In the monolayer spectrum, the main peak is not shifted relative to the multilayer signal, while a minor component appears at 778.6 eV (shifted by -1.6 eV relative to the multilayer signal). Again, the monolayer spectrum shows satellite structures at higher binding energies due to the unpaired electron(s) of the Co ion. The integrals of the peaks, from low to high binding energies, in the deconvoluted CoOEP monolayer spectrum have the ratios 1 : 1.5 : 0.85 : 0.76 : 0.7. The intensity ratio of the shifted component at 778.6 eV to the remaining part of the spectrum is 1 : 3.1. With the same argument as in the case of CoTPP, the component at 778.6 eV contributes probably more to the Co $2p_{3/2}$ signal than suggested by this ratio.
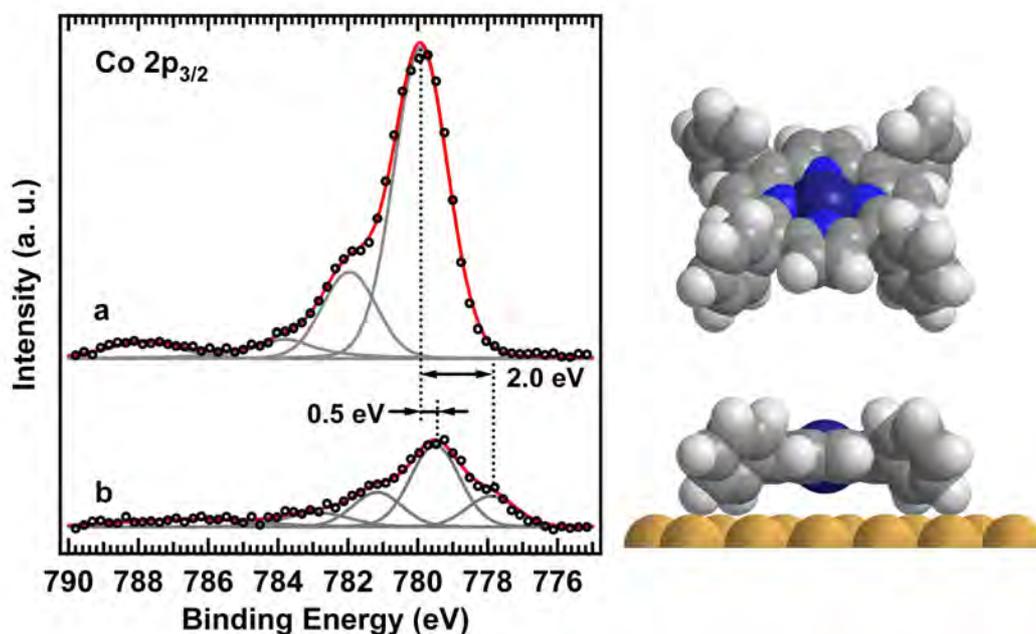
Figure 6-8. Co $2p_{3/2}$ XP spectra of CoOEP on Au(111). (a) CoOEP multilayer (~ 10 monolayers), (b) CoOEP monolayer.

As already mentioned in Section 6.1.1, due to the detection with grazing emission, it is hard to determine the multilayer desorption temperature accurately. Although 510 K was chosen as the desorption temperature to prepare a CoOEP monolayer, annealing at 510 K may leads to incomplete desorption of the CoOEP monolayer, i.e., the multilayer desorption temperature may be higher than 510 K, and annealing at 510 K may leave a CoOEP bilayer which gives rise to the minor component at 778.5 eV in Figure 6-8 b. In order to exclude this possibility, CoOEP multilayer was also annealed up to 600 K, which is near the decomposition temperature of CoOEP (Figure 6-4). The Co $2p_{3/2}$ XP spectra taken after annealing at 600 K is shown in Figure 6-9 b, where the peak has the same area as the peak in Figure 6-8 b. (However,

the whole spectrum is shifted to lower binding energy by about 0.65 eV probably due to decomposition.) With the same shape of the Co $2p_{3/2}$ XP spectra in Figure 6-9 we conclude that 510 K is sufficient for the multilayer desorption, and the minor component in Figure 6-8 b does not come from a CoOEP bilayer. Since a minor component in the Co $2p_{3/2}$ XP spectrum was also observed for CoTPP monolayer, the same annealing procedure should also be performed in the future to exclude the possibility of obtaining a bilayer.
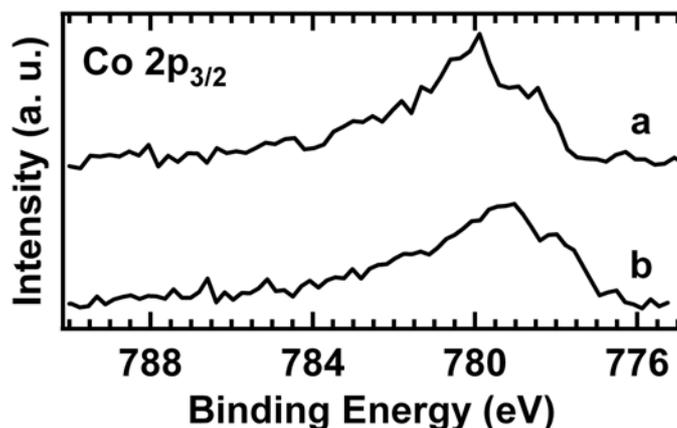
Figure 6-9. Co $2p_{3/2}$ XP spectra of CoOEP after heating the multilayer at 510 K (a) and at 600 K (b).

The difference in binding energy between the Co 2p multilayer signals and the respective shoulders at the low-binding energy side of the monolayer signals is in same range as was found on Ag(111) (-1.8 eV for CoTPP/Ag(111), -1.9 eV for CoOEP/Ag(111)).[Lu07] [Ba09] The main difference to Ag(111) is that here, on Au(111), only a small fraction of the signal is shifted by this large amount, while on Ag(111) the whole signal is shifted. This observation will be discussed following in the context of the herringbone reconstruction of Au(111), which leads to lateral variations in height and in electronic structure.[Ba90] [Wö89]

To clarify whether the core level shifts of the other elements in the complex follow the same trend, comparison with the N 1s and C 1s shifts between multilayer and monolayer is made for the Co porphyrins and the metal-free ligands. The N 1s XPS data have been shown in Figure 6-5 and 6-6; the Co 2p, N 1s and C 1s shifts for all four species are listed in Table 6-1. The data show that the major component of the Co signal shifts by the same amount as the N 1s and C 1s signals (0.6 eV for CoTPP, 0.0 eV for CoOEP); all these shifts are attributed to final state effects (relaxation shift). The much larger shift of the minor fraction of the Co signal has no equivalent in the other signals; here we clearly observe indications for a specific interaction between the Co ion and the substrate.

Table 6-1. XPS core-level shifts between multilayer and monolayer coverage of various porphyrins on Au(111). All signals shift toward lower BE in the monolayer.

	CoTPP	2HTPP	CoOEP	2HOEP
Co 2p$_{3/2}$	-0.6 eV / -2.0 eV	-	0.0 eV / -1.6 eV	-
C 1s, N 1s	-0.5 eV	-0.5 eV	0.0 eV	-0.4 eV

UPS and work function changes

Figure 6-10 shows the UP spectra of CoTPP monolayers and multilayers on Au(111), in comparison to the spectrum of the clean gold surface. For better recognition, the secondary electron cutoff (left) and the region around E_F (right) are shown separately. Compared to the spectrum of clean Au(111) (curve (a)), the spectrum of the CoTPP monolayer (curve (b)) shows several new signals, which are attributed to the molecular orbitals of CoTPP. The energetic positions of the most intense signals are listed in Table 6-2.
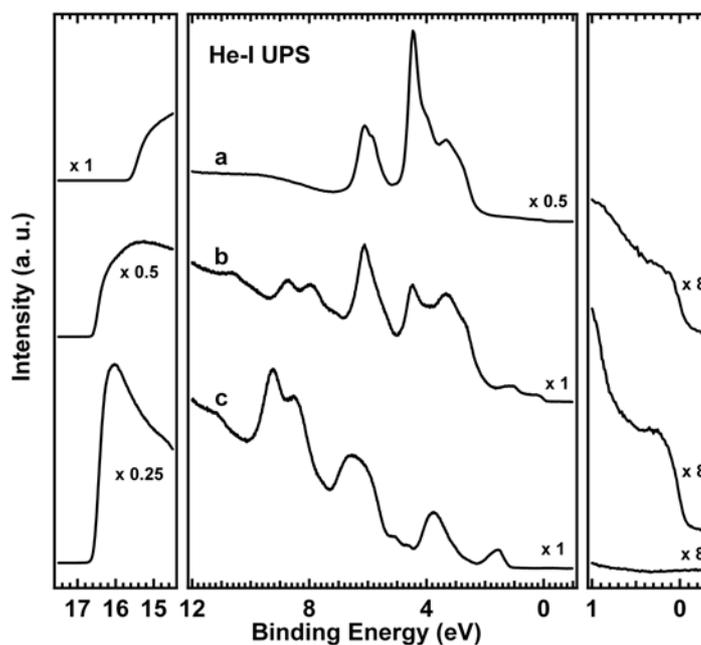
Figure 6-10. UP spectra of CoTPP on Au(111). (a) clean Au(111) surface, (b) CoTPP monolayer, (c) CoTPP multilayer. The right frame shows a magnified view of the region around the Fermi edge, the left frame the secondary electron cutoffs.

Comparison with the peak positions in the multilayer spectrum (c) shows that all signals undergo a uniform relaxation shift by 0.5 eV toward lower binding energy in

the monolayer. Table 6-2 also shows the gas phase peak positions of NiTPP from ref. [Kh75]. After subtraction of the work function of Au(111) with one monolayer of CoTPP, 4.52 eV, these values compare reasonably well to the multilayer peak positions for the peaks below the SOMO peak, if an additional shift of all signals by 0.7±0.1 eV due to the extramolecular relaxation is taken into account. Gas phase data for CoTPP itself have not been reported, but the variations in the UPS peak position of Mg, Mn, Fe, Ni, Cu and Zn tetraphenylporphyrins (as reported in the same publication [Kh75]) are so small that very similar values can be expected for CoTPP, in particular for the levels below the SOMO.

The most interesting feature of the monolayer spectrum is the additional intensity in the direct vicinity of E_F (0-0.4 eV), which has no counterparts in the multilayer spectrum nor in the spectrum of clean Au(111). Therefore, it is likely that this feature arises from the electronic interaction between the molecules in the monolayer and the Au surface.

Table 6-2. UPS peak positions (in eV) for CoTPP monolayer and multilayer. For comparison, the peak position in the gas phase UP spectrum of NiTPP is shown.[Kh75]

CoTPP monolayer	0-0.4	1.1	3.3	(~6.0)	8.0	8.8
CoTPP multilayer	-	1.6	3.8	6.4	8.5	9.3
NiTPP gas phase	-	6.62 6.44	8.93	11.72	13.77	14.54
NiTPP gas phase – Φ (Φ = 4.52 eV)	-	2.10 1.92	4.41	7.20	9.25	10.02

To obtain more detailed information about character and origin of this interaction-induced signal, Figure 6-11 shows a close-up of the CoTPP multilayer and monolayer UP spectra in the range directly below E_F (curves (a) and (b)). The peak at 1.6 eV in the multilayer spectrum (a) is attributed to the singly occupied molecular orbital (SOMO) of the complex. [Lu07] (Note that CoTPP has at least one unpaired electron due to the d^7 electron configuration of the Co ion.) Comparison of the CoTPP monolayer spectrum (curve (b)) with the spectrum of the clean Au(111) surface (curve (c)), which is placed directly underneath, clearly shows the increased intensity between E_F and ~0.4 eV. In addition, the CoTPP monolayer spectrum features the SOMO-related signal, which is shifted to 1.1 eV, i.e., by the same -0.5 eV relative to the multilayer as the other adsorbate-related peaks (relaxation shift, cf. Table 6-2 for the valence levels and Table 6-1 for the core levels).

To clarify the role of the Co ion in the formation of the new electronic state around 0-0.4 eV, the UP spectrum of a 2HTPP monolayer on Au(111) was recorded (curve (d)). 2HTPP differs from CoTPP only insofar as the Co ion is replaced by two hydrogen

atoms bound to pyrrolic nitrogen atoms (cf. Figure 1 c and d). As can be seen, the 2HTPP monolayer spectrum (d) is very similar to the spectrum of clean Au(111) in the vicinity of E_F and, in particular, the feature around 0-0.4 eV seen in the CoTPP monolayer spectrum is here missing. Since the new valence state apparently requires that Co ions have direct contact to the substrate, we conclude that it arises from the electronic interaction between the Co ion and the Au(111) surface. Note that similar conclusions have been drawn previously in the case of CoTPP on Ag(111), where a new signal at 0.6 eV below E_F appears in the monolayer spectrum, but again neither in the CoTPP multilayer nor in the 2HTPP monolayer spectra.[Lu07] The signal around 0.6 eV on Ag(111) is more intense than the interaction induced signal on Au(111), which could indicate that the Co ion interacts more strongly with Ag(111) than with Au(111) or, alternatively, that only a fraction of the Co ions in the monolayer interacts with the substrate in the case of Au(111).
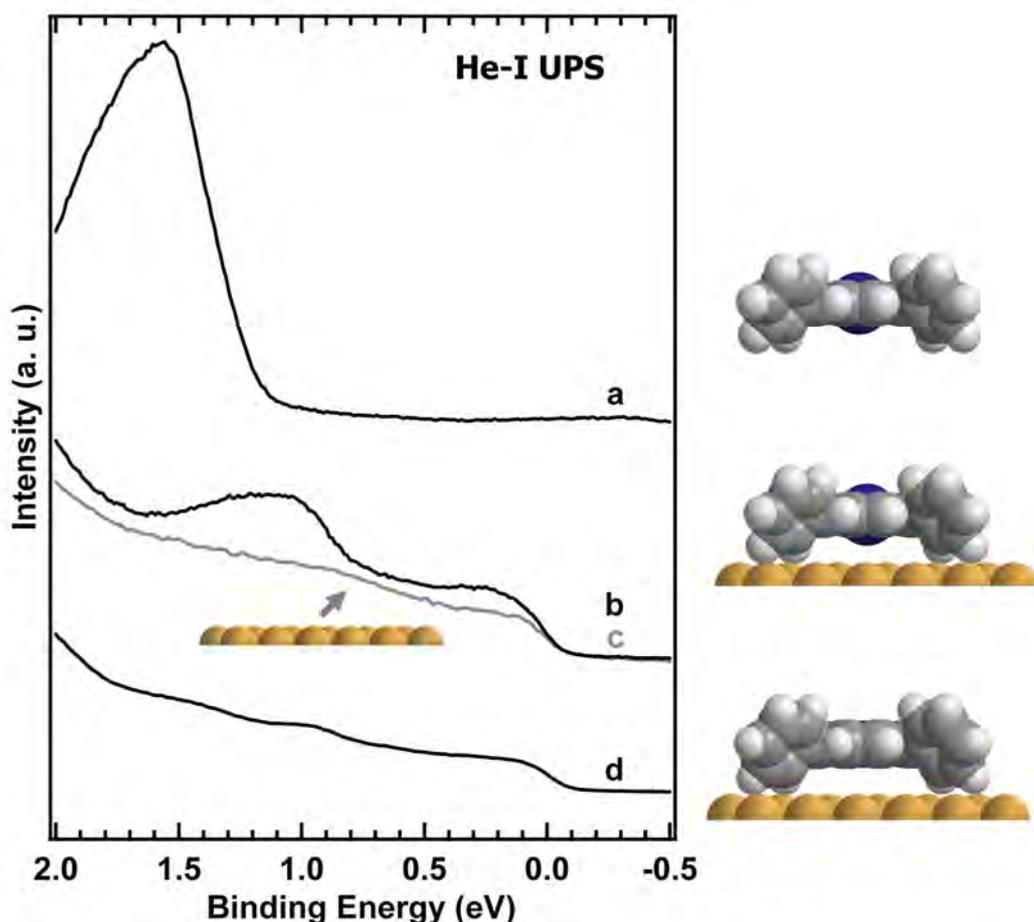
Figure 6-11. He–I UP spectra in the vicinity of the Fermi edge. (a) CoTPP multilayer (~5 monolayers) on Au(111), (b) CoTPP monolayer on Au(111), (c) clean Au(111) surface, and (d) 2HTPP monolayer on Au(111).

The study has been extended to the UP spectra of CoOEP, which are shown in Figures 6-12 and 6-13. The overview UP spectra for CoOEP monolayer and multilayers on Au(111) in Figure 6-12 (b) and (c) differ notably from the respective CoTPP spectra in Figure 6-10. Instead of the discrete peak structure seen in the CoTPP multilayer spectrum (Figure 6-10c), the CoOEP multilayer spectrum in Figure 6-12c shows several broad features, with the most intense signals in the range between 4.0 eV and 8.0 eV. Since the structural differences between CoTPP and CoOEP concern only the periphery of the molecule, which consists of four σ-bonded phenyl groups in CoTPP and eight ethyl groups in CoOEP, the differences in the valence electronic structure between CoTPP and CoOEP must be related to these side groups. A spectrum very similar to Figure 6-12c has been reported previously for NiOEP multilayers on Au(111).[Sc02]

In agreement with the broad structures in the CoOEP multilayer spectrum, the monolayer spectrum (Figure 6-12, curve (c)) shows no pronounced localized features, but adsorbate-related intensity is visible in the ranges between 7.0 eV and 11.0 eV (center frame of Figure 6-12) and between E_F and ~0.5 eV (right frame of Figure 6-12). For a closer inspection of the valence states in the vicinity of the E_F, this energy region is magnified in Figure 6-13.
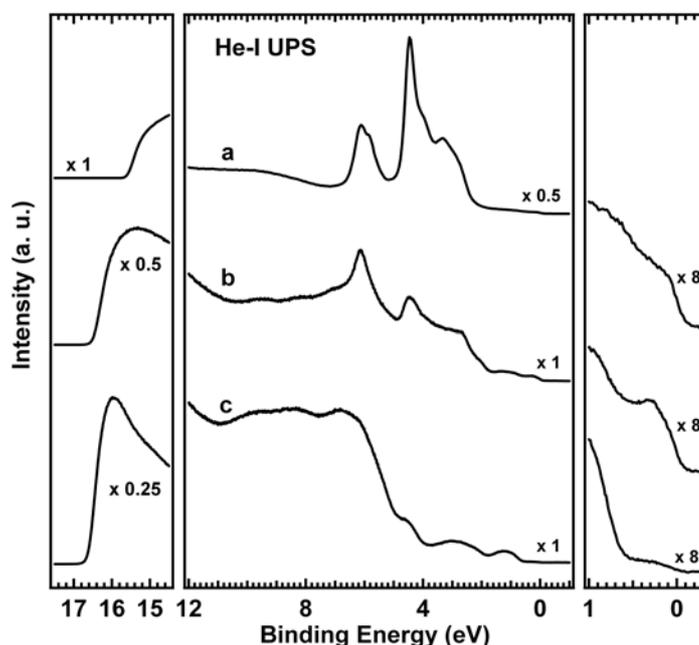
Figure 6-12. UP spectra of CoOEP on Au(111). (a) clean Au(111) surface, (b) CoOEP monolayer, (c) CoOEP multilayer. The right frame shows a magnified view of the region around the Fermi edge, the left frame the secondary electron cutoffs.

The CoOEP multilayer spectrum in Figure 6-13, curve (a), shows a signal centered at 1.2 eV. This signal has a width of 0.73 eV (full width at half maximum, FWHM) and

is thus considerably broader than the SOMO related signal of CoTPP with a FWHM of 0.54 eV. Most likely, this peak consists of at least two overlapping contributions from valence states of slightly different energy (e.g., SOMO and SOMO-1). The two contributions are more clearly visible in the CoOEP monolayer spectrum, where the signal is centered around 1.1 eV (Figure 8, curve (b)). The apparent change in peak shape is not due to a further separation of the components, since the FWHM does not increase. (In fact, the FWHM even decreases to 0.66 eV. Note that the FWHM of the CoTPP SOMO signal changes in a similar way; it is 0.54 eV in the multilayer and 0.50 eV in the monolayer spectrum.) The center of the monolayer SOMO signal is shifted by only about 0.1 eV relative to the multilayer signal, which is much less than in the case of CoTPP, where a 0.5 eV shift was observed. Whether the other CoOEP valence signals shift by the same amount cannot be clarified, because all other valence peaks are too strongly overlapping or obscured by the Au 5d signal. However, the smallness of the shift of the SOMO signal parallels our observation that the major part of the Co 2p signal as well as the N 1s and C 1s signals have almost identical energetic positions in mono- and multilayer spectra.
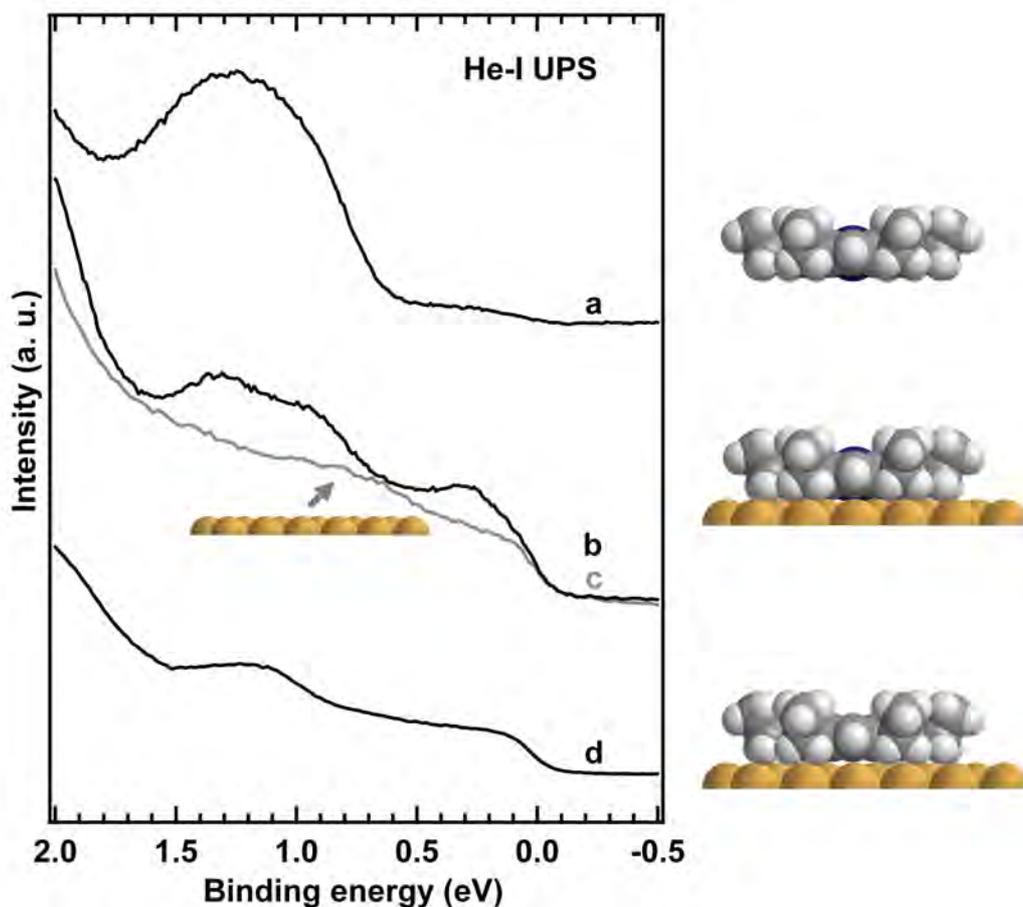
Figure 6-13. He–I UP spectra of (a) CoOEP multilayer (~5 monolayers) on Au(111), (b) CoOEP monolayer on Au(111), (c) the clean Au(111) surface, and (d) 2HOEP monolayer on Au(111).

In agreement with the findings for CoTPP, the CoOEP monolayer spectrum shows additional intensity in the range between E_F and 0.5 eV. This contribution is clearly seen by direct comparison with the spectrum of the clean Au(111) (curve c) and it is more intense than in the case of CoTPP. The signal is absent in the CoOEP multilayer spectrum and thus can be attributed to the interaction with the substrate. Comparison with curve (d), the spectrum of the 2HOEP monolayer, show that this signal is absent if the Co ion is replaced by two pyrrolic H atoms. As in the case of CoTPP, this again underlines the central role of the Co ion in the interaction.

Adsorbate-induced work function changes were extracted from the shifts of the secondary electron cutoffs of the UP spectra, which are shown in the left frames of Figures 6-10 and 6-12. Reductions of the work function by adsorption of organic molecules, as found for all here investigated species, have frequently been observed in the past and have been attributed to Pauli repulsion between the electrons of the molecule and those of the metal. This 'cushion effect' leads to a depletion of charge density between molecule and metal and thus to a modification of the dipole layer.[Wi05] The work function shifts for the Co porphyrins and their free-base counterparts are shown in Table 6-3. All species lower the work function, but the free-base porphyrins consistently cause larger changes than the metal complexes and there are also significant differences between the tetraphenylporphyrins and the octaethylporphyrins.

Table 6-3. Work function changes $\Delta\Phi$ (in eV) for CoTPP, 2HTPP, CoOEP and 2HOEP monolayers, relative to the work function of the clean Au(111) surface (5.37 eV).

CoTPP	2HTPP	CoOEP	2HOEP
0.85	1.1	0.75	1.2

Figure 6-14 shows a schematic energy diagram of the CoTPP/Au(111) and CoOEP/Au(111) interfaces as derived from the UP spectra in Figures 6-10 and 6-12.
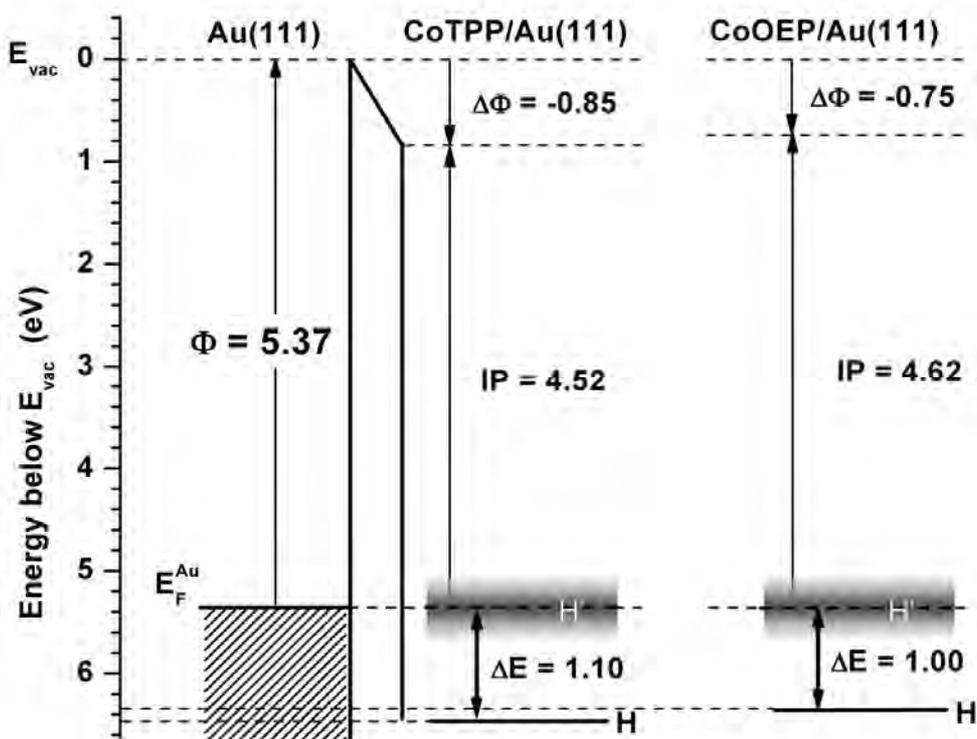
Figure 6-14. Schematic energy diagram of the electronic levels at the CoTPP/Au(111) and CoOEP/Au(111) interfaces at monolayer coverage. Φ is the work function of clean Au(111) and $\Delta\Phi$ the adsorbate-induced work function shift or shift of the vacuum level. IP denotes the ionization potential of the adsorbed CoTPP. H' is the highest occupied molecular level related to the adsorbate, induced by the interaction between the CoTPP or CoOEP molecules and the substrate. H is the former highest occupied level of the CoTPP molecule. Since the interaction-induced valence state is located in direct vicinity of E_F, it is likely that it extends beyond the Fermi energy as schematically indicated in the Figure.

Discussion

Previous XPS, UPS and STM studies of cobalt porphyrins on Ag(111) show various indications for a direct electronic interaction between the coordinated Co ions and the substrate, in particular adsorption-related chemical shifts of Co core levels as well as new electronic states in the valence region and enhanced tunnelling probabilities, which occur only if the Co ions are in direct contact to the substrate.[Lu07] [Fl07B][Fl07C] [Co08] [Ba09] [Go09] The uniformity of the Co 2p shifts indicates that the interactions are laterally homogeneous, i.e., virtually all Co ions interact in the same way with the Ag substrate.

The here presented results for Au(111) reveal that this substrate influences the Co porphyrins very differently than Ag(111). Instead of the uniform peak shift observed on Ag(111), the Co 2p signal of Co porphyrin monolayers splits in (at least) two

components. The larger fraction shifts only marginally relative to the multilayer (-0.6 eV for CoTPP, 0 eV for CoOEP), whereas a minor contribution shifts by a much larger amount, -2.0 eV for CoTPP and -1.6 eV for CoOEP. These dramatic shifts towards lower binding energies suggest that a certain fraction of the Co ions in the monolayers interacts strongly with the Au surface and are partially reduced, while the majority of the molecules interact less strongly and less specifically with the substrate.

The most obvious explanation for the signal splitting and the different behaviour of parts of the adsorbed Co porphyrins is related to the complex surface structure of Au(111). Gold is the only fcc metal with a reconstructed (111) surface. The top layer of Au(111) undergoes an uniaxial compression along [1-10]. In this direction, which is parallel to the long side of the $\begin{pmatrix} 22 & 0 \\ -1 & 2 \end{pmatrix}$, 63×4.7 Å^2 unit cell, 23 atoms occupy 22 bulk sites.[Ha85] [Wö89] [Ba90] The compression of the surface layer leads to a lateral sequence, along the [1$\overline{1}$0] direction, of alternating regions with fcc and hcp type stacking and transition regions between them. The ratio between the areas covered by fcc and hcp regions is ~2:1, indicating that the former are more stable. The Au atoms in the top layer occupy hollow sites of the second layer in the fcc and hcp regions, but quasi-bridge sites in the transition regions. This has two structural consequences: First, the atoms in the transition regions are elevated by ~0.2 Å relative to the fcc regions and second, the distance, along [1$\overline{1}$0], between atomic rows in [11$\overline{2}$] direction is largest in the transition regions and shortest in the hcp regions (2.8 vs 2.6 Å). The corrugation (in STM) is also larger in the transition region than in the fcc or hcp regions, possibly reflecting a drain of charge density from the more delocalized Au 6sp states in favour of the more localized Au 5d states.[Wö89] [Ba90]

The vertical and horizontal (out of the hollow sites) displacement of the atoms in the transition regions leads to an increased reactivity of these parts of the surface. For example, it has been noted that, upon deposition of potassium, the Au atoms in the transition regions are the most reactive. On a larger length scale, the Au(111) surface features a zigzag superstructure that results from periodic changes of the direction of contraction by ±120°.[Ba90] The elbow regions of the zigzag pattern are preferential adsorption sites for organic molecules[Bö99] or metal atoms[Ch91].

Adsorption of metalloporphyrins on Au(111) does not lift the surface reconstruction.[Sc00] [Sc01] [Sc02] [Ba04] Therefore, we propose that the different components in the split Co 2p signals of the Co porphyrin monolayers result from adsorption on different regions within the unit cell of the Au(111) surface. In particular, Co porphyrins adsorbed on the transition regions interact more strongly and give rise to the strongly shifted Co 2p components (-2.0 eV for CoTPP and -1.6 for CoOEP, relative to the respective multilayer signals). In contrast, Co porphyrins adsorbed on fcc and hcp regions are related to the other signal components with shifts

of only -0.6 eV (CoTPP) and 0 eV (CoOEP) (main peaks of the monolayer signal at 779.9 eV and 780.2 eV). Note that the energetic separations between the main peak and the strongly shifted component in the monolayer spectra are almost identical for both porphyrins; their values are -1.5 eV for CoTPP und -1.6 eV for CoOEP.

Further support for this interpretation comes from previous STM investigations of CoTPP monolayers on Au(111), which show that the adsorbed complexes enhance the contrast associated with the surface reconstruction.[Sc01] This means that molecules adsorbed on the more elevated transition regions, which appear with increased brightness in the STM images, further enhance tunnelling in this regions relative to molecules adsorbed in fcc and hcp regions. Since it is known that the electronic interaction between the Co ion and the surface leads to an increased tunnelling contribution through the metal ion,[Lu, 1996] [Hi96] [Sc02] [Ba04] [Co08] [Ba09] this observation indicates that the Co ions interact more strongly with the transition regions, in agreement with our interpretation of the XPS data. Alternatively, one may consider that the sites of increased Co-Au interaction are located in the elbow regions of the zigzag pattern. However, considering the relatively large fraction of strongly interacting molecules (18-24%), it is unlikely that the elbow regions alone can account for this finding. For direct identification of the sites of strong Co-Au interaction, application of local probe techniques such a scanning tunnelling microscopy are suggested for further investigation.

Alternatively, the split Co $2p_{3/2}$ signals in the monolayer spectra may be related to final state effects, in particular charge transfer screening. According to a model proposed by Gunnarsson and Schönhammer[Gu78], initially unoccupied valence orbitals of the metalloporphyrin (here especially vacant Co 3d levels) can be lowered beneath the Fermi level by Coulomb attraction of the core hole in the photoion and consequently be occupied by electrons from the Fermi sea. In this model, the strongly shifted component of the monolayer signals would correspond to the more efficiently screened photoions. It is expected that Co ions with the stronger interaction to the substrate in the initial state are also more efficiently screened in the final state, because in both cases the overlap of wave functions plays an important role. Therefore, this approach is also consistent with the assumption of a non-uniform monolayer containing Co species with different interaction to the substrate in the initial state. The main difference to the initial state model described above is that transfer of electron density from the substrate to the Co ion occurs in the undisturbed system in this model, whereas the final state approach assumes that electron density is transferred during the photoemission process. It should be noted that even a single adsorbate species can give rise to several XPS peaks because of charge transfer screening, as was shown for example for CO on Cu(100)[Gu78] and N_2 on various transition metal surfaces.[Um84] This is due to the statistical nature of the charge

transfer event: only if a certain event is sufficiently fast, the excess energy is transferred to the photoelectron.

Finally, it should be considered that the Co ions in the monolayer are exposed to a different ligand field than the Co ions in the multilayers. This could result in a different spin state of the Co ions in the monolayer and thus explain the increased complexity of the Co $2p_{3/2}$ monolayer signals. More insight into these effects and generally into the influence of the substrate can be obtained by deliberate suppression of the Co-Au interaction with axial ligands such as nitric oxide coordinated to the Co ion.[Fl07B] The respective studies are presently underway in our laboratory.

All here investigated molecules lower the work function of the Au(111) surface. The remarkable fact that the free-base porphyrins cause a more negative change than the Co porphyrins can be understood on the basis of our previously developed model for the interfacial electronic interaction.[Lu07] [Go09] According to this model, the large shift of parts of the Co 2p signal towards lower binding energy is interpreted as due to transfer of electron density from the Au surface to the Co ion. Since substrate-to-adsorbate electron transfer often results in a work function increase, the effects of the Co-Au interaction are likely to counteract the negative work function change caused by the porphyrin ligand. Partly, the different work function changes of Co porphyrins and free base porphyrins may also be related to differences in the molecular conformations (and the resulting different dipole moments) of the adsorbed species. The differences in work function change between CoTPP and CoOEP and between 2HTPPP and 2HOEP indicate that such factors can indeed play a role.

Conclusion

Using X-ray and UV photoelectron spectroscopy, the coordinative interactions between CoTPP and CoOEP complexes and an Au(111) surface have been investigated. The drastic shift of parts of the Co $2p_{3/2}$ signal toward lower binding energy in the monolayer XP spectra (CoTPP: -2.0 eV, CoOEP: -1.6 eV relative to the multilayer signals) indicates that some of the coordinated Co ions interact strongly with the Au surface and are partially reduced by electrons from the substrate. The monolayer UP spectra of CoTPP and CoOEP show a new valence state, which is located in the direct vicinity of the Fermi edge. This valence state is not present in monolayer UP spectra of the free-base porphyrins and hence attributed to the interaction between the Co ions and the Au surface. The fact that the larger part of the Co $2p_{3/2}$ signal is only marginally influenced by the substrate shows that the majority of the complexes only weakly interact with the Au(111) surface. This contrasts with previous findings for CoTPP and CoOEP monolayers on Ag(111), in which virtually all complexes interact strongly with the substrate. The coexistence of weakly and strongly interacting complexes on the gold substrate attributed to the herringbone

reconstruction of Au(111), which leads to periodic lateral variations of the surface reactivity. In particular, it is proposed that the Co ions interact strongly with the transition region, in which the Au atoms in the topmost layer have elevated positions and sit on quasi-bridge sites, but only weakly with the fcc and hcp sites. Comparison of the spectra of CoTPP and CoOEP also show that the interaction with Au(111) is more sensitive to the structural differences between the porphyrins than the previously studied interaction with Ag(111).

6.2 Phthalocyanine thin films on a Au(111) surface

The studies of CoOEP monolayer and multilayer on Au(111) in the previous section have raised questions, such as why there is no energy shift of C 1s and N 1s XP spectra between multilayer and monolayer. These could be a consequence of the thermal decomposition of CoOEP molecules, since the CoOEP molecule contains eight ethyl groups, which may partly be lost during thermal deposition and subsequent annealing process. Thus, 2HPc and CoPc thin layers have also been investigated on Au(111) with XPS and UPS, because both molecules have flat frameworks (similar to adsorbed CoOEP and 2HOEP) and are expected to be more thermally stable.

6.2.1 Multilayer desorption series of 2HPc and CoPc on Au(111)

Figure 6-15 shows the multilayer thermal evolution series of 2HPc on Au(111) measured with XPS. The C 1s peak intensity decreased rapidly from 400 K to 560 K. The C 1s peak position started to shift at 540 K and remained stable until 650 K. However, in the spectrum after annealing at 540 K, some component from the multilayer can still be seen, thus 560 K was chosen as the temperature to prepare 2HPc monolayer from a multilayer.
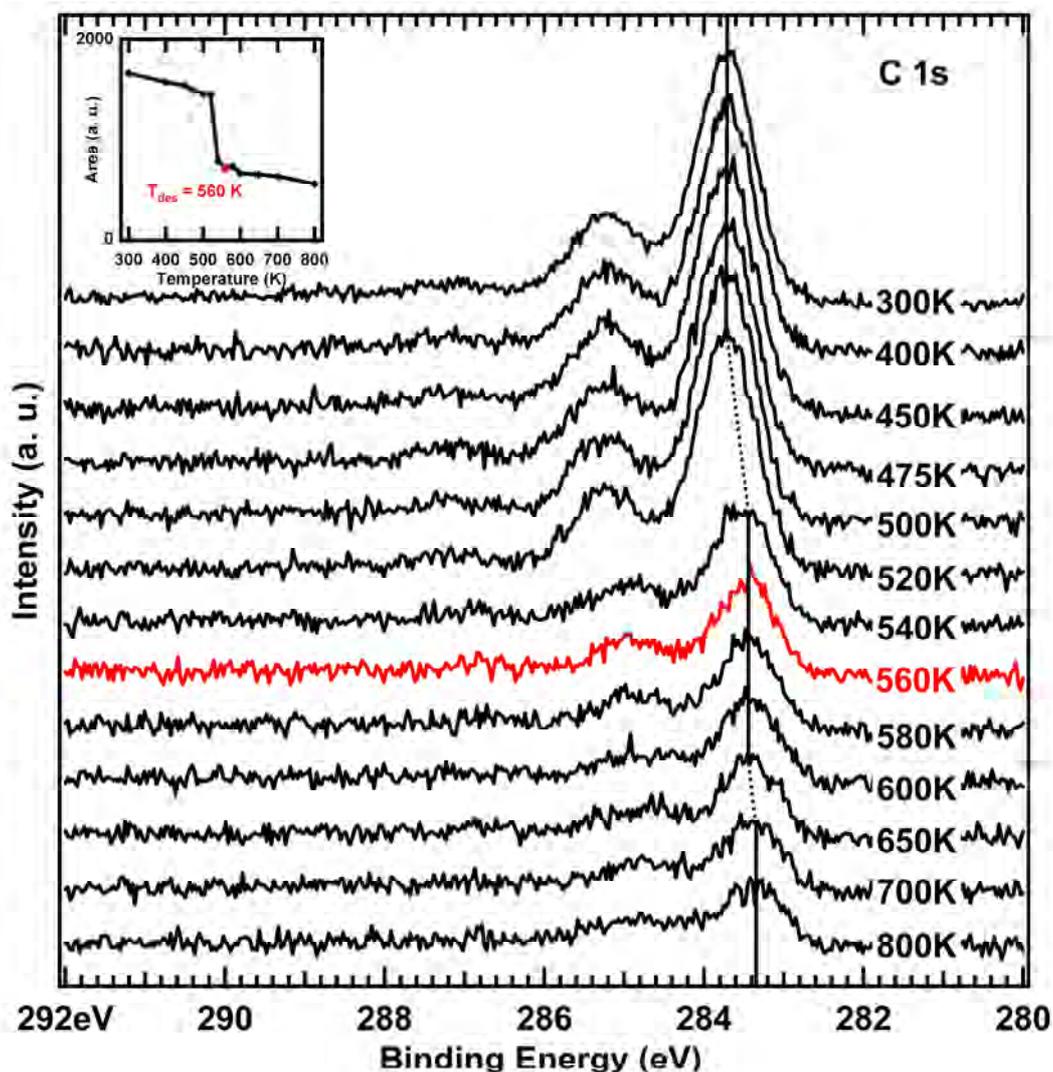
Figure 6-15. C 1s spectra taken after annealing of a 2HPc multilayer (~ 5 monolayers) on the Au(111) surface at the indicated temperatures for 30 s. Inset: integrated peak areas of the spectra at different temperatures. The measurements were performed at room temperature with a detection angle of 70°.

Similarly, Figure 6-16 shows the multilayer thermal desorption series of CoPc on Au(111) measured with XPS. There was a sudden decrease of the C 1s peak intensity at 600 K, and the peak also started to shift at this temperature. Thus 600 K was chosen as the temperature to prepare CoPc monolayer from a multilayer.
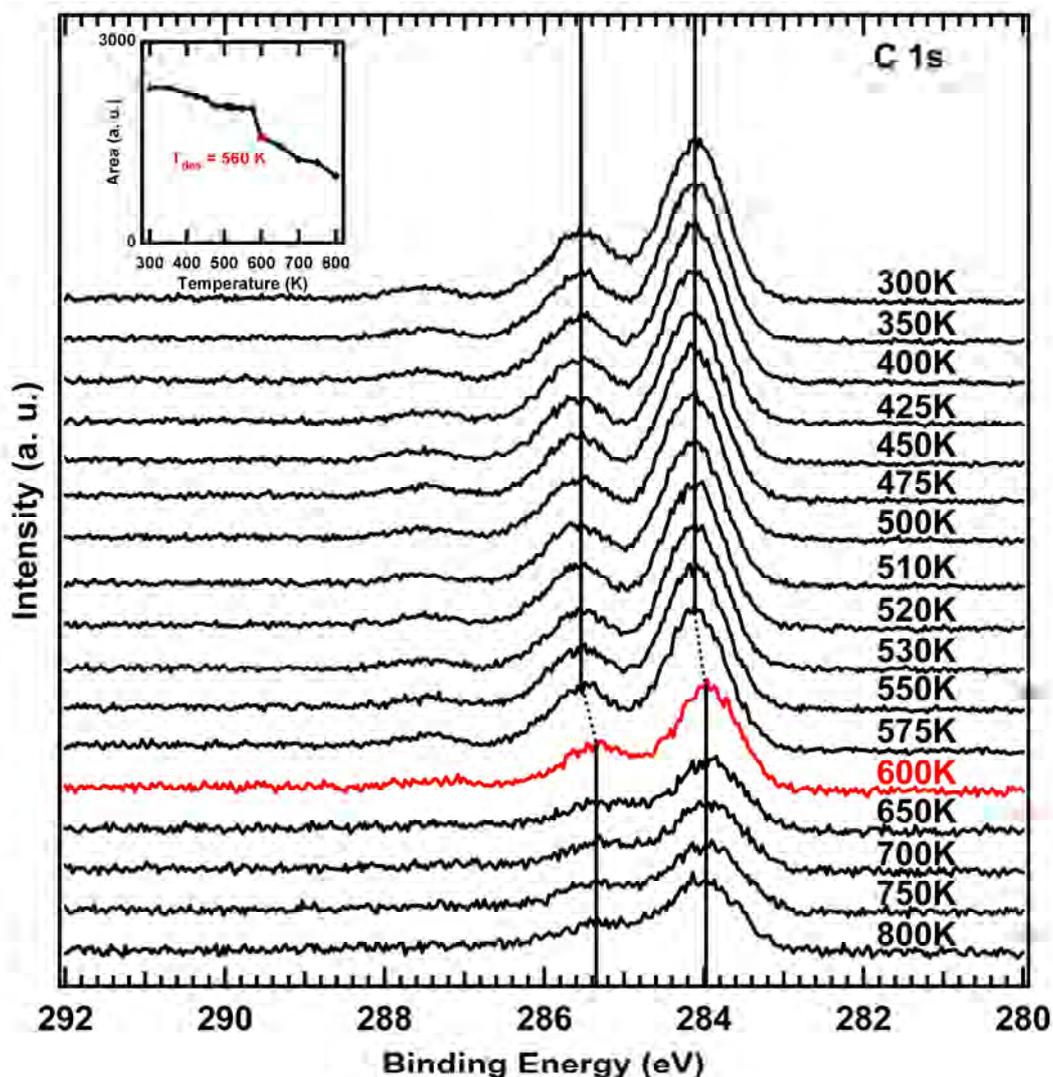
Figure 6-16. C 1s spectra taken after annealing of a CoPc multilayer (~ 5 monolayers) on the Au(111) surface at the indicated temperatures for 30 s. Inset: integrated peak areas of the spectra at different temperatures. The measurements were performed at room temperature with a detection angle of 70°.

6.2.2 XP spectra in C 1s and N 1s region for monolayers and multilayers of 2HPc and CoPc on Au(111) surface

Figure 6-17 shows XP spectra in the C 1s region for the 2HPc multilayer and the monolayer on Au(111). The multilayer C 1s spectrum is very similar to that on Ag(111) surface (see Section 5.1.1). It shows three peaks at 284.3 eV, 285.8 eV and 287.6 eV. Similar to the C 1s spectrum of a 2HPc multilayer on Ag(111), according to the peak position and the relative ratio of the peak areas, the peak at 285.8 eV is attributed to the hetero carbon atoms, which are directly connected to nitrogen atoms, and the other peak at 284.3 eV is attributed to the remaining carbon atoms, which are

only connected to other carbon atoms. The small signal at 287.6 eV presents the shake-up satellite feature of the C 1s photoelectrons of the 2HPc multilayer, which is typical for organic molecules with extended conjugated π systems[Sc04]. In the monolayer spectrum, this satellite feature becomes rather small. In the C 1s spectra, there is a small shift of about 0.3 eV to lower binding energy from multilayer to monolayer. One may notice that all the C atoms in both 2HTPP and 2HPc molecules are sp^2 hybridized, however, they show very different XP spectra on Ag(111) and Au(111). The XP spectra of 2HTPP show only one sharp peak, indicating that all carbon atoms are in the same chemical environment, although some C atoms are directly connected to N atoms while others are not. On the contrary, the XP spectra of 2HPc clearly show the difference between the hetero C atoms and the rest. This may be due to the different number of N atoms connected to the hetero C atoms in 2HTPP and 2HPc, i.e., in a 2HTPP molecule every hetero C atom is connected to only one N atom, while in a 2HPc molecule every hetero C atom is connected to two N atoms, which influence the chemical environment of the hetero C atoms more effectively.
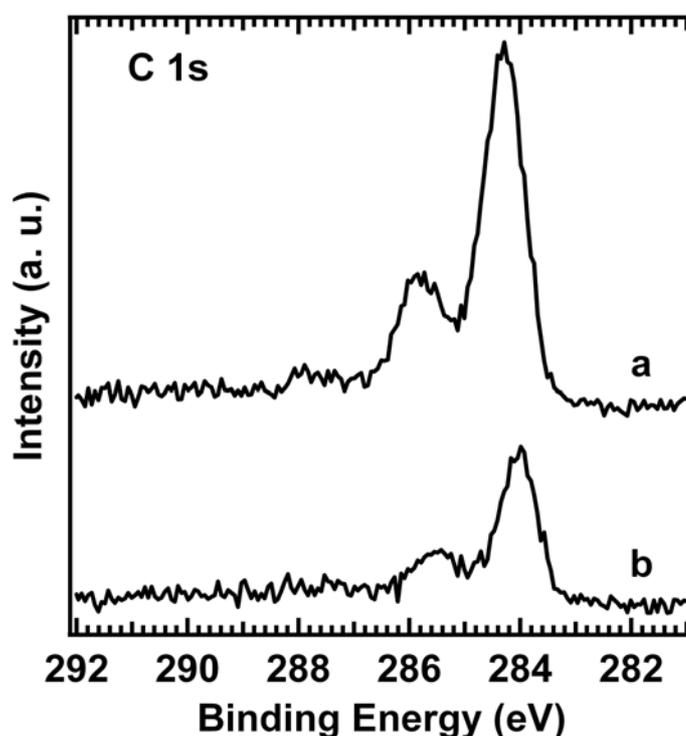
Figure 6-17. C 1s XP spectra for 2HPc multilayer and monolayer on Au(111): (a) multilayer, (b) monolayer.

Figure 6-18 shows XP spectra in the N 1s region for 2HPc multilayer and monolayer on Au(111). Similar to the spectra on Ag(111) (Section 5.1.1), there are two peaks in the N 1s region, presenting the different nitrogen atoms in a 2HPc molecule, i.e., two pyrrolic (-NH-) and six iminic nitrogen atoms (=N-). The monolayer spectrum is shifted to lower binding energy by approximately 0.5 eV.
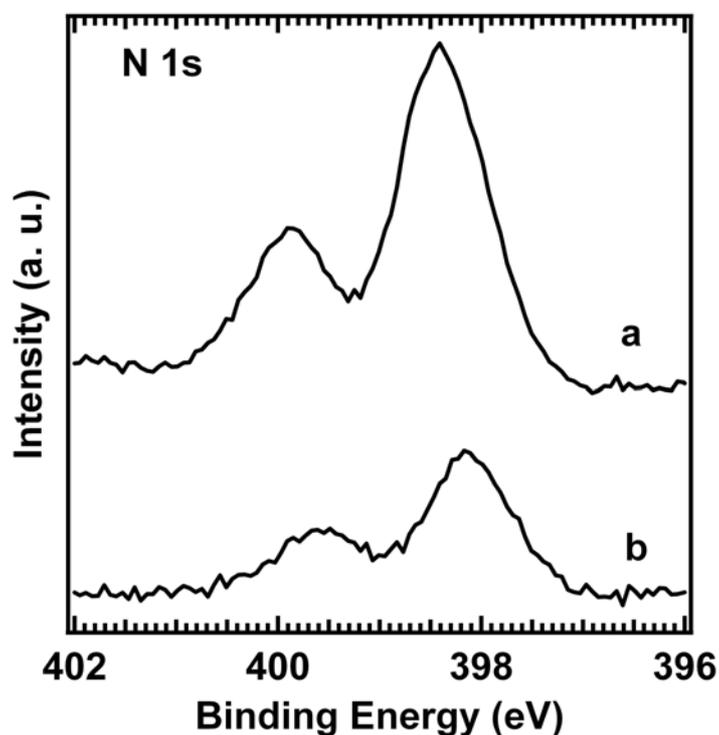
Figure 6-18. N 1s XP spectra for 2HPc multilayer and monolayer on Au(111): (a) multilayer, (b) monolayer.

Figure 6-19 shows the C 1s XP spectra for CoPc multilayer and monolayer on Au(111), which have very similar features to the C 1s XP spectra of 2HPc. The multilayer C 1s spectrum shows three peaks at 284.2 eV, 285.5 eV and 287.5 eV, in which the one at 285.5 eV is attributed to the hetero carbon atoms, and the other one at 284.2 eV is attributed to the homo carbon atoms. The small signal at 287.5 eV is the shake-up satellite feature of the C 1s photoelectrons of the 2HPc multilayer, which almost vanished in the monolayer spectrum. In the C1s spectra the binding energy is shifted about 0.3 eV towards lower binding energy direction from CoPc multilayer to monolayer.
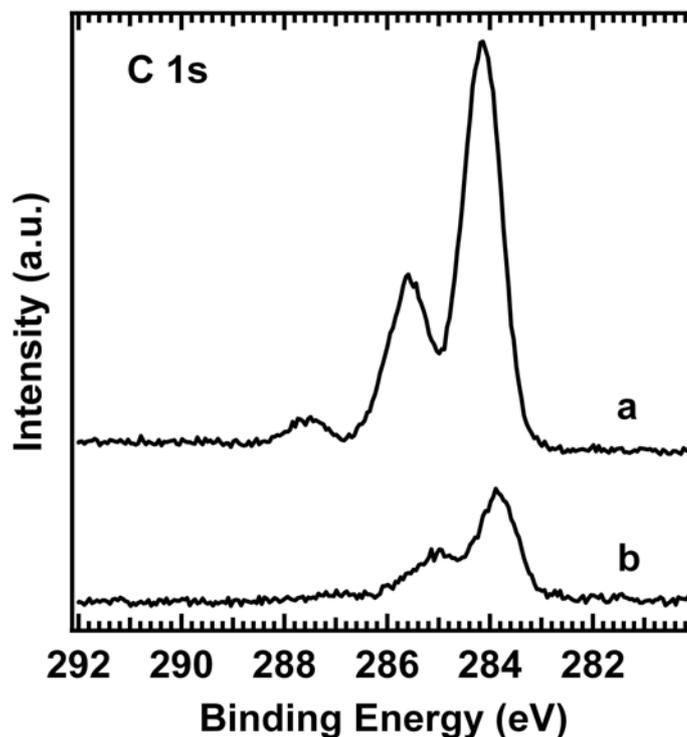
Figure 6-19. C 1s XP spectra for CoPc multilayer and monolayer on Au(111): (a) multilayer, (b) monolayer.

Figure 6-20 shows the XP spectra in N 1s region for CoPc monolayer and multilayer. Since the CoPc molecule contains only iminic nitrogen atoms, one observes only one main peak in this region. The binding energy is shifted by about 0.5 eV to the lower binding energy side from CoPc multilayer to CoPc monolayer, which is typical due to the higher effectiveness of the core hole screening in the CoPc monolayer.
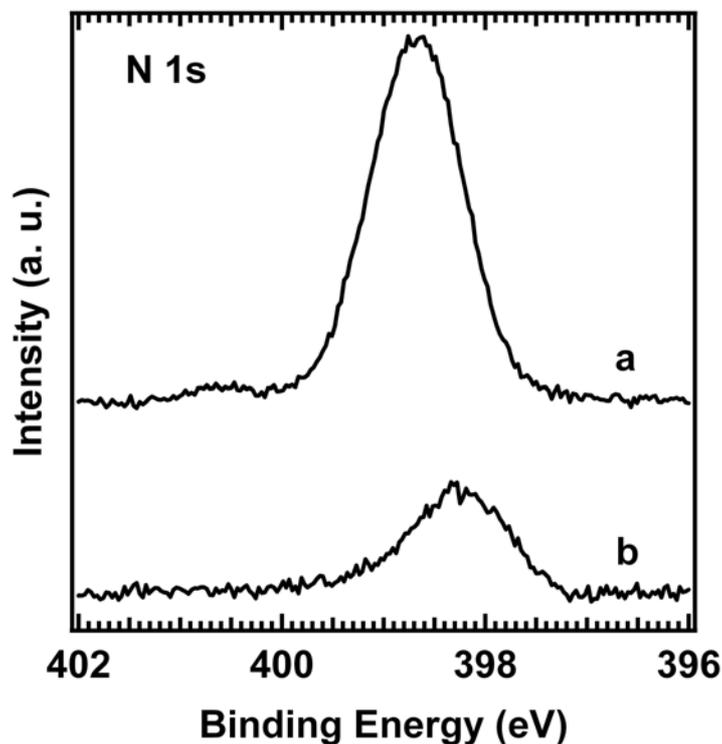
Figure 6-20. N 1s XP spectra for CoPc multilayer and monolayer on Au(111): (a) multilayer (b) monolayer.

6.2.3. Interaction between adsorbed CoPc molecules and the underlying Au(111) surface

Previous studies have revealed that the metal ions in metalloporphyrin monolayers undergo covalent electronic interaction with the substrate, accompanied by transfer of electron density from the substrate to the metal ions.[Ba04] [Fl07B] [Lu07] [Co08] [Go09] [Ba09] Since metallophthalocyanine molecules have similar structure to metalloporphyrins, and they form well ordered monolayer on Au(111) surface,[Ba04] [Lu96] it is likely that this kind of interaction also exists for adsorbed metallophthalocyanine monolayers on metal substrates. For example, on the Ag(111) surface, the binding energy difference of Co $2p_{3/2}$ signal between FePc multilayer and monolayer is about 1.8 eV, suggesting a transfer of electron density from the Ag substrate to the Fe ion.[Ba08] In order to further study the electronic interaction between metallophthalocyanines and the metal surfaces, we studied CoPc and 2HPc thin layers on Au(111) surface with UPS and XPS.

UPS measurements

Figure 6-21 shows the UP spectra of CoPc monolayers and multilayers on Au(111) in comparison to the spectrum of the clean gold surface. For better recognition, the secondary electron cutoff (left) and the region around E_F (right) are shown separately. Compared with the spectrum of the clean Au(111) surface, the spectrum of CoPc monolayer shows some new features. However, it is more like in the CoOEP case, where the new signals are not as pronounced or localized as in the CoTPP case. Table 6-4 shows the positions of the main signals in the CoPc multilayer UP spectrum, together with the main signal positions in CoTPP and CoOEP multilayer spectra. CoPc has similar values to CoOEP at about 1.2 eV, 6.5 eV, 8.4 eV and 8.7 eV, and CoTPP also shows similar values to CoPc at about 1.6 eV, 3.8 eV, 6.4 eV, and 8.5 eV.
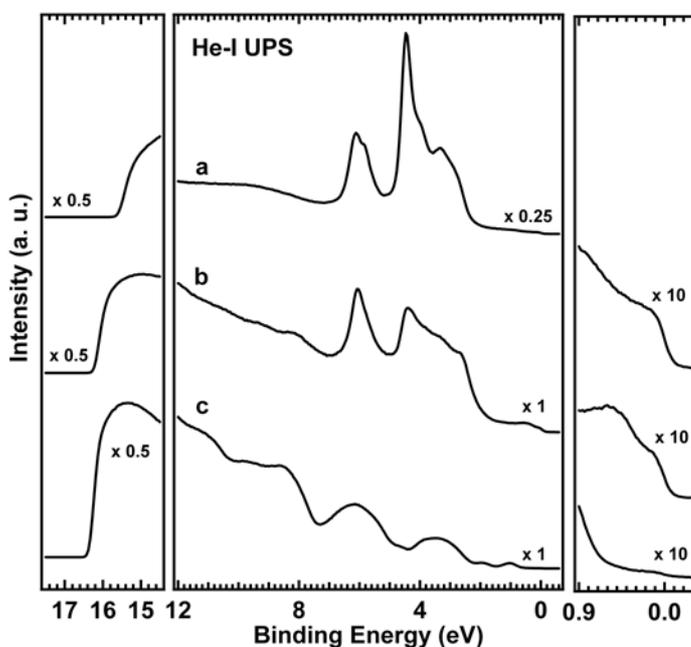
Figure 6-21. The overview UPS spectra of (a) the clean Au(111) surface, (b) a CoPc monolayer on Au(111), and (c) a CoPc multilayer on Au(111).

Table 6-4. Positions of the main signals (in eV) in the UP spectra of CoPc, CoTPP and CoOEP multilayers.

CoPc multilayer	1.1	1.7	-	3.4	-	-	6.1	8.4	8.7
CoTPP multilayer	1.6	-	-	3.8	4.6	5.1	6.4	8.5	9.3
CoOEP multilayer	1.2	-	2.8	-	4.5	-	6.5	8.4	8.7

Figure 6-22 shows the UP spectra in the region near the Fermi edge for pure Au(111), for CoPc monolayer and multilayer and for 2HPc monolayer. 6-22a shows the UV

spectrum of a CoPc multilayer on Au(111). The SOMO peak is located at about 1.1 eV below the Fermi energy. In the CoPc monolayer UV spectrum (6-22b) one observes a new electronic state at about 0.5 eV below the Fermi energy, which is absent in the UV spectrum for pure Au substrate (6-22c). Since in the UV spectrum for 2HTPP (6-22d), no new electronic state can be observed close to the Fermi edge, the new state in spectrum 6-21b most likely come from the interaction between the CoPc monolayer and the underlying Au(111) substrate. This electronic state is at a higher binding energy position than in the cases of CoTPP and CoOEP.
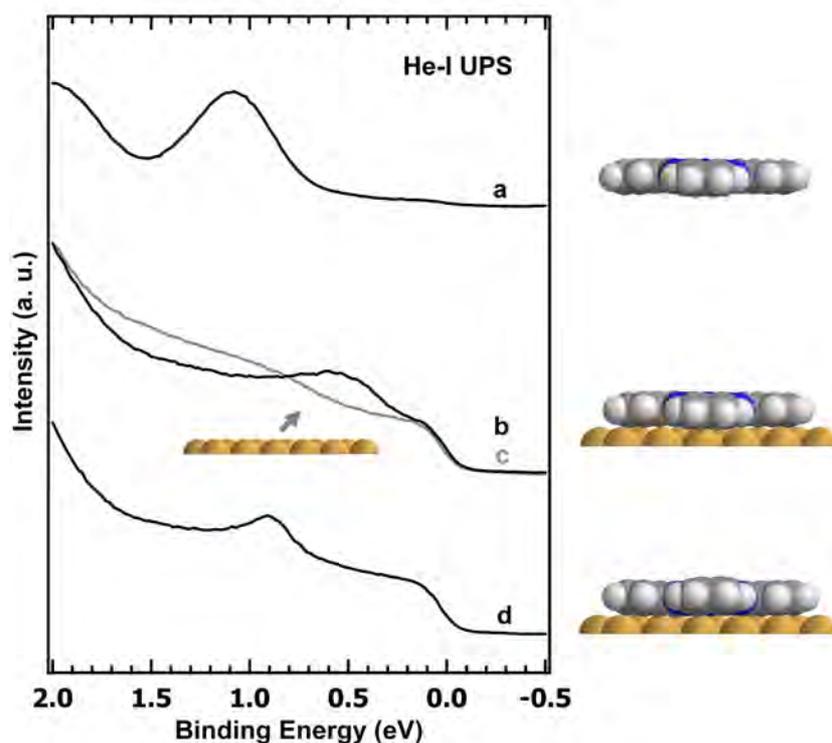
Figure 6-22. UP spectra for CoPc and 2HPc on Au(111): (a) CoPc multilayer, (b) CoPc monolayer, and (c) 2HPc monolayer

XPS measurements

Further evidence for the interaction between the Co ion and the Au(111) surface comes from XPS measurements in the Co $2p_{3/2}$ region. The results are shown in Figure 6-23.
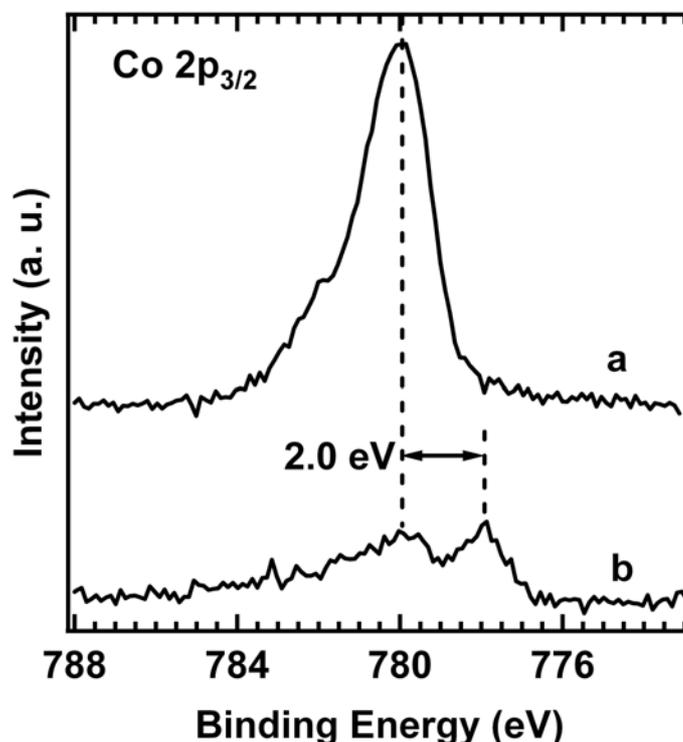
Figure 6-23. Co $2p_{3/2}$ XP spectra for CoPc multilayer and monolayer on Au(111): (a) multilayer, (b) monolayer.

Curve 6-23a shows the XP spectrum of a CoPc multilayer on Au(111), where one observes a main peak at about 780.0 eV, a typical Co(II) position, and some satellite features at the higher binding energy side. In 6-23b, the XP spectrum for a CoPc monolayer on Au(111) surface, the main signal split into two peaks. One component remains at 780.0 eV and the other component shifted to 777.8 eV, a typical Co(0) position. The appearance of the new component at 777.8 eV is most likely due to the partial reduction of a part of Co ions in the monolayer by the electrons from the Au(111) surface, which supports the conclusion that the new electronic state observed in the UP spectrum is due to the interaction between the Co ion and the underlying Au(111) surface. The form of the CoPc monolayer Co $2p_{3/2}$ XP spectrum is similar to that of CoTPP and CoOEP on Au(111) surface (shown in Figure 6-24), but different from CoTPP and CoOEP on Ag(111) surface, where there is only one peak at a typical Co(0) position. We conclude that the Co-Au(111) interaction for CoPc monolayer is not as strong as on the Ag(111) surface, thus only a portion of the Co ions are partially reduced and there exist two Co species, which give rise to the

energetic seperation in the XP spectrum. To confirm this conclusion, further study of CoPc on Ag(111) surface is necessary.
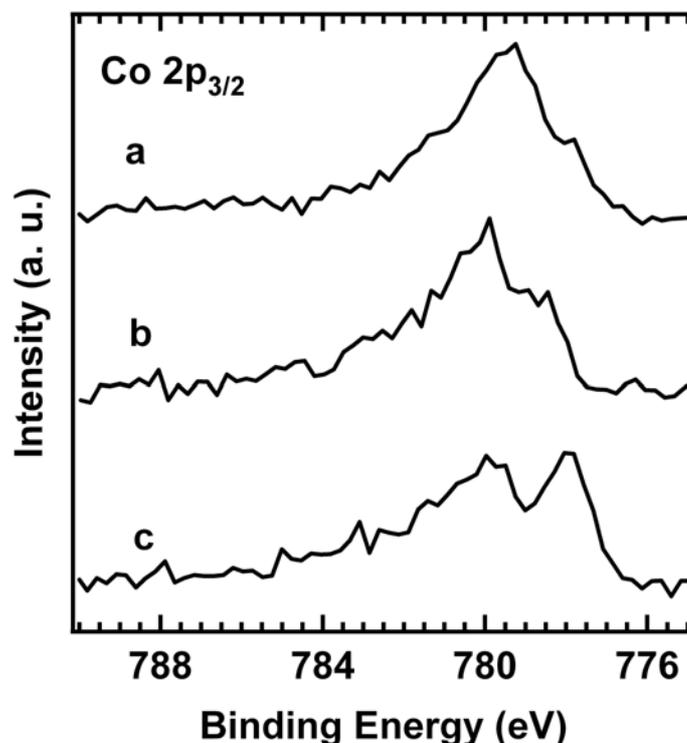
Figure 6-24 $2p_{3/2}$ XP spectra for CoTPP, CoOEP and CoPc monolayers on Au(111). (a) CoTPP monolayer, (b)CoOEP monolayer, and (c) CoPc monolayer.

Conclusion

The coordinative interaction between CoPc and an Au(111) surface has been investigated with XPS and UPS. The shift of the main Co $2p_{3/2}$ signal toward lower binding energy in the monolayer spectrum indicates that a part of the Co ions interact with the surface strongly and are partially reduced by the electrons from the Au(111) surface. The UP spectrum of the CoPc monolayer shows a new valence state, which is absent in both the CoPc multilayer UV spectrum and the 2HPc monolayer spectrum. This provides further evidence that the Co ions in the CoPc monolayer coordinately interact with the Au(111) surface.

Summary

Adsorbed tetrapyrrole complexes on well defined metal surfaces have been studied with X-ray photoelectron spectroscopy (XPS), UV photoelectron spectroscopy (UPS) and X-ray standing wave technique (XSW) in this thesis. The investigations include the preparation of Fe(II)-phthalocyanine and Fe(II)-porphyrin monolayers on a Ag(111) surface by direct metalation, studies of the interaction between the underlying surface and the metal ion in tetrapyrroles on Ag(111) and Au(111), determination of the vertical distance between the Ag(111) surface and the atoms in an adsorbed porphyrin monolayer, and the coordination of small gas molecules to the metal center of metalloporphyrins.

Preparation of tetrapyrrole thin layers on Ag(111) and Au(111) surface

Thin layers of tetrapyrroles were prepared on well defined surfaces of metal single crystals, namely Ag(111) and Au(111). Multilayers were prepared by physical vapour deposition of the tetrapyrrole molecules. The thickness depends on the temperature and the duration of deposition. Normally for thermal deposition of the tetrapyrrole molecules an evaporation temperature between 500 K and 700 K was chosen. Well defined monolayers were prepared by thermal desorption of the corresponding multilayers, where by the temperature of desorption was determined by the intensity and position of the C 1s signal in the XP spectrum. The quality and structure of the thin layers were investigated with low energy electron diffraction (LEED) and scanning tunneling microscopy (STM). In contrast to the quadratic arrangement of the tetraphenylporphyrin and the phthalocyanine monolayers, the octaethylporphyrin monolayers exhibit an oblique (almost hexagonal) arrangement. Since Ag(111) surface exhibits three-fold symmetry, the square geometry of the tetraphenylporphyrin and phthalocyanine monolayers indicates that the structure of the adsorbate lattice is more determined by intramolecular interactions than by the adsorbate-substrate interactions.

Direct synthesis of metallotetrapyrrole complexes

Conventionally, metallotetrapyrrole complexes are prepared by wet chemical methods. However for the preparation of reactive metallotetrapyrrole complexes, e.g., Fe(II)-tetraphenylporphyrin, it is difficult to obtain the pure products since they react readily with air. An alternative is to synthesize this kind of metallotetrapyrroles directly under ultra-high vacuum (UHV) conditions by depositing the corresponding metal atoms onto a pre-deposited thin layer of the metal-free base, or vice versa. In this thesis, Fe(II)-phthalocyanine was prepared in an UHV environment by depositing Fe atoms to a metal-free phthalocyanine monolayer on Ag(111). This metalation reaction happens already at room temperature with a high yield. Fe(II)-

116

tetraphenylporphyrin was also prepared by direct metalation under UHV conditions, however, in a reversed order, i.e., the metal-free tetraphenyl porphyrin (2HTPP) was deposited onto pre-deposited Fe atoms. This reaction needs to be activated by heating the mixed Fe/2HTPP layer to 550 K, indicating a reaction barrier at room temperature.

Study of the interaction between the adsorbed tetrapyrroles and the underlying metal substrates (XPS measurements)

The interaction between adsorbed cobalt porphyrin complexes and a Ag(111) surface has been studied with XPS and UPS in previous investigations.[Lu07] In this thesis this interaction was further exploded with porphyrin and phthalocyanines complexes on not only Ag(111), but also Au(111). In the study of CoOEP/2HOEP on Ag(111) with XPS, similar to the CoTPP/2HTPP on Ag(111) case, binding energy shift of about 1.9 eV between the multilayer spectrum and the monolayer spectrum was observed in the Co $2p_{3/2}$ region, indicating the presence of a covalent interaction between the Co ion and the Ag(111) surface and transfer of electron density from the Ag surface to the Co ion. CoTPP/2HTPP and CoOEP/2HOEP were also studied on a Au(111) surface. In the XP spectra for both CoTPP and CoOEP multilayers on Au(111), a main signal at a typical Co(II) position was observed, along with satellite features at higher binding energy positions. Unlike on Ag(111), the XP spectra of the CoTPP and CoOEP monolayers on Au(111) feature a main peak with a minor component at lower binding energy position in the Co $2p_{3/2}$ region, with an energetic seperation of about 1.5 eV (for CoTPP) and 1.6 eV (for CoOEP). This indicates the coexistence of weakly and strongly interacting complexes on the gold substrate and is attributed to the herringbone reconstruction of Au(111), which leads to periodic lateral variations of the surface reactivity. In particular, it is proposed that the Co ions interact strongly with the transition regions between areas with fcc and hcp stacking. In these transition regions, the Au atoms in the topmost layer have elevated positions and sit on quasi-bridge sites. In the case of CoPc on Au(111), the Co $2p_{3/2}$ XP spectrum of CoPc multilayer shows one main signal along with some satellite features on higher binding energy side. Similar to CoTPP and CoOEP monolayers on Au(111), in the Co $2p_{3/2}$ XP spectrum of CoPc monolayer this main peak splits into two signals with a energy difference of 2.0 eV. However, the signal at lower binding energy position is much more significant than in CoTPP and CoOEP monolayer spectra, which suggests a higher ratio of the species at lower binding energy in CoPc monolayer.

Study of the interaction between the adsorbed tetrapyrroles and the underlying metal substrates (UPS measurements)

More evidence of the presence of a covalent interaction between the metal ion and substrates was provided with UPS measurements. For a CoOEP monolayer on Ag(111), a new electronic state was observed around 0.6 eV below the Fermi energy.

This state does not appear in the UP spectrum of a 2HOEP monolayer or of a CoOEP multilayer. Since CoOEP molecules do not undergo saddle-shaped distortion upon adsorption on the Ag(111) surface (a change that could also modify the valence electronic structure), this new electronic state can only result from the interaction between the Co ion and the underlying Ag(111) surface. on Au(111), we observed a new weak and broad feature around 0.3 eV below the Fermi energy for both CoOEP and CoTPP monolayers, which indicates the presence of an electronic interaction also between the Co ion and the Au(111) surface. CoPc on a Au(111) surface also gives rise to a new electronic state at around 0.5 eV, which is similar to the new electronic state of CoTPP and CoOEP monolayers on Ag(111).

Determination of the distance between the substrate surface and the metal ions in the porphyrin molecules

In previous studies it was assumed that when the peripheral substituents in a metalloporphyrin were replaced by significantly bigger or smaller groups, the distance between the substrate surface and the metal ion in the porphyrin molecule would be changed, thus the strength of the interaction between the substrate and the metal ion would also be changed.[Lu07] In order to verify this assumption, the distance between the substrate surface and the metal ion was measured with the XSW technique. It was initially assumed that the Co-Ag(111) distance was larger for the CoTTBPP monolayer than for the CoTPP monolayer, because of the much larger substituents. However, the distance measured with XSW was 5.16 Å for CoTTBPP and 5.27 Å for CoTPP, and both distances seem too long to be in agreement with a covalent interaction between the Co ion and the Ag surface, as observed by UPS and XPS. Since XSW technique only measures the distance between the atoms in an adsorbed molecule and the Bragg diffraction plane, it does not determine the distance between the atoms in an adsorbed molecule and an atom from the substrate surface at the local adsorption site. To resolve the apparent contradiction between XPS/UPS and XSW results, we propose that silver atoms can be trapped between the coordinated Co ions of the Co(II)-porphyrin molecules and the Ag(111) surface, which reduces the Co-Ag distance by approximately 2.36 Å, the distance between two adjacent Ag(111) planes. The resulting distance of about 2.91 Å allows for an electronic interaction between the Co ion and the Ag atom. For all three metalloporphyrins (CoTPP, CoTTBPP and ZnTPP), relatively low coherent fraction for N 1s was acquired, which suggests different heights of N atoms in porphyrin molecules. This is probably due to the previously observed saddle-shaped distortion of the molecules.[We08]

Coordinaation of small gas molecules to Fe(II)TPP monolayer on the Ag(111) surface

In order to prepared the O_2-Fe(II)TPP complex, oxygen molecules were dosed at room temperature to an *in situ* prepared Fe(II)TPP monolayer on Ag(111). The chemical changes, especially at the metal center, were monitored using the Fe $2p_{3/2}$ XPS signal. Before dosing oxygen, the main signal in the Fe$2p_{3/2}$ XP spectrum was at a binding energy of 707.2 eV, which is near a typical Fe(0) position. After oxygen attachment the main signal was shifted to a binding energy of 709.3 eV, while a small signal remained at the Fe(0) position. The change of the Fe $2p_{3/2}$ spectrum illustrated that oxygen molecules have been coordinated to the Fe ion. The change of electron density on Fe may be the result of different effects. Firstly, it can come from the direct transfer of electron density from Fe to O_2, which leads to the formation of superoxide (O_2^-) or peroxide (O_2^{2-}). Secondly, as already observed for NO coordination on CoTPP and FeTPP,[Fl07C] [Fl07B] the coordination of O_2 on FeTPP may also suppress the electronic interaction between the Fe ion and the underlying substrate due to the trans effect, thus weakens the electron density on Fe. The XP O 1s spectrum shows two components with the same intensity, suggesting an end-on coordination geometry of the oxygen molecule on the central Fe atom. The exchange by a CO molecule of an oxygen molecule coordinated on the central Fe atom was not observed at room temperature, although according to a DFT calculation[Sh10], the binding energy of CO with the central Fe atom is much higher than that of O_2. This suggests the existence of an activation barrier of the exchange experiment.

Zusammenfassung

Adsorbierte Tetrapyrrolkomplexe auf wohldefinierten Metalloberflächen wurden in dieser Arbeit mittels Röntgenphotoelektronenspektroskopie (XPS) UV-Photoelektronenspektroskopie (UPS) und X-ray Standing Wave Technik (XSW) untersucht. Dies beinhaltet die *in situ* Synthese von ultra reinen Fe(II)-Phthalocyanin und Fe(II)-Porphyrin Monolage auf einer Ag(111) Oberfläche, die Untersuchungen der Wechselwirkung zwischen der Substratoberfläche und dem zentralen Metallionen der Tetrapyrrole auf Ag(111) und Au(111) Oberflächen, als auch die Bestimmung des vertikalen Abstands zwischen dem Substrat und den Atomen der Moleküle in einer Monolage.

Präparation von dünnen Tetrapyrrolschichten auf Ag(111) und Au(111)

Die untersuchten Tetrapyrrolmultilagen wurden durch Gasphasenabscheidung der entsprechenden Moleküle auf wohldefinierte Ag(111) und Au (111) Einkristalloberflächen hergestellt. Je nach verwendetem Tetrapyrrolkomplex wurde eine Temperatur zwischen 500 K und 700 K für die Abscheidung gewählt. Die Herstellung von entsprechenden Monolagen wurde durch thermische Desorption von überschüssig aufgedampften Multilagenmolekülen erreicht. Die Desorptionstemperatur konnte über die Intensität und die Position des C 1s Signal im XP Spektrum bestimmt werden. Die Qualität und die Struktur der dünnen Schichten wurden mit Beugung niederenergetischer Elektronen (LEED) und Rastertunnelmikroskopie (STM) untersucht. Auf Ag(111) zeigten die Tetraphenylporphyrinmonolagen und die Phthalocyaninmonolagen eine quadratische Anordnung, während Octaethylporphyrine in einer schiefwinkligen, fast hexagonalen Struktur aggregierten. Auf Ag (111), da die Metalloberfläche Dreifachsymmetrie besetzt, zeigt die quadratische Geometrie der Tetraphenylporphyrin- und Phthalocyanin-Monoschichten, dass die Struktur des Adsorbat Gitters mehr durch intramolekulare Wechselwirkungen als durch die Wechselwirkungen zwischen dem Adsorbat und dem Substrat bestimmt wird.

Direkte Synthese von Metallotetrapyrrolen

Konventionell werden Metallotetrapyrrolkomplexe durch nass-chemische Verfahren hergestellt. Allerdings ist die Herstellung von reaktiven Metallotetrapyrrolkomplexen, z. B. Fe(II)-Tetraphenylporphyrin, auf diese Weise schwierig, da Reaktionen mit der umgebenden Luft nicht ausgeschlossen werden können. Eine Alternative ist, diese Art von Metallotetrapyrrolen direkt unter UHV-Bedingung zu synthetisieren. Hierbei werden die entsprechenden Metallatome auf eine Monolage der metallfreien Base aufgedampft oder umgekehrt. In dieser Arbeit wurden Fe-Atome auf eine adsorbierte metallfreie

Phthalocyaninmonolage (2HPc) aufgedampft, und FePc mit hoher Ausbeute hergestellt. Darüber hinaus wurde auch Fe(II)-Tetraphenylporphyrin durch diese Art der direkten Metallierung unter UHV-Bedingungen synthetisiert. Anders als bei FePc-Synthese wurde hier das metallfreie Tetraphenylporphyrin auf eine Ag(111)-Oberfläche mit bereits adsorbierten Fe-Atomen aufgedampft. Diese Reaktion muss durch Erhitzen der Probe auf 550 K aktiviert werden, was auf eine Reaktionsbarriere schließen lässt, die bei Raumtemperatur nicht überwunder werden kann.

Untersuchung der Wechselwirkung zwischen den adsorbierten Tetrapyrrolen und Ag(111) bzw. Au(111) mittels XPS

In dieser Arbeit wurde die Wechselwirkung von Porphyrinen und Phthalocyaninen mit Ag(111) und Au(111) Oberflächen untersucht. Bei der Untersuchung von CoOEP auf Ag(111) mittels XPS zeigte sich eine Verschiebung des Co $2p_{3/2}$ Signals um 1.9 eV zu niedrigerer Bindungsenergie, beim Übergang von der Multilage zur Monolage. Dieser Effekt deutet auf eine kovalente Wechselwirkung zwischen dem zentralen Cobaltion und der Silberoberfläche hin, die möglicherweiser auch mit einer Ladungsübertragung vom Ag-Substrat zum Co-Ion verbunden ist. Ähnliche Effekte wurden bei früheren Experimenten mit CoTPP auf Ag(111) beobachtet.[Lu07] Um den Einfluss des Substrates auf diese Effekte zu charakterisieren wurden CoOEP und CoTPP Multi- und Monolagen auf Au(111) untersucht. Hier zeigte sich nur eine geringe Verschiebung des dominierenden Co $2p_{3/2}$ Signals von ~0.5 eV bei CoTPP und kaum Verschiebung bei CoOEP, beim Übergang von der Multilage zur Monolage. Neben dem Hauptsignal zeigten die Spektren aber auch einen stark zu niedrigeren Bindungsenergien verschobenen Anteil. Die Verschiebung, relativ zum Hauptsignal im Monolagenspektrum, betrug für CoTPP etwa 1.5 eV und für CoOEP 1.6 eV. Dies deutet auf die Koexistenz von stark und schwach wechselwirkenden Komplexen auf der Goldoberfläche hin, was vermutlich in Zusammenhang mit der Au(111) Rekonstruktion steht. Diese Oberflächenrekonstruktion führt u.a. zu periodischen lateralen Variationen der Oberflächenstruktur (fcc, hcp und Übergangsbereich) sowie der Reaktivität der Oberfläche. Insbesondere könnten die Übergangsregionen zwischen fcc und hcp Bereichen Adsorptionsplätze mit der Möglichkeit zu stärkerer Wechselwirkung zwischen den Co-Ionen und dem Substrat darstellen. In diesem Übergangsbereich besetzen die Au-Atome relativ zum übrigen Gitter erhöhte Positionen. Ein Vergleich der Spektren von CoPc, CoTPP und CoOEP Monolagen zeigt weiterhin, dass die Wechselwirkung mit dem Au(111) Substrat zum Teil von der Molekülgeometrie beeinflusst wird. So ist der relative Signalanteil der stark verschobenen Co $2p_{3/2}$ Komponente im Fall von CoPc Monolagen wesentlich höher als in CoOEP und CoTPP Spektren. Das deutet darauf hin, dass in CoPc Monolagen ein größerer Anteil der adsorbierten Moleküle stark mit dem Substrat wechselwirken kann.

Untersuchung der Wechselwirkungen zwischen den adsorbierten Tetrapyrrolen und Ag(111) bzw. Au(111) mittels UPS

Weitere Indizien für die elektronische Wechselwirkung zwischen den Metallionen und Substraten wurden mit UPS Messungen erbracht. Im Fall von CoOEP Monolagen auf Ag(111) zeigte sich ein neuer elektronischer Zustand etwa 0.6 eV unterhalb der Fermienergie. Dieses Signal fehlte sowohl im CoOEP Multilagenspektrum als auch im entsprechenden Spektrum für die metallfreie Monolage aus 2HOEP Molekülen. Da sich die CoOEP Moleküle in der Monolage nicht geometrisch verformen, wie das z.B. von Tetraphenylporphyrinen bekannt ist, kann auch dieser Effekt als mögliche Ursache für die neue elektronische Struktur ausgeschlossen werden. Somit kann dieser neue elektronische Zustand allein der Wechselwirkung zwischen dem Co-Ion und der Ag(111) Oberfläche zugeschrieben werden. Bei CoOEP, CoTPP und CoPc Monolagen auf Au(111) zeigt sich diese oberflächen-induzierte Struktur ebenfalls. Im Falle von CoOEP und CoTPP erscheint sie etwa 0.3 eV unterhalb der Fermikante, allerdings schwächer ausgeprägt als auf Ag(111). Im Fall von CoPc Monolagen befindet sie sich etwa 0.5 eV unterhalb der Fermikante.

Bestimmung des Abstandes zwischen der Substratoberfläche und der Metallionen in den Porphyrinmolekülen

Um den Abstand des zentralen Metallions von Metalloporphyrinen von der Substratoberfläche zu variieren, wurden in einer vorangegangenen Studie[Lu07] die entsprechenden Porphyrine mit unterschiedlichen seitlichen Substituenten versehen. So sollte der Abstand zwischen Metallion und Oberfläche im CoTTBPP aufgrund der größeren Substituenten auch größer sein als der entsprechende Abstand beim CoTPP. Mit dieser Variation des Abstandes sollte sich auch die Stärke der Wechselwirkung zwischen dem Metallzentrum und dem Substrat ändern. [Lu07] Um diese postulierte Abstandsänderung zu messen wurden X-ray standing wave (XSW) Experimente durchgeführt. Diese Technik ermöglicht es, den Abstand von Adsorbaten zur Oberflächenebene festzustellen. Abweichend von diesen Erwartungen zeigten die XSW Messungen einen Metallion-Substrat Abstand von 5.16 Å für CoTTBPP und 5.27 Å für CoTPP. Diese Abstände sind wesentlich größer als die Distanzen, die normalerweise typisch für kovalente Wechselwirkungen sind. Die gemessenen Distanzen beziehen sich allerdings nur auf die Oberflächenebene, d.h. XSW ist nicht in der Lage unterschiedliche lokale Distanzen festzustellen. Bei den gemessenen Abständen wäre es durchaus denkbar, dass sich zwischen den koordinierten Metallionen und der Oberflächenebene ein einzelnes Ag-Atom befindet. Diese Hypothese würde die starke kovalente Wechselwirkung der beiden Adsorbate trotz des großen Abstandes zur Ag(111) Ebene erklären. In diesem Fall würde sich der Abstand zwischen dem Metallion und dem nächsten Ag-Atom um etwa 2.36 Å verringern, wodurch eine starke Wechselwirkung zwischen Metall-Zentrum und Substrat plausibel erscheint. Eine Analyse der Abstände der Stickstoffatome von der

Ag(111) Ebene offenbart für CoTPP, CoTTBPP und ZnTPP Monolagen niedrige Kohärenzfaktoren, was ein Indiz für eine unregelmäßige Höhenverteilung der N-Atome darstellt. Diese Ergebnisse stehen mutmaßlich im Zusammenhang mit einer Verformung der Moleküle in eine sattelförmige Konformation, über die in der Literatur berichtet wird [We08].

Koordination kleiner Gasmoleküle an einer Fe(II)TPP Monoschicht auf einer Ag (111) Oberfläche

Um die Koordination kleiner Moleküle an Metalloporphyrine zu studieren, wurden Sauerstoffmoleküle auf eine *in situ* hergestellte Fe(II)TPP Monolage dosiert. Mit XPS konnte eine Änderung im Fe $2p_{3/2}$ Spektrum beobachtet werden, die in Zusammenhang mit der Adsorption der Sauerstoffmoleküle an die Fe-Zentralionen steht. Vor der Sauerstoffdosierung lag das Hauptsignal im Fe $2p_{3/2}$ XP Spektrum bei einer Bindungsenergie von 707.2 eV und damit im Bereich einer typischen Fe(0) Position. Nach der Sauerstoffdosierung wurde das Hauptsignal zu einer Bindungsenergie von 709.3 eV verschoben. Die Änderung des Fe $2p_{3/2}$ Spektrums zeigt, dass Sauerstoff-Moleküle auf die Fe-Ionen koordiniert wurden. Die Veränderung der Elektronendichte an Fe kann Ursachen haben. Erstens kann sie vom direkten Transfer der Elektronendichte von Fe zu O_2 kommen, die zur Bildung von Superoxid (O_2^-) oder Peroxid (O_2^{2-}) führt. Zweitens, kann wie bereits für NO Koordinierung mit CoTPP und FeTPP beobachtet, [Fl07B] [Fl07C] die Koordinierung von O_2 auf FeTPP ebenfalls die elektronische Wechselwirkung zwischen den Fe-Ionen und dem Substrat aufgrund des trans-Effekts unterdrücken und damit die Elektronendichte an Fe schwächen. Das XP Spektrum im Bereich der O 1s Region zeigte zwei Komponenten, die auf einen end-on Modus von der Adsorption eines Sauerstoffmoleküles auf das zentrale Eisenatom hindeuten. In einem weiteren Experiment sollten die komplexierten Sauerstoffmoleküle durch CO-Moleküle verdrängt werden. DFT–Rechnungen zeigen für eine Bindung an das Fe Zentralion eine wesentlich höhere Bindungsstärke von CO als für O_2. Die XPS Spektren nach der CO Dosierung lassen allerdings keine Rückschlüsse darauf zu, ob und gegebenenfalls wie weit diese Verdrängungsreaktion abläuft. Dies weist auf das Vorliegen einer Aktivierungsbarriere für die Austauschreaktion hin.

References

[Åh06] J. Åhlund, K. Nilson, J. Schiessling, L. Kjeldgaard, S. Berner, N. Mårtensson, C. Puglia, B. Brena, M. Nyberg and Y. Luo, *J. Chem. Phys.*, 2006, **125**, 034709.

[Al05A] Y. Alfredsson, B. Brena, K. Nilson, J. Åhlund, L. Kjeldgaard, M. Nyberg, Y. Luo, N. Mårtensson, A. Sandell, C. Puglia and H. *J.* Siegbahn *Chem. Phys.*, 2005, **122**, 214723.

[Al05B] Y. Alfredsson, J. Åhlund, K. Nilson, L. Kjeldgaard, J. N. O'Shea, J. Theobald, Z. Bao, N. Mårtensson, A. Sandell, C. Puglia and H. Siegbahn, *Thin Solid Films*, 2005, **493**, 13-19.

[Au07A] W. Auwärter, A. Weber-Bargioni, S. Brink, A. Riemann, A. Schiffrin, M. Ruben and J. V. Barth, *ChemPhysChem*, 2007, **8**, 250-254.

[Au07B] W. Auwärter, F. Klappenberger, A. Weber-Bargioni, A. Schiffrin, T. Strunskus, C. Wöll, Y. Pennec, A. Riemann and J. V. Barth, *J. Am. Chem. Soc.*, 2007, **129**, 11279-11285.

[Au08] W. Auwärter, A. Schiffrin, A. Weber-Bargioni, Y. Pennec, A. Riemann and J. V. Barth, *Int. J. Nanotechnol.*, 2008, **5**, 1171-1193.

[Ba90] J. V. Barth, H. Brune, G. Ert, and R. J. Behm, *Phys. Rev. B*, 1990, **42**, 9307-9318.

[Ba04] D. E. Barlow, L. Scudiero, and K. W. Hipps, *Langmuir*, 2004, **20**, 4413-4421.

[Ba07] J. V. Barth, *Annu. Rev. Phys. Chem.*, 2007, **58**, 375-407.

[Ba08] Y. Bai, F. Buchner, M. T. Wendahl, I. Kellner, A. Bayer, H.-P. Steinrück, H. Marbach and J. M. Gottfried, *J. Phys. Chem. C*, 2008, **112**, 6087-6092.

[Ba09] Y. Bai, F. Buchner, I. Kellner, M. Schmid, F. Vollnhals, H.-P. Steinrück, H. Marbach and J. M. Gottfried, *N. J. Phys.,* 2009, **11**, 125004.

[Be06] S. Berner, S. Biela, G. Ledung, A. Gogoll, J. E. Backvall, C. Puglia and S. Oscarsson, *J. Cat.*, 2006, **244**, 86-91.

[Be07] W. J. Belcher, K. I. Wagner and P. C. Dastoor, *Solar Energy Materials & Solar*, Cells 2007, **91**, 447–452.

[Be07] A. Bendounan, F. Forster, A. Schöll, D. Batchelor, J. Ziroff, E. Umbach and F. Reinert, *Surf. Sci.*, 2007, **601**, 4013-4017.

[Bö99] M. Böhringer, K. Morgenstern, W.-D. Schneider, R. Berndt, F. Mauri, A. De Vita and R. Car, *Phys. Rev. Lett.*, 1999, **83**, 324.

[Br90] Practical Surface Analysis Volume 1: *Auger and X-ray Photoelectron Spectroscopy*, Edited by D. Briggs and M. P. Seah, John Wiley & Sons Ltd 1990 (2nd Ed.).

[Br09] J. Brede, M. Linares, S. Kuck, J. Schwöbel, A. Scarfato, S.-H. Chang, G. Hoffmann, R. Wiesendanger, R. Lensen, P. H. J. Kouwer, J. Hoogboom, A. E. Rowan, M. Bröring, M. Funk, S. Stafström, F. Zerbetto and R. Lazzaroni, *Nanotechnol.*, 2009, **20**, 275602-275612.

[Bu07A] F. Buchner, K. Comanici, N. Jux, H.-P. Steinrück and H. Marbach, *J. Phys. Chem. C*, 2007, **111**, 13531-13538.

[Bu07B] F. Buchner, V. Schwald, K. Comanici, H.-P. Steinrück and H. Marbach, *ChemPhysChem*, 2007, **8**, 241-243.

[Bu08] F. Buchner, K. Flechtner, Y. Bai, E. Zillner, I. Kellner, H.-P. Steinrück, H. Marbach and J. M. Gottfried, *J. Phys. Chem. C,* 2008, **112**, 15458-15465.

[Bu09] F. Buchner, K.-G. Warnick, T. Wölfle, A. Görling, H.-P. Steinrück, W. Hieringer and H. Marbach, *J. Phys. Chem. C*, 2009, **113**, 16450-16457.

[Ca07] W. M. Campbell, K. W. Jolley, P. Wagner, K. Wagner, P. J. Walsh, K. C. Gordon, L. Schmidt-Mende, M. K. Nazeeruddin, Q. Wang, M. Gratzel and D. L. Officer, *J. Phys. Chem. C*, 2007, **111**, 11760-11762.

[Ca09] S. T. Castaman, S. Nakagaki, R. R. Ribeiro, K. J.Ciuffi and S. M. Drechsel, *J. Mol. Cat. A: Chemical*, 2009, **300**, 89-97.

[Ch91] D. D. Chambliss, R. J. Wilson and S. Chiang, *Phys. Rev. Lett.*, 1991, **66**, 1721.

[Ci07] J. J. Cid, J. H. Yum, S. R. Jang, M. K. Nazeeruddin, E. M. Ferrero, E. Palomares, J. Ko, M. Gratzel and T. Torres, *Angew. Chem. Int. Ed.*, 2007, **46**, 8358-8362.

[Cl06] S. Clair, S. Pons, S. Fabris, S. Baroni, H. Brune, K. Kern and J. V. Barth, *J. Phys. Chem. B*, 2006, **110**, 5627-5632.

[Co08] K. Comanici, F. Buchner, K. Flechtner, T. Lukasczyk, J. M. Gottfried, H.-P. Steinruck and H. Marbach *Langmuir*, 2008, **24**, 1897-1901.

[ESRF] http://www.esrf.eu/, 2010.

[Fi06] D. Filippini, A. Alimelli, C. Di Natale, R. Paolesse, A. D'Amico and I. Lundstrom, *Angew. Chem. Int. Ed.*, 2006, **45**, 3800-3803.

[Fl07A] K. Flechtner, A. Kretschmann, L. R. Bradshaw, M. M. Walz, H. P. Steinrück and J. M. Gottfried, *J. Phys. Chem. C*, 2007, **111**, 5821-5824.

[Fl07B] K. Flechtner, A. Kretschmann, H.-P. Steinrück, and J. M. Gottfried, *J. Am. Chem. Soc.*, 2007, **129**, 12110-12111.

[Fl07C] K. Flechtner, *Dissertation*, Universität Erlangen-Nürnberg, Erlangen, 2007.

[Gl98] K. Glöcker, C. Seidel, A. Soukopp, M. Sokolowski, E. Umbach, M. Böhringer, R. Berndt and W.-D. Schneider, *Surf. Sci.*, **199**8, 405, 1-20.

[Go06] J. M. Gottfried, K. Flechtner, A. Kretschmann, T. Lukasczyk and H. P. Steinrück, *J. Am. Chem. Soc.*, 2006, **128**, 5644-5645.

[Go09] J. M. Gottfried and H. Marbach, *Z. Phys. Chem.-Int. J. Res. Phys. Chem. Chem. Phys.*, 2009, **223**, 53-74.

[Gu35] R. W. Gurney, *Phys. Rev.*, 1935, **47**, 479-482.

[Gu78] O. Gunnarsson and K. Schönhammer, *Phys. Rev. Lett.*, 1978, **41**, 1608-1612.

[Ha85] U. Harten, A. M. Lahee, J. P. Toennies and C. Wöll, *Phys. Rev. Lett.*, 1985, **54**, 2619.

[He07] S. K. M. Henze, O. Bauer, T.-L. Lee, M. Sokolowski and F. S. Tautz, *Surf. Sci.*, 2007, **601**, 1566-1573.

[Hi96] K. W. Hipps, X. Lu, X. D. Wang and U. Mazur, *J. Phys. Chem.*, 1996, **100**, 11207.

References

[Hi10] W. Hieringer et al., Surface Coordination Chemistry with Metalloporphyrins, in Preparation.

[Hu07] B. Hulskeni, R. Van Hameren, J. W. Gerritsen, T. Khoury, P. Thordarson, M. J. Crossley, A. E. Rowan, R. J. M. Nolte, J. A. A. W. Elemans and S. Speller, *Nat. nanotechnol.*, 2007, **2**, 265-289.

[Is99] H. Ishii, K. Sugiyama, E. Ito and K. Seki, *Adv. Mater.*, 1999, **11**, 605-625.

[Kh75] C. Khandelwal and J. Roebber, *Chem. Phys. Lett.*, 1975, **34**, 355-359.

[Ki75] K. S. Kim, *Phys. Rev. B*, 1975, **11**, 2177-2185.

[Ki06] L. Kilian, E. Umbach and M. Sokolowski, *Surf. Sci.*, 2006, **600**, 2633-2643

[Kl08] F. Klappenberger, A. Weber-Bargioni, W. Auwarter, M. Marschall, A. Schiffrin and J. V. Barth, *J. Chem. Phys.*, 2008, **129**, 214702.

[Ko34] T. Koopmans, *Physica*, 1934, **1**, 104-113.

[Kr07] A. Kretschmann, M.-M. Walz, K. Flechtner, H.-P. Steinrück and J. M. Gottfried, *Chem. Commun.*, 2007, 568-570.

[Ku10] Personal Contact. Forschungszentrum Jülich, Institute of Bio- and Nanosystems, c.kumpf@fz-juelich.de.

[La32] I. Langmuir, *J. Am. Chem. Soc.*, 1932, 54, 2798-2832.

[La05] J. G. Speight, *Lange's Handbook of Chemistry* (section 1.3 The Elements), Mcgraw-Hill Publ. Comp., 2005 (16th Ed.).

[Li06] N. Lin, S. Stepanow, F. Vidal, K. Kern, M. S. Alam, S. Strömsdörfer, V. Dremov, P. Müller, A. Landa and M. Ruben, *Dalton Trans.*, 2006, 2794-2800

[Li08] N. Lin, S. Stepanow, M. Ruben and J. V. Barth, *Topics in Current Chemistry- Templates in Chemistry III*, 2009, **287**, 1-44.

[Lu96] X. Lu, K. W. Hipps, X. D. Wang and U. Mazur, *J. Am. Chem. Soc.*, 1996, **118**, 7197.

[Lu07] T. Lukasczyk, K. Flechtner, L. R. Merte, N. Jux, F. Maier, J. M. Gottfried and H. P. Steinrück, *J. Phys. Chem. C*, 2007, **111**, 3090-3098.

[Ma84] N. Mårtensson R. Nyholm and B Johansson, *Phys. Rev. B*, 1984, **29**, 4800-4802.

[Mo80] I. Mochida, K. Tsuji, K. Suetsugu, H. Fujitsui and K. Takeshita, *J. Phys. Chem.*, 1980, **84**, 3159-2162.

[Mo82a] I. Mochida, K. Suetsugu, H. Fujitsu and K. Takeshita, *J. Cat.*, 1982, **77**, 519-526.

[Mo82b] I. Mochida, K. Suetsugu, H. Fujitsu and K. Takeshita, *J. Chem. Soc., Chem. Commun.*, 1982, 166-167.

[Mo83] I. Mochida, K. Suetsugu, H. Fujitsu and K. Takeshita, *J. Phys. Chem.* 1983, **87**, 1524-1529.

[Ni06] N. Nicoara, E. Román, J.M. Gómez-Rodríguez, J. A. Martín-Gago and J. Méndez, *Org. Electro.*, 2006, **7**, 287–294.

[Og06] A. Ogunrinde, K. W. Hipps and L. Scudiero, *Langmuir*, 2006, **22**, 5697-5701.

[Pa06] G. B. Pan, H. J. Yan and L. J. Wan, *Nano*, 2006, **1**, 95-100.

[Po74] R. A. Pollak, L. Ley, F. R. McFeely, S. P. Kowalczyk and D. A. Shirley, *J. Electron Spectrosc. Relat. Phenom.*, 1974, **3**, 381-398.

[Pr07] L. D. Prockop and R. I. Chichkova, *J. Neuro. Sci.*, 2007, **262**, 122–130.

[Ra06] L. Ramoino, M. von Arx, S. Schintke, A. Baratoff, H. J. Guntherodt and T. A. Jung, *Chem. Phys. Lett.*, 2006, **417**, 22-27.

[Ra00] N. A. Rakow and K. S. Suslick, *Nature*, 2000, **406**, 710-713.

[Ri08] J. R. Gispert, *Coordination Chemistry.*, Wiley-VCH, 2008.

[Sc97] T. Schmitz-Hübsch, T. Fritz, F. Sellman, R. Staub and K. Leo, *Phys. Rev. B*, 1996, **55**, 7972-7976.

[Sc00] L. Scudiero, D. E. Barlow and K.W. Hipps, *J. Phys. Chem. B*, 2000, **104**, 11899-11905.

[Sc01] L. Scudiero, D. E. Barlow, U. Mazur and K. W. Hipps, *J. Am. Chem. Soc.*, 2001, **123**, 4073-4080.

[Sc02] L. Scudiero, D. E. Barlow and K. W. Hipps, *J. Phys. Chem. B*, 2002, **106**, 996-1003.

[Sc04] A. Schöll, Y. Zou, M. Jung, Th. Schmidt, R. Fink and E. Umbach, *J. Chem. Phys.*, 2004, **121**, 10260-10267.

[Sc05] L. Schmidt-Mende, W. M. Campbell, Q. Wang, K. W. Jolley, D. L. Officer, M. K. Nazeeruddin and M. Gratzel, *Chemphyschem*, 2005, **6**, 1253-1258.

[Sc07] L. Scudiero and K. W. Hipps, *J. Phys. Chem. C*, 2007, **111**, 17516-17520.

[Sc08] C. H. Schwalb, S. Sachs, M. Marks, A. Schöll, F. Reinert, E. Umbach, and U. Höfer, *Phys. Rev. Lett.*, 2008, **101**, 146801.

[Se79] M. P. Seah and W. A. Dench, *Surf. Interf. Anal.* 1979, **1**, 1-11.

[Sh72] D.A. Shirley*, Phys. Rev. B*, 1972, **5**, 4709-4714.

[Sh07] T. E. Shubina, H. Marbach, K. Flechtner, A. Kretschmann, N. Jux, F. Buchner, H.-P. Steinrück, T. Clark and J. M. Gottfried, *J. Am. Chem. Soc.*, 2007, **129**, 9476-9483.

[Sh10] T. E. Shubina and T. Clark, Universität Erlangen-Nürnberg, Computer-Chemie-Centrum, clark@chemie.uni-erlangen.de, Personal Contact.

[St06] C. Stadler, S. Hansen, F. Pollinger, C. Kumpf, E. Umbach, T.-L. Lee and J. Zegenhagen, *Phys. Rev. B*, 2006, **74**, 035404.

[Ta08] S. L. Tait, Y. Wang, G. Costantini, N. Lin, A. Baraldi, F. Esch, L. Petaccia, S. Lizzit and K. Kern, *J. Am. Chem. Soc.*, 2008, **130**, 2108–2113.

[Ta08] B. R. Takulapalli, G. M. Laws, P. A. Liddell, J. Andreasson, Z. Erno, D. Gust and T. J. Thornton, *J. Am. Chem. Soc.*, 2008, **130**, 2226-2233.

[To27] J. Topping, *Proc. Roy. Soc. London A*, 1927, **114**, 67-72.

[Ts02] E. V. Tsiper, Z. G. Soos, W. Gao and A. Kahn, *Chem. Phys. Lett.*, 2002, **360**, 47-52.

[Um95] E. Umbach, C. Seidel, J. Taborski, R. Li and A. Soukopp, *Phys. Stat. Sol.* (B), 1995, **192**, 389-406.

[Va96] A. A. Vaughan, M. G. Baron and R. Narayanaswamy, *Anal. Commun.*, 1996, **33**, 393-396.

[Va04] H. Van Ryswyk, E. E. Moore, N. S. Joshi, R. J. Zeni, T. A. Eberspacher and J. R. Collman, *Angew. Chem. Intern. Ed.*, 2004, **43**, 5827-5830.

[Wa79] C. D. Wagner, W. M. Riggs, L. E. Davis and J. F. Moulder, Editor: G. E. Muilenberg, *Handbook of X-Ray Photoelectron Spectroscopy*, Perkin-Elmer Corporation (Physical Electronics Division) 1979 (1st Ed.).

[Wa05] Q. Wang, W M. Carnpbell, E. E. Bonfantani, K. W. Jolley, D. L. Officer, P. J. Walsh, K. Gordon, R. Humphry-Baker, M. K. Nazeeruddin and M. Gratzel, *J. Phys. Chem. B*, 2005, **109**, 15397-15409.

[Wa09] R. Wang, B. Gao and W. Jiao, *App. Surf. Sci.*, 2009, **255**, 4109-4113.

[We07] H. Wende, M. Bernien, J. Luo, C. Sorg, N. Ponpandian, J. Kurde, J. Miguel, M. Piantek, X. Xu, P. Eckhold, W. Kuch, K. Baberschke, P. M. Panchmatia, B. Sanyal, P. M. Oppeneer and O. Eriksson, *Nat. Mater.*, 2007, **6**, 516-520.

[We08A] A. Weber-Bargioni, W. Auwärter, F. Klappenberger, J. Reichert, S. Lefrancois, T. Strunskus, C. Wöll, A. Schiffrin, Y. Pennec and J. V. Barth, *ChemPhysChem*, 2008, **9**, 89-94.

[We08B] A. Weber-Bargioni, J. Reichert, A. P. Seitsonen, W. Auwarter, A. Schiffrin and J. V. Barth, *J. Phys. Chem. C*, 2008, **112**, 3453-3455.

[Wi05] G. Witte, S. Lukas, P. S. Bagus and C. Wöll, *App. Phys. Letts*, 2005, **87**, 263502.

[Wö08] T. Wölfle, A. Görling and W. Hieringer, *Phys. Chem. Chem. Phys.*, 2008, **10**, 5739-5742.

[Wö89] C. Wöll, S. Chiang, R. J. Wilson and P. H. Lippel, *Phys. Rev. B*, 1989, **39**, 7988.

[Wu97] X. Wu, Y. Li, B. Gründig, N.-T. Yu and R. Renneberg, *Electroanalysis*, 1997, **9**, 1288-1290.

[Yo96] D. Yoshimura, H. Ishii, S. Narioka, M. Sei, T. Miyazaki, Y. Ouchi, S. Hasegawa, Y. Harima, K. Yamashita and K. Seki, *J. Electron Spectrosc. Relat. Phenom.*, 1996, **78**, 359-362.

[Yo04] S. Yoshimoto, J. Inukai, A. Tada, T. Abe, T. Morimoto, A. Osuka, H. Furuta and K Itaya, *J. Phys. Chem. B*, 2004, **108**, 1948-1954.

[Yo06] S. Yoshimoto, S. Sugawara and K. Itaya, *Electrochemistry*, 2006, **74**, 175-178.

[Yu08] J. H. Yum, S. R. Jang, R. Humphry-Baker, M. Gratzel, J. J. Cid, T. Torres and M. K. Nazeeruddin, *Langmuir*, 2008, **24**, 5636-5640.

[Zo06] Y. Zou, L. Kilian, A. Schöll, T. Schmidt, R. Fink and E. Umbach, *Surf. Sci.*, 2006, **600**, 1240-125.

List of Figures

List of Tables

List of publications

1. Direct Metalation of a Phthalocyanine Monolayer on Ag(111) with Coadsorbed Iron Atoms
Y. Bai, F. Buchner, M. Wendahl, I. Kellner, A. Bayer, H.-P. Steinrück, H. Marbach, and J. M. Gottfried
J. Phys. Chem. C, 2008, **112**, 6087-6092

2. Coordination of Iron Atoms by Tetraphenylporphyrin Monolayers and Multilayers on Ag(111) and Formation of Iron-Tetraphenylporphyrin
F. Buchner, K. Flechtner, Y. Bai, E. Zillner, I. Kellner, H.-P. Steinrück, H. Marbach, and J. M. Gottfried
J. Phys. Chem. C, 2008, **112**, 15458–15465

3. A Comparative Study of a Triphenylene Tricarbonyl Chromium Complex and its Uncoordinated Arene Ligand on the Ag(111) Surface: Influence of the Complexation on the Adsorption
C. Schmitz, C. Rang, Y. Bai, I. Kossev, J. Ikonomov, Y. Su, K. Kotsi, S. Subach, O. Neucheva, S. Tautz, F. Neese, H-P Steinrück, J. M. Gottfried, K. Doetz, and M. Sokolowski
J. Phys. Chem. C, 2009, **113**, 6014–6021

4. Formation of the Calcium/Poly(3-Hexylthiophene) Interface: Structure and Energetics
J. Zhu, F. Bebensee, W. Zhao, J. H. Baricuatro, J. Farmer, Y. Bai, H.-P. Steinrück, J. M. Gottfried, and C. T. Campbell
JACS, 2009, **131**, 13498-13507

5. Adsorption of Cobalt(II) Octaethylporphyrin and 2H-Octaethylporphyrin on Ag(111): New Insight into the Surface Coordinative Bond
Y. Bai, F. Buchner, I. Kellner, M. Schmid, F. Vollnhals, H.-P. Steinrück, H. Marbach, and J. M. Gottfried
New J. Phys., 2009, **11**, 125004

6. Interfacial Coordination Interactions Studied on Cobalt Octaethylporphyrin and Cobalt Tetraphenylporphyrin Monolayers on Au(111)
Y. Bai, M. Sekita, M. Schmid, T. Bischof, H.-P. Steinrück, and J. M. Gottfried
PCCP, 2009, in press

7. Interface Formation between Calcium and Electron-Irradiated Poly(3-Hexylthiophene)
F. Bebensee, J. Zhu, J. H. Baricuatro, J. A. Farmer, Y. Bai, H.-P. Steinrück, Ch. T. Campbell, and J. M. Gottfried
Langmuir, 2010, submitted

8. Determining the Distance Between the Atoms in Adsorbed Metalloporphyrins and the Underlying Ag(111) Surface Using NIXSW Technique
Y. Bai, I. Kröger, F. Bebensee, H.-P. Steinrück, C. Kumpf, and J. M. Gottfried

In preparation

Acknowledgement

Lebenslauf

Persönliche Daten

Name: Bai

Vorname: Yun

Geburtsdatum: 19.05.1981

Geburtsort: Jingzhou, China

Nationalität: Chinesisch

Schulbildung

09.1987 – 07. 1992: Grundschule, Jingzhou, China

09.1992 – 07.1995: Sekundärschule, Jingzhou, China

09.1995 – 07.1998: Jingzhou-Gymnasium, Jingzhou, China

Hochschullaufbahn

09.1998 – 06.2002: Wuhan Universität, China

06.2002: Bachelor of Science in Chemie

10.2004 – 09.2006: Freie Universität Berlin

09.2006: Master of Science in Chemie

Tätigkeiten

10.2002 – 06.2004: Wissenschaftliche Übersetzerin bei der Firma „China
Patent" Beijing, China

01.2006 – 06.2006: Studentische Hilfskraft in der Technischen Fakultät der
Universität Kiel

Seit 11.2006: Wissenschaftliche Mitarbeiterin am Lehrstuhl für Physikalische Chemie
II an der Universität Erlangen-Nürnberg